FY21 NRL DOD HPCMP ANNUAL REPORTS

U.S. NAVAL RESEARCH LABORATORY

FY21 NRL DoD High Performance Computing Modernization Program Annual Reports

Edited by
Bonnie J. Assad

Prepared by
Portia A. Shingler and Beth A. Howell

Center for Computational Science
Information Technology Division

August 9, 2022

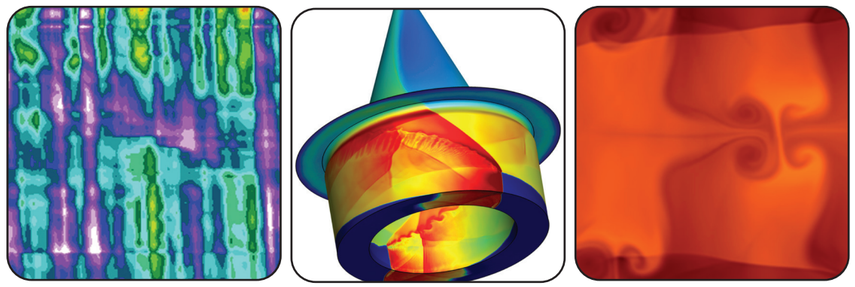

REVIEWED AND APPROVED
NRL/PU/5594--22-667
IR-5594-22-1-U
August 2022

Center for Computational Science
Information Technology Division

Introduction

This book is a compilation of reports on all the work accomplished by NRL scientists and engineers and their collaborators using the DoD High Performance Computing Modernization Program's (HPCMP) resources for fiscal year 2020. The reports encompass work performed by researchers at all three NRL sites: Washington, DC, Stennis Space Center, Mississippi, and Monterey, California.

These reports are categorized according to the primary Computational Technology Area (CTA) as specified by the HPCMP and include resources at the DOD Supercomputing Resource Centers (DSRC) as well as the Affiliated Resource Centers (ARC). This volume includes three indices for ease of reference: an author index, a site index, and an NRL hierarchical index of reports from the branches and divisions in the Laboratory.

THIS PAGE INTENTIONALLY LEFT BLANK

Table of Contents

Computational Structural Mechanics (CSM)

Computational Fluid Dynamics (CFD)

Computational Biology, Chemistry, and Materials Science (CCM)

Computational Electromagnetics and Acoustics (CEA)

Climate Weather Ocean Modeling (CWO)

Signal Image Processing (SIP)

Space and Astrophysical Science (SAS)

Other (OTH)

CSM

Computational Structural Mechanics

CSM covers the high-resolution multidimensional modeling of materials and structures subjected to a broad range of loading conditions including quasistatic, dynamic, electromagnetic, shock, penetration, and blast. It also includes the highly interdisciplinary research area of materials design, where multiscale modeling from atomistic scale to macroscale is essential. CSM encompasses a wide range of engineering problems in solid mechanics, such as material or structural response to time- and history-dependent loading, large deformations, fracture propagation, shock wave propagation, isotropic and anisotropic plasticity, frequency response, and nonlinear and heterogeneous material behaviors. High-performance computing for CSM addresses the accurate numerical solution of conservation equations, equations of motion, equations of state, and constitutive relationships to model simple or complex geometries and material properties, subject to external boundary conditions and loads. CSM is used for basic studies in continuum mechanics, stress analysis for engineering design studies, predicting structural and material response to impulsive loads, and modeling response of heterogeneous embedded sensors/devices. DoD application areas include conventional underwater explosion and ship response, structural acoustics, coupled field problems, space debris, propulsion systems, structural analysis, total weapon simulation, weapon systems' lethality/survivability (e.g., aircraft, ships, submarines, and tanks), theater missile defense lethality analyses, optimization techniques, and real-time, large-scale soldier- and hardware-in-the-loop ground vehicle dynamic simulation.

Title: Geometric, Constitutive and Loading Complexities in Structural Materials
Author(s): S.A. Wimmer,[1] R.N. Saunders,[1] A. Arcari,[1] C. Farhat,[2] A. Iliopoulos,[1] L.P. Kuna,[3] J.G. Michopoulos,[1] and S.N. Rodriguez[1]
Affiliation(s): [1]Naval Research Laboratory, Washington, DC, [2]CMSoft, Inc., Palo Alto, CA, [3]National Academies of Sciences, Engineering, and Medicine, Washington, DC
CTA: CSM

Computer Resources: HPE SGI 8600 [AFRL, OH], [NAVY, MS]

Research Objectives: The research strives to develop rational bases and mathematical descriptions of complex material responses for structural and novel evolving materials. Structural integrity and life cycle evaluations require an understanding of material responses. Analytical models and techniques cannot describe complex materials and often do not account for interactions, complex geometries, or multiphysics loading. Finite-element methods are used to develop models involving multifunctional materials, novel evolving materials, and multiphysics. In order to accurately model the nonlinear response of conventional structural materials, rate dependence, large deformation, and damage-accumulation mechanisms must be understood and accurately represented. The performance of the overall structure or system is also examined via parameters such as kinematics, geometric complexities, loading path dependencies, and interaction between loading types.

Methodology: The project uses finite-element methods extensively. Nonlinear material constitutive response features are highlighted in much of the work. Implicit and explicit solutions methods are used as appropriate. The primary finite-element code used is ABAQUS. Coupled material responses such as electric-thermal or electrical-mechanical-thermal are exercised for evaluation of these effects. Model development is done with CUBIT, ABAQUS/CAE, ScanIP, or in-house software. Large run times and large model size are often required for the multistep nonlinear finite-element analysis jobs.

Results: This project involves work in several topical areas. Work has been performed on creating image-based microstructural models, modeling multilayer ceramic structures, modeling stress corrosion cracking, modeling biofoulants, and modeling transparent armor delamination. Representative results for the topic of modeling stress corrosion are discussed. Crystallographic microstructures influence the evolution of pitting corrosion. Pitting corrosion can lead to failure through initiation of stress-corrosion cracking. Grain shape, grain boundary characteristics, and second-phase precipitates, among other features, all have been identified as potential influences on corrosion initiation sites in stainless steel alloys. Figure 1 shows a representative volume with its microstructure. The microstructure comes from measured data. Using the multiphysics platform PRISMS-PF, the initial pit is allowed to evolve and grow. Computational results of pit growth for three samples are shown in Fig. 2. Figure 3 shows the stress concentrations for all samples and for a homogeneous case. Stress concentrations are found to be significantly greater than and more localized than for a homogeneous sample.

DoD Impact/Significance: Pitting corrosion can lead to stress corrosion cracking and failure of metal components in water environments. The role of material microstructure, specifically grain boundaries and second-phase precipitates on the growth of corrosion pits in stainless steel alloys, is not well characterized. The results of this study will enable better mitigation of pit growth to prevent or reduce stress corrosion cracking and improved intergranular corrosion models for accurate life cycle predictions for current and future naval structure designs.

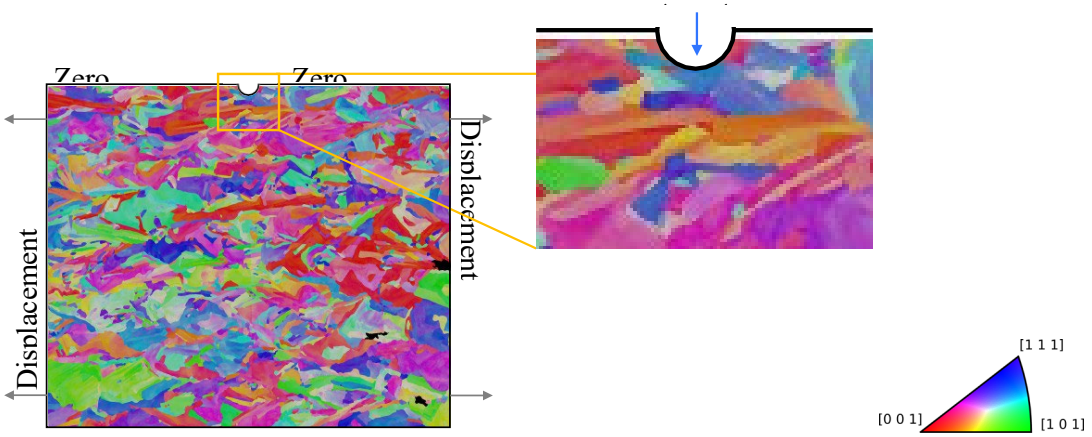

Figure 1. Schematic of computational problem domain with applied boundary conditions. The color notates the grain orientations of austenitic stainless steel, 316L. The 2D analysis volume was 114.7 x 97.5 micrometers. The initial pit radius was 5.7 micrometers.

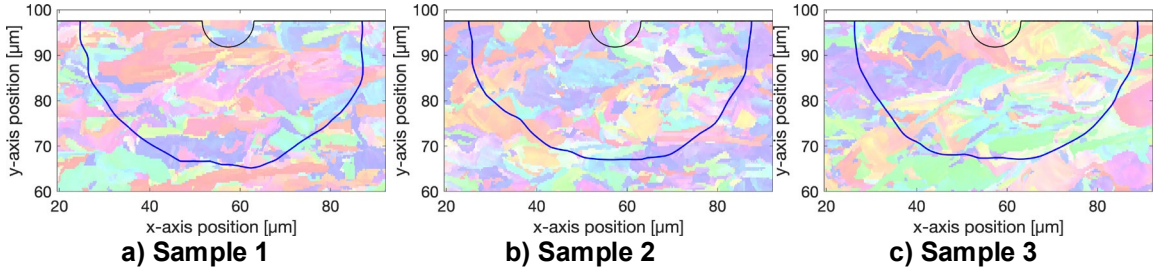

Figure 2. Evolved pit fronts at the end of the simulation time for three samples. The grain colors are lightened to highlight the pit front, but are the same scale as seen in Fig. 1.

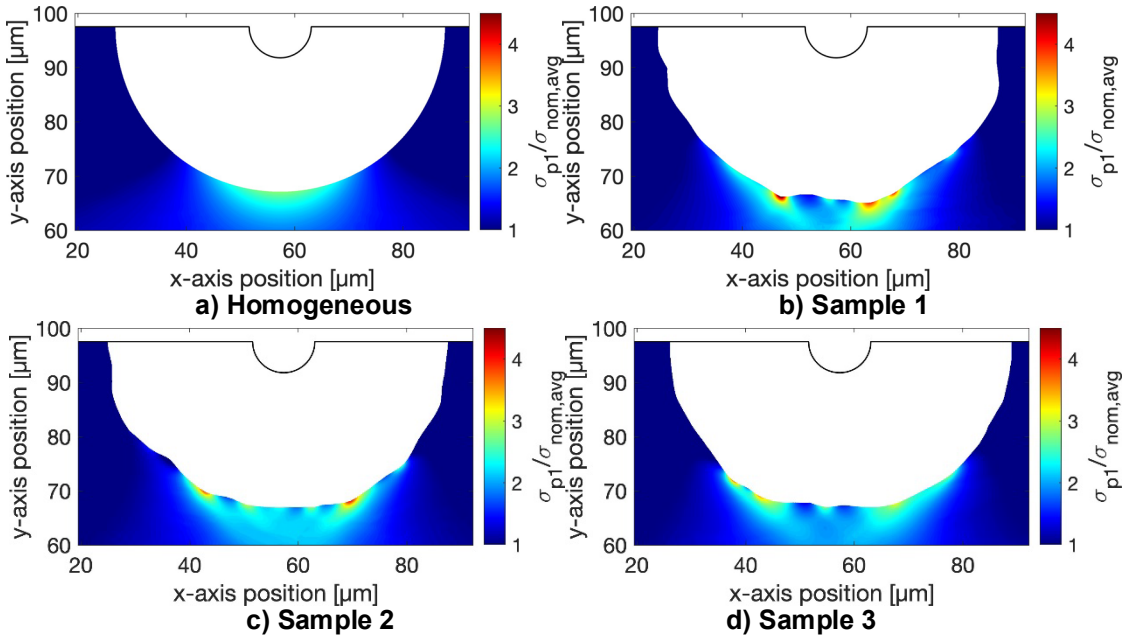

Figure 3. Comparison of stress concentrations, the ratio of first principal stress, $\boldsymbol{\sigma}_{p1}$, normalized by the nominal stress along the boundary, $\boldsymbol{\sigma}_{norm}$, for all model cases at the end of the simulation.

Title: Stochastic Methods for Uncertainty Quantification in Computational Mechanics
Author(s): K. Teferra,[1] L. Kuna,[2] and R.N. Saunders[1]
Affiliation(s): [1]Naval Research Laboratory, Washington, DC, [2]National Research Council Postdoctoral Research Associate, Naval Research Laboratory, Washington, DC
CTA: CSM

Computer Resources: Cray XC40/50 [ERDC, MS]; HPE SGI 8600 [NAVY, MS]

Research Objectives: The research objective for the work in FY21 is to be able to predict the microstructure evolution of additively manufactured (AM) 316L stainless steel and to evaluate the effect of different build conditions on microstructural features. Additive manufacturing is a promising materials-processing technique because of its ability to tailor part geometry. However, being a new processing technique having a significantly different thermal history than traditional, wrought-processing techniques, the effect on material microstructure and properties is not established at the level of reliability required for design standards. Understanding the effect of heat source-processing parameters on the temperature field and microstructure evolution falls within microstructure characterization, which is a necessary and essential component of material accreditation. Our goal is to be able to model and simulate this process in order to establish validated, predictive modeling capability such that rapid assessment of build strategies can be made.

Methodology: This work focuses on implementing modifications to the cellular automata finite-element (CAFE) model necessary to make it optimal for simulating solidification of AM metals in order to simulate large enough polycrystalline microstructures such that crystallographic texture can be analyzed sufficiently. An implementation of the CAFE model was developed to efficiently utilize distributed memory systems using the MPI library, enabling large-scale simulations. This implementation of the CAFE model is used to explore the effect of processing parameters, such as laser scan path, for both bulk material and thin-walled domains.

Results: Large polycrystalline microstructures are simulating for AM 316L processed through laser powder bed fusion. Material properties are derived from its composition as well as microstructural configuration, which depends on the processing technique used in fabrication. Common laser scan patterns and laser parameters, including scan speed and laser power, were analyzed. Figure 1 shows results of a laser grid that rotates 67 degrees per layer along with 3 pole figure plots, followed by a thin-walled section compared to experimental electron backscatter diffraction data.

DoD Impact/Significance: Enhanced structural material performance in terms of durability and strength-to-weight ratio, as well as manufacturability, are essential ingredients toward transforming fleet capabilities. Additive manufacturing (AM) may eventually become a commonplace manufacturing technique for both military and civilian applications. Understanding the relationship between AM processing parameters and microstructure morphology can provide guidance to material designers to achieve manufacturing of materials with desired properties.

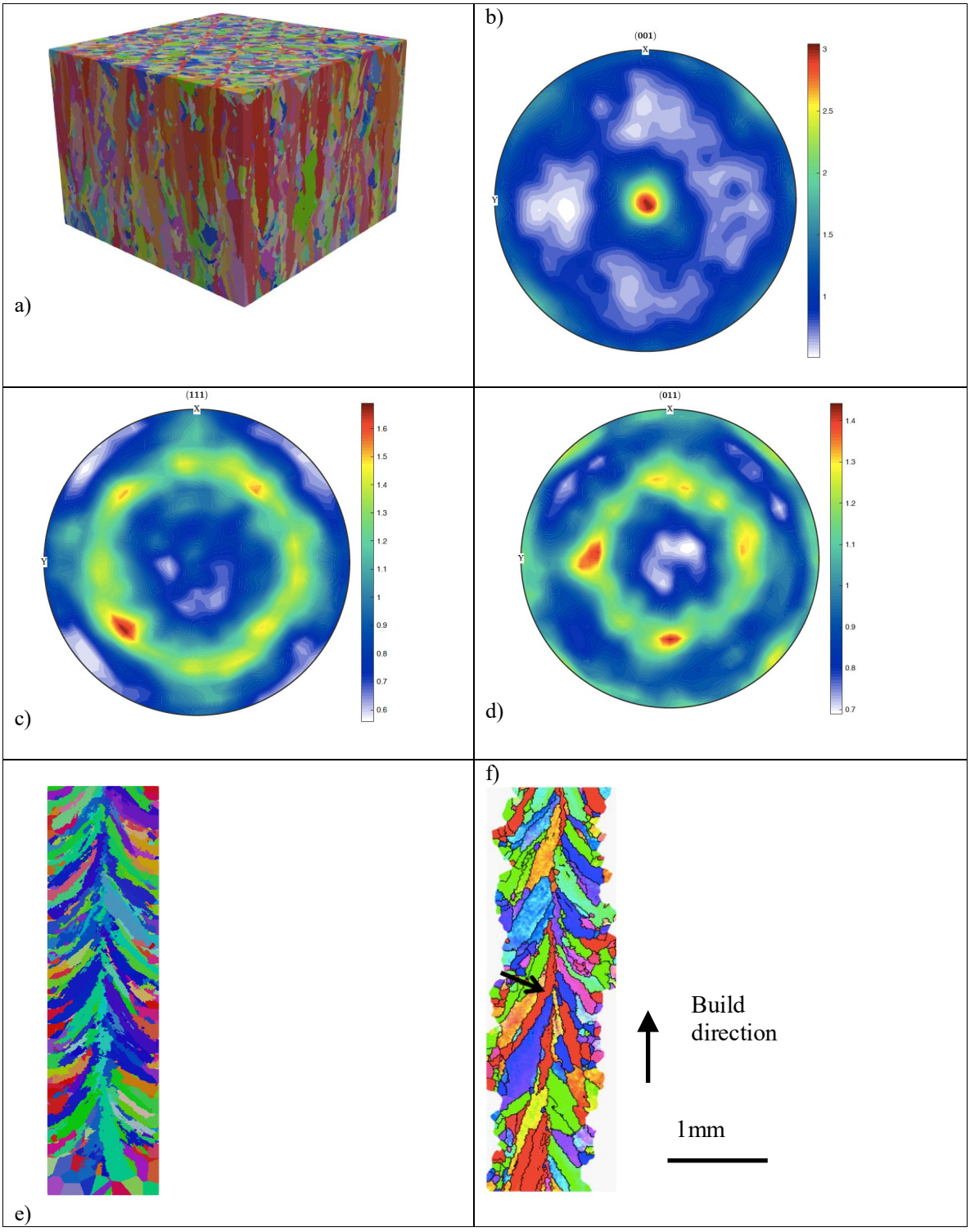

Figure 1. Results of a cellular automata finite element simulation. a) Isometric view of simulation, b) <0 0 1> pole figure of sample. c) <1 1 1> pole figure of sample. d) < 0 1 1> pole figure of sample, e) View of thin wall simulation, f) EBSD image of thin-wall sample.

Title: Computational Analysis of Warfighter Brain Injury and Protective Equipment
Author(s): X.G. Tan and R.N. Saunders
Affiliation(s): Naval Research Laboratory, Washington, DC
CTA: CSM

Computer Resources: HPE SGI 8600 [AFRL, OH], [NAVY, MS]; Cray XC40 [ARL, MD]

Research Objectives: The research objective of this project is developing methods to prevent and mitigate injury to warfighters. This involves computational analysis of ballistic/blunt impacts on personal protective equipment (PPE) and blast-induced traumatic brain injury (TBI). Computational methods, such as finite-element analysis, are used to conduct the simulation analysis. The use of HPC resources is vitally important to this project due to the high fidelity of the models of interest. A typical model to analyze traumatic brain injury requires approximately 24 hours on 216 CPUs. One of the primary outcomes of this research will be the accumulation of a significant number of simulations that will be used to construct the correspondence relationship between humans and animals and to optimize the design of protective equipment.

Methodology: The project uses finite-element methods extensively, but the work is not restricted to finite-element methodologies. Nonlinear material mechanical constitutive response features are highlighted in much of the work performed. Implicit and explicit solution methods are used as appropriate. The primary finite-element codes used are Abaqus, CoBi and CTH. User subroutines are used for specialized material constitutive response when applicable. Multiphysics analysis is used to capture the fluid/acoustic structure interaction, thermomechanical and electromagneto-mechanical effects. Typically, Abaqus/Viewer, ParaView, VisIt, IDL, and Matlab are used for visualization of results in formats such as VTU and HDF5, including animation. For model development, the project typically uses CUBIT, ABAQUS/CAE, Simpleware, IDL, and in-house code. Large run times and large model sizes are often required for the multiphysics/multistep nonlinear finite-element/volume analysis jobs.

Results: This project involves work in several topical areas. Work has been performed in the development of a method to map biomechanical results to clinical imaging data for improved understanding of the causes and effects of blunt-impact incidents that may augment clinical diagnosis and injury assessment. Shown in Fig.1, the multifidelity modeling approach was used to analyze the biomechanical response of real-world head-impact accidents. The simulation results then were mapped to clinical imaging data. The correlation analyses show different biomechanical measures and thresholds can be used to explain different blunt-impact injury modalities. One of advanced MRI modalities, ADC, was found to be appropriate for MRI data interpretation and digitization of clinical assessment for quantitative analyses and injury assessments. This methodology of integrating computational and clinical analyses leads to further developments to understand, quantify, and interpret brain injury, to refine injury criteria and to predict injury risk.

DoD Impact/Significance: Insights gained from this project are necessary for the advancement from concept to application. Navy/DoD expected results are an improved understanding of traumatic brain injury for naval/DoD applications. New insights will be gained through quantifying the effects of anatomical and material property differences on the mechanical response of quantities correlated with traumatic brain injury, which will affect warfighter health in terms of improved protective gear and improved understanding of the correlation between mechanical response thresholds and traumatic brain injuries. The development of techniques to model population-wide anatomical variability will provide insight into the importance of the fit of protective gear.

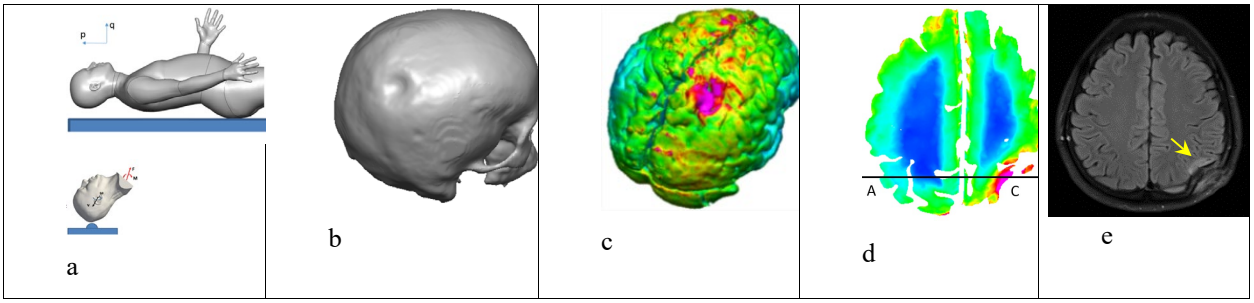

Figure 1. Comparison of biomechanical simulation with clinical imaging data: a) biodynamic simulation of accidental fall, b) resulting skull indentation from high-fidelity head-impact simulation, c) contour of maximum strain rate on brain, d) contour of maximum strain rate in transverse plane passing through the indented region, e) MRI image of transverse plane passing through the indented region.

Title: Atomistic Modeling of Structural Materials
Author(s): E. Antillon, N. Bernstein and M. Johannes
Affiliation(s): Naval Research Laboratory, Washington, DC
CTA: CSM

Computer Resources: HPE SGI 8600 [AFRL, OH]; SGI ICE X [ARL, MD]; Cray XC40/50 [ERDC, MS]

Research Objectives: The basic objective is to understand fundamental deformation mechanisms responsible for mechanical strength and stability for superior alloys in naval applications. Of particular importance are austenitic steels, which can achieve a balance of strength, ductility, stability, and corrosion resistance. Because of the large content of iron, spin-polarized calculations become necessary to capture a magneto-volume coupling that arises on this class of alloys. First-principles codes are used to measure critical inputs to an Integrated Computational Materials Engineering (ICME) framework that replaces the trial-and-error design approaches with a more predictive material design approach.

Methodology: The Vienna Ab initio Simulation Package (VASP) is used to perform all density functional theory calculations. Austenitic steel alloys prove to be challenging because these materials are stable only in the paramagnetic state, which is an intrinsically high-temperature phenomenon involving dynamically disordered spins, which break local symmetry but produce FCC structure, on average. To emulate the paramagnetic state, we follow an averaging scheme that couples the lattice and magnetic degrees of freedom in a supercell via a statistical-averaging method known as magnetic sampling method. This approach is applied to measure elastic and point-defect properties in a model 316L steel alloy composition.

Results: We have focused our investigations on a model austenitic steel alloy, $Fe_{0:70}Ni_{0:12}Cr_{0:18}$, and explored the role of magnetic moments on various material properties. In steel alloys, magnetic moments can be strongly coupled to atomic lattice displacements, and as a result, they can influence phase stability and related atomic-scale properties. One example of this is the elastic constants on single crystals for the aforementioned composition. Figure 1 compares the elastic constants obtained using first-principles calculations under various magnetic arrangements with experimental values from Ledbetter et al. Here, first-principles calculations are carried out using nonmagnetic density functional theory (DFT) and spin-polarized DFT, with the magnetic moments arranged in either ferrimagnetic orientation or approximately disordered paramagnetic state as described in the methodology section. It is clear that the nonmagnetic calculations show larger elastic moduli values, followed by the paramagnetic state, while ferrimagnetic state shows the smallest values. At the atomic level, this trend can be attributed to the Pauli forces' slightly increasing the effective size of the atoms compared to nonmagnetic calculations, making the system less compact and softer. Our results suggest that both the presence of magnetic moments and their disordered orientations are necessary to properly describe elastic properties from first-principles calculations.

DoD Impact/Significance: The objectives as given above have immediate relevance for military interests. The problems of designing superior steel alloys is relevant to designing surface and underwater naval vessels. Our calculations provide a fundamental input into the integrated computational materials engineering (ICME) framework to connect accurate atomic-scale calculations of deformations modes to the overall mechanical properties of steel alloys. This framework opens the possibility to combine computational and experimental methods to achieve the desired balance of superior strength and stability relative to 316L stainless steel that is currently in use.

Elastic Constants [GPa]	DFT Non-Magnetic	DFT Para-Magnetic	DFT Ferri-Magnetic	Experiment [Fe-12Ni-18Cr]
C_{11}	360 ±2	238±15	150 ±6	191-216
C_{12}	219 ±1	126±8	93 ±2	118-145
C_{44}	193 ±1	141±3	103 ±1	129-139
B	266 ±1	163±8	112 ±8	142-168
E	293 ±1	216±4	138 ±8	204-208
G	111 ±1	84±2	53 ±4	78-83
ν	0.317 ±0.001	0.279 ±0.010	0.294 ± 0.002	0.25-0.29

Figure 1. Comparison of elastic constants obtained under various magnetic orientation using first-principles calculations. The experimental values are from H. M. Ledbetter phys. stat. sol. (a) 86, 89 (1984)

THIS PAGE INTENTIONALLY LEFT BLANK

CFD

Computational Fluid Dynamics

CFD covers high-performance computations whose goal is the accurate numerical solution of the equations describing fluid motion and the related use of digital computers in fluid dynamics research. CFD is used for basic studies of fluid dynamics for engineering design of complex flow configurations and for predicting the interactions of chemistry with fluid flow for combustion and propulsion. It is also used to interpret and analyze experimental data and to extrapolate into regimes that are inaccessible or too costly to study. Work in the CFD CTA encompasses all Reynolds number flow regimes and scales of interest to the DoD. Incompressible flows are generally slow (e.g., governing the dynamics of submarines, slow airplanes, pipe flows, and air circulation) while compressible flows are important at higher speeds (e.g., controlling the behavior of transonic and supersonic planes, missiles, and projectiles). Fluid dynamics itself involves some very complex physics, such as boundary layer flows, transition to turbulence, and turbulence dynamics, that require continued scientific research. CFD also must incorporate complex additional physics to deal with many real-world problems. These effects include additional force fields, coupling to surface atomic physics and microphysics, changes of phase, changes of chemical composition, and interactions among multiple phases in heterogeneous flows. Examples of these physical complexities include direct simulation Monte Carlo and plasma simulation for atmospheric reentry, microelectromechanical systems (MEMS), materials processing, and magnetohydrodynamics (MHD) for advanced power systems and weapons effects. CFD has no restrictions on the geometry and includes motion and deformation of solid boundaries defining the flow.

Title: Hypersonic Reactive Flow Modeling
Author(s): G. Goodwin
Affiliation(s): Naval Research Laboratory, Washington, DC
CTA: CFD

Computer Resources: SGI ICE X [ARL, MD]

Research Objectives: The objective of this research is to characterize the effect of turbulence on flame stability and combustor efficiency. This research encompasses a broad range of system types, sizes, and scales, from smaller combustors used for analyzing the fine details of the underlying combustion physics to larger applied systems, such as ramjets and supersonic combustion ramjets (scramjets), in which quantification of combustor efficiency and reliability is a primary goal.

Methodology: One of the predominant challenges in using air-breathing engines for hypersonic flight (typically, greater than five times the speed of sound) is that the extremely fast flow speeds through the engine present a challenging environment for reliable ignition of the fuel and stable combustion. The methodology for this research is to use high-fidelity computational fluid dynamics (CFD) to simulate the high-speed reactive flow in the combustors of air-breathing hypersonic vehicles. Boundary conditions, fuel chemistry, combustor geometry, and turbulence levels are varied to catalog the effects of these phenomena on achieving stable ignition and complete combustion. For the results described in this paper, the combustor of a dual-mode scramjet with an inflow Mach number of 0.6 was used as the computational domain. The inflow is a mixture of ethylene and air at an equivalence ratio of 0.6, a pressure of 1.72 atm, and a temperature of 1,125 K. A synthetic turbulence generator was implemented to generate isotropic turbulence at the inflow boundary such that the turbulence intensity in the combustor ranges from 10 to 15%. Simulations were performed both with and without the synthetic turbulence. Combustion is modeled using a calibrated single-step reaction model using an Arrhenius form.

Results: The turbulent inflow generates vorticity in the free stream that causes the flame to wrinkle and roll up. Simulations were performed both with and without this turbulence. The accompanying figure shows isosurfaces of vorticity magnitude, ϖ, of 100 x 10^3 s^{-1} colored by temperature for the laminar and turbulent cases. In the laminar case, the vorticity is present in the boundary layers on the top and bottom walls and in the flame and the cavity, but not in the freestream upstream of the flame. The roll-up of the flame in the shear layer is apparent and several hairpin vortices are visible in the burned product downstream. There are streaks visible in the boundary layers immediately downstream of the inflow, which may indicate a transition from a laminar to turbulent boundary layer. These streaks are also visible in the top wall boundary layer above the flame near the outflow boundary. At this location, the streaks are likely the result of the boundary layer interactions with the pressure waves generated by the flame in the extender section. The synthetic turbulence inflow boundary condition generates considerable vorticity in the freestream, which is densely populated with ϖ = 100 x 10^3 s^{-1} isosurfaces. Vorticity at this magnitude is prevalent throughout the entire domain, but some attenuation is observed as the vortices pass through the flame. This attenuation results from gas expansion within the flame and is visible where there is an absence of ϖ = 100 x 10^3 s^{-1} isosurfaces in the product gas just upstream of the outflow boundary.

DoD Impact/Significance: The impact of this research is an increased fundamental understanding of the fine-scale ignition and combustion physics in scramjet engines. Using high-fidelity computational fluid dynamics to simulate scramjet combustion is a critical step in the engine research-and-development process. The simulations are run in tandem with accompanying experiments for validation and comparison.

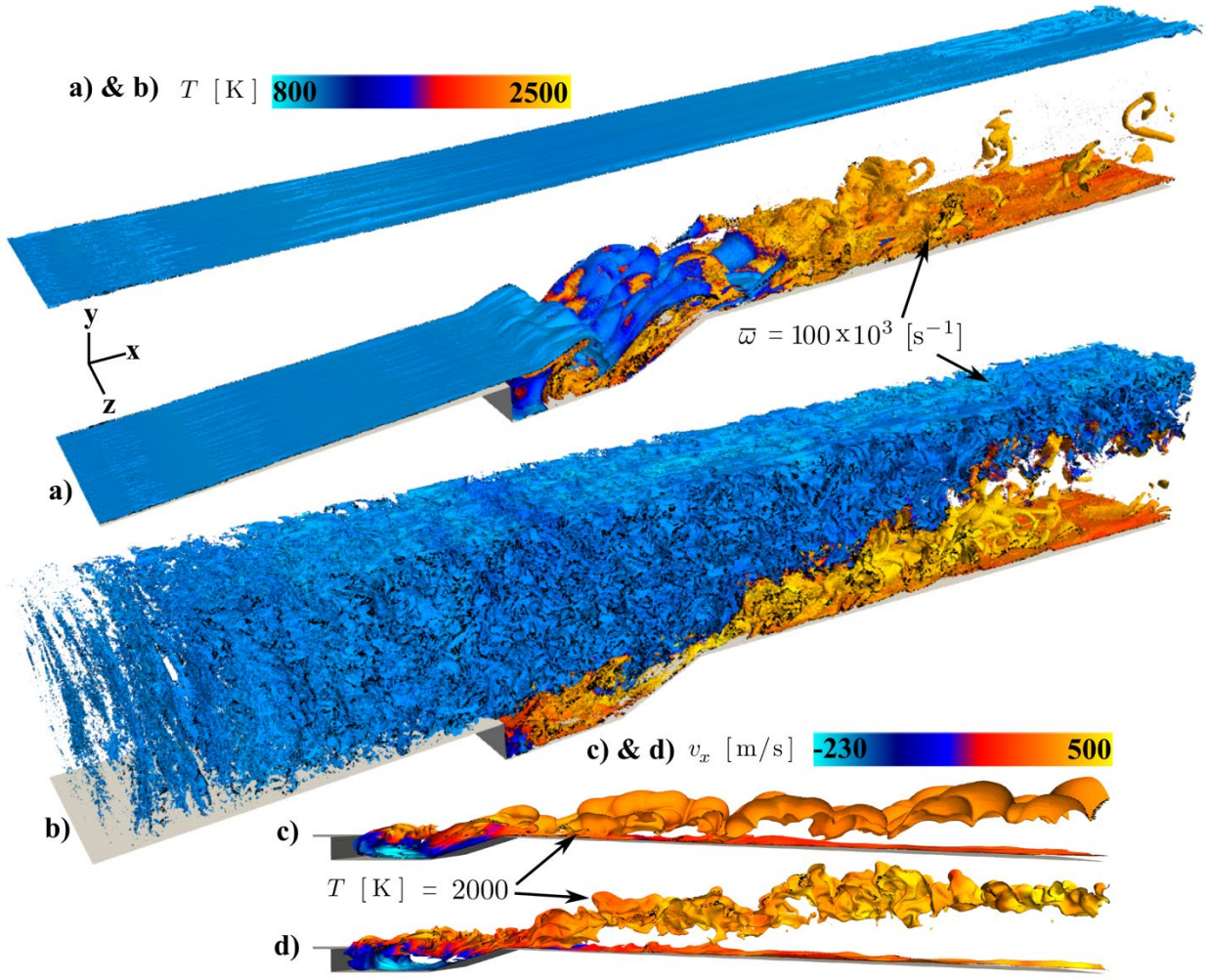

Figure 1. Three-dimensional simulations of combustion in a cavity flameholder. The images show isosurfaces of vorticity colored by temperature (in a and b) and streamwise velocity (in c and d). Images a and c are taken from simulations with the synthetic turbulence inflow.

Title: Numerical Simulations of Noise Generated by Non-Circular Advanced Military Aircraft Nozzles
Author(s): K. Viswanath and R. Ramamurti
Affiliation(s): Naval Research Laboratory, Washington, DC
CTA: CFD

Computer Resources: SGI ICE X, Cray XC40 [ARL, MD]; Cray XC40/50 [ERDC, MS]; Cray Shasta [NAVY, MS]

Research Objectives: To predict details of turbulent flow structures and noise generation in supersonic noncircular asymmetric exhaust jets from representative military aircraft jet engine nozzles. This information will be used to investigate and assess promising jet noise-reduction concepts in support of the ongoing testing program.

Methodology: Simulations are performed using the Jet Noise Reduction (JENRE®[1]) code developed at the Naval Research Laboratory. JENRE® provides unsteady compressible flow solver capabilities that support various numerics and cell-centered finite volume or nodal finite-element methods, while delivering high throughput on calculations. It was developed with an emphasis on raw performance and the ability to exploit emerging massively parallel, HPC architectures. It supports HPC parallel programming paradigms for message passing such as MPI, OpenMP, CUDA, and hybrid models. JENRE® supports parallel IO via MPI/IO or the adaptable IO system (ADIOS) to further complement the multiple levels of parallelism. JENRE® uses an edge-based formulation for all flux integration and limiting algorithms. The Taylor-Galerkin finite-element method with second-order spatial accuracy for tetrahedral cells is used with the finite element flux corrected transport (FEM-FCT) method. The multidimensional FCT flux limiter provides an implicit subgrid stress model, which ensures monotonicity at shocks and sharp gradients with minimal artificial dissipation. JENRE® also features a wall model that supports high-speed flows and surface roughness effects while significantly reducing grid resolution requirements.

Results: Simulations of supersonic twin jets at a highly overexpanded baseline operating condition nozzle pressure ratio of 2.5 were investigated with the operating conditions within each nozzle differing by small increments relative to each other. This sets up jets from each nozzle that are slightly different, hence their interaction is also different from the baseline case, with both nozzles with identical jets. This simulates potential realistic conditions and helps us understand the asymmetric noise characteristics and evaluate noise-reduction techniques. A twin-jet rectangular nozzle (equivalent diameter D = 0.018 m), with an aspect ratio of 2 and a centerline nozzle separation distance of 2.3 D, as shown in Fig. 1, was simulated and its noise production and flow features were compared with experimental data from the University of Cincinnati (UC). The simulations matched the far-field noise and the spatial variation of the noise compared to UC data best for a differential operating condition of 5%, shown in Fig. 2. Figure 3 compares the normalized time averaged contours of the streamwise jet plume velocity, showing the shock cell structures and the jet core plume breakdown regions for all cases. Without differential conditions, the simulations show stronger shock cells, near nozzle exit, compared to UC data, while using 10% differential brings the simulations closer to the experimental data. This points to experimental setups' having initial conditions that are slightly different from what is intended and how much it can affect the noise generation and jet interaction.

DoD Impact/Significance: The results of our work will provide better understanding of the noise production for both industrial and military aircraft, and will aid the current effort of noise reduction, especially for supersonic aircraft, to reduce the impact of the jet noise on shipboard health and safety issues.

[1] JENRE® is a registered trademark of the Department of the Navy.

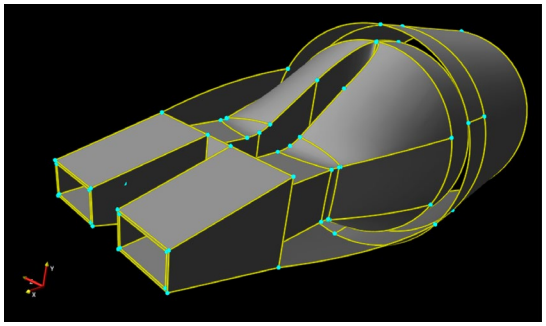

Figure 1. Twin-jet nozzle geometry, aspect ratio 2 nozzles with separation distance of 2.3 D.

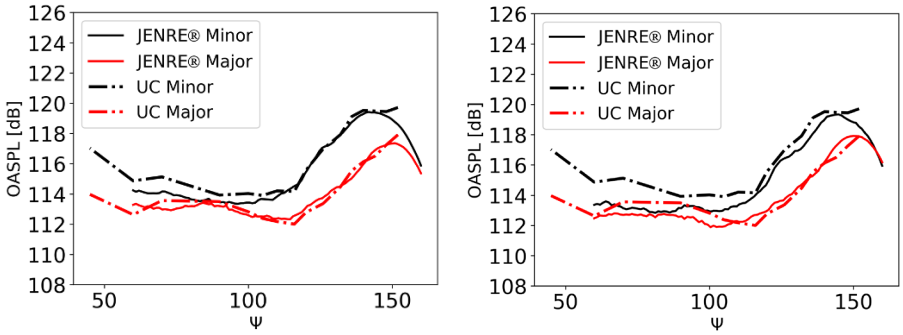

Figure 2. Far-field noise comparison at 60D for the NPR 2.5 case twin-jet plume with differential operation condition between the two jets. Left shows 5% differential conditions. Right shows a 10% difference in NPR.

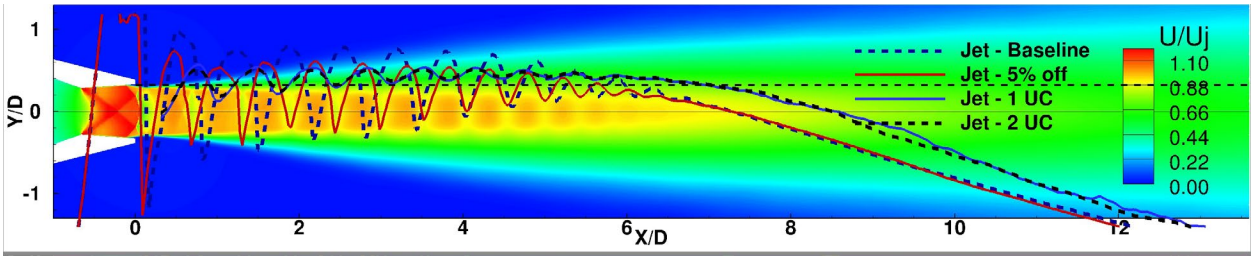

JENRE® data comparison with 5% differential NPR

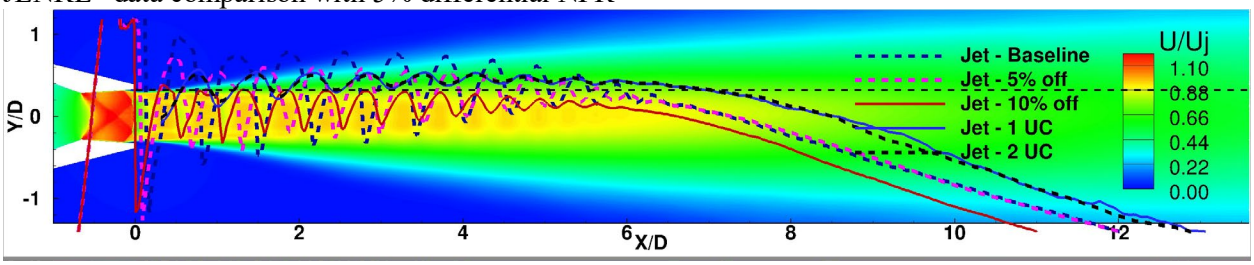

JENRE® data comparison with 10% differential NPR

Figure 3. Overlay with UC data centerline jet velocity of the time-averaged flow field from JENRE® simulation comparisons for differential twin-jet nozzle conditions. Top shows 5% difference in NPR between the twin jets. Bottom shows 10% differential condition.

Title: Numerical Simulations of Turbulence Impact on Optical Signal Transmission and Near-Surface Turbulence
Author(s): S. Matt
Affiliation(s): Naval Research Laboratory, Stennis Space Center, MS
CTA: CFD

Computer Resources: SGI ICE X, Cray XC40 [ARL, MD]

Research Objectives: The objective is to refine work on the computational fluid dynamics (CFD) representation of numerical tanks to support and augment companion laboratory experiments. The laboratory tanks emulated are the Simulated Turbulence and Turbidity Environment (SiTTE) laboratory and similar Rayleigh-Bénard (RB) tanks designed to generate convective, optically active turbulence, and the laminar-to-turbulent-flow tank flowSiTTE for boundary-layer dynamics and drag reduction, as well as the large, state-of-the-art SUrge-STructure-Atmosphere INteraction (SUSTAIN) facility at the University of Miami. Results from numerical simulations of the RB tanks are geared toward providing the basis for optical modeling and the description of beam wander due to optical turbulence. This work supported development of a new underwater communications system based on orbital angular momentum (OAM), novel fiber-sensor technologies, a new system for active boundary-layer control and drag reduction, as well as insight into the dynamics underlying near-surface turbulence and boundary-layer processes to improve air-sea-interface flux parameterizations.

Methodology: To accurately reproduce the turbulence dynamics, the representation of the numerical tanks is accomplished using large-eddy simulation (LES) and the full physical domain size of the respective tanks. The numerical experiments build on our previous work with OpenFOAM. We expanded our simulations of RB convection for simulation in air and for a wider range of boundary conditions and geometries, including a new physical RB tank in development at NRLDC (UWOC project, PI Judd).

Results: We performed simulations of different configurations of convective turbulence tanks with the goal of providing phase screens for modeling of optical propagation through turbulence (Figs.1–3). We emulated the laboratory tank setup and compared results to data from a comparable spectral model. Simulations investigating the impact of boundary oscillations on channel flow to study the dynamics of drag reduction near active boundaries corroborate lab results and show that boundary actuation may reduce frictional drag. Numerical experiments at higher wind-wave conditions for the SUSTAIN tank setup were completed to compare more closely to laboratory conditions and to support a new base program project on air-sea-wave dynamics.

DoD Impact/Significance: CFD simulations emulating the convective SiTTE tank, the flow SiTTE tank, and the SUSTAIN wind-wave tank, are critical for the success of research on a novel optical communication system based on orbital angular momentum (OAM), novel methodologies for active boundary-layer control and drag reduction, new fiber-optics sensor development (temperature, flow), and parameterization of air-sea-interface dynamics.

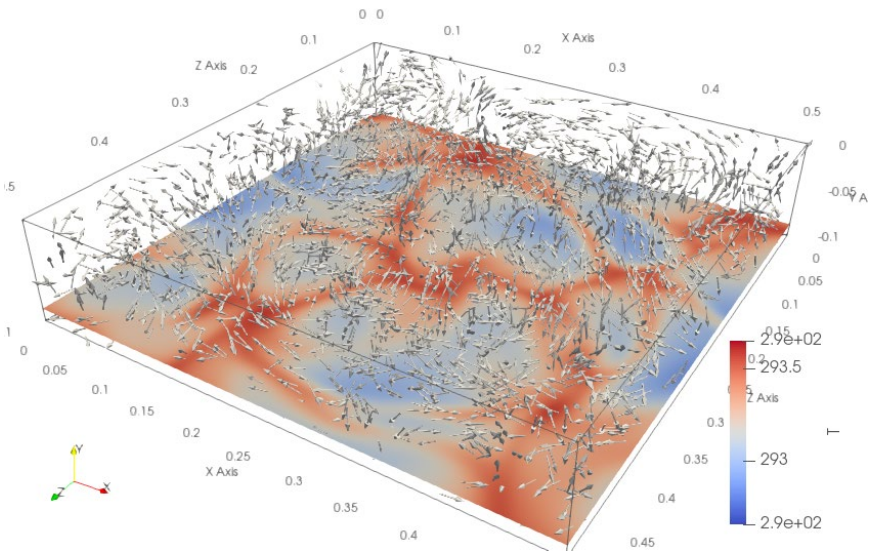

Figure 1. Numerical RB tank to study optical propagation in air for comparison to Direct Numerical Simulation with a spectral model. Plane at 1.25 cm above the bottom shows temperature T at model time t = 180 s. Arrows indicate the velocity field. ΔT between bottom/top is 1 K. Temperature in K, tank dimensions are 0.1 m by 0.1 m by 0.5 m.

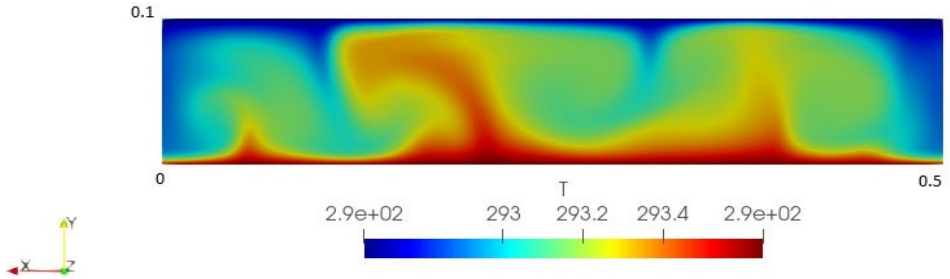

Figure 2. Cross-section (x-y plane, note y is the vertical dimension in this configuration) at x = 25 cm of the model shown in Fig. 1 illustrates convective up- and downdrafts in the domain. Temperature in K.

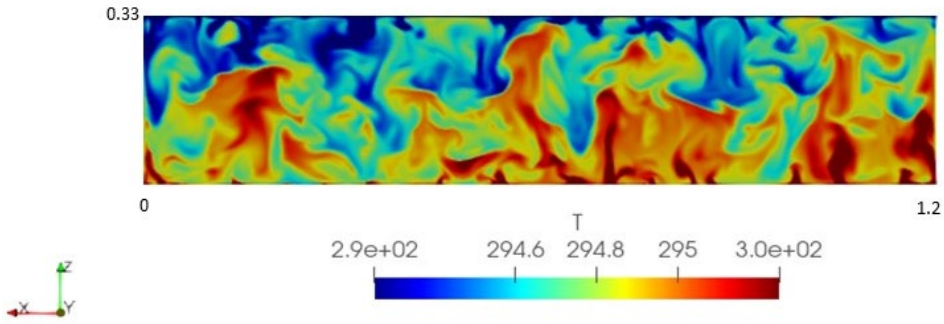

Figure 3. Section along the centerline (x-z plane, note z is the vertical dimension in this configuration), i.e., at y = 16.5 cm, of the simulations of the RB physical tank in development at NRLDC (UWOC project). ΔT between bottom/top is 13.5 K. This results in much stronger convection and smaller-scale features than in the setup shown in Figs. 1 and 2. Temperature in K, tank dimensions in m.

Title: Jet Noise Reduction Studies
Author(s): Y. Khine
Affiliation(s): Naval Research Laboratory, Washington, DC
CTA: CFD

Computer Resources: HPE SGI 8600 [AFRL, OH]; SGI ICE X [ARL, MD]; Cray XC40/50 [ERDC, MS]; Cray Shasta [NAVY, MS]

Research Objectives: The goal of this project is to investigate and assess jet noise-reduction concepts for representative military aircraft jet engines in order to address work place health and safety issues and environmental concerns.

Methodology: Jet noise simulations require a very large computational domain to include both the near and far fields for long enough duration of physical time to study the effect of noise propagation. Thus, it requires significant HPC resources to simulate realistic conditions. For this project, the NRL-developed flow solver JENRE®[1] is used to simulate turbulent flows in nozzles. JENRE® is a large-eddy simulation (LES) model that uses a nodal finite-element method and is implemented with multiple levels of parallelism. Both structured and unstructured meshes can be used with JENRE®, and it has been verified to provide an ideal scalability for thousands of processors. Various jet conditions are considered for a noise-reduction technology called chevrons. In this project, azimuthally varying chevrons are implemented on model-scale faceted nozzles that are representative of GE-F40 nozzles. It is expected that the presence of chevrons at the end of a military aircraft nozzle possibly can reduce supersonic jet noise. Many parameters play important roles in producing desired effects from using the chevrons, and various cases of simulations are needed to understand the effects caused by the presence of chevrons.

Results: This work is in collaboration with the University of Cincinnati (UC) and a sample converging-diverging nozzle with chevrons is presented in Fig. 1. In Fig. 2, Mach number distributions for a baseline nozzle and the chevron nozzle shown in Fig. 1 are presented for nozzle pressure ratio of 3.0 and the nozzle temperature ratio of 3.0. It can be seen that the baseline nozzle shows oblique shock cells inside and outside the nozzle (Fig. 2(a)). In Fig. 2(b) for the chevron nozzle, the shock wave in the distribution of the chevron nozzle is already in the chevron region outside the nozzle. We have studied three chevron shapes and the chevron geometry with the least blockage area presents the best thrust-based noise-reduction performance. Our results reveal that the chevron geometry with a large blockage area not only increases the thrust penalty, but also can impact the flow inside the nozzle adversely and can affect the engine performance.

DoD Impact/Significance: Hearing disability caused by the noise generated by supersonic military aircraft has been a very serious concern for DoD. These studies offer better insight of the physical phenomena for different jet conditions and allow us to optimize chevrons that can provide significant reduction in noise level. This research also supports ongoing jet noise-reduction studies at other government agencies and in academia.

[1] JENRE® is a registered trademark of the Department of the Navy.

Figure 1. Sample faceted nozzle with chevrons

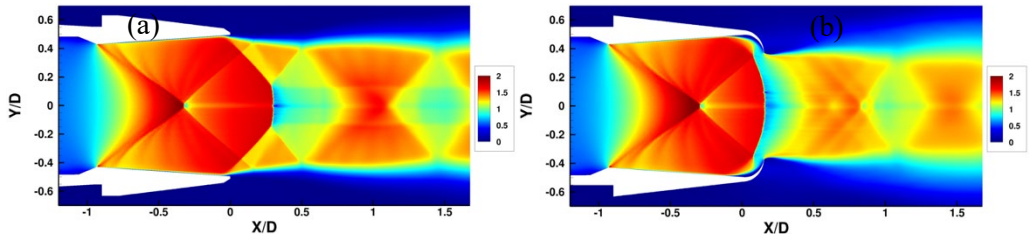

Figure 2. Sample Mach number distributions for nozzle pressure ratio of 3.0 and the nozzle temperature ratio of 3.0. (a) Baseline nozzle. (b) Chevron nozzle shown in Fig. 1.

Title: Detonations with Multi-Phase Flows for Propulsion
Author(s): D.A. Schwer
Affiliation(s): Naval Research Laboratory, Washington, DC
CTA: CFD

Computer Resources: HPE SGI 8600 [AFRL OH]; Cray XC40 [ARL, MD]

Research Objectives: The main research goal is to study high- and low-speed multiphase reacting flows for further understanding of advanced engine concepts, with the specific application for detonation engines.

Methodology: We have used two modeling codes for our research into blast and detonation engine simulations. Our main development and simulation code is the JENRE®[1] code. Due to our extensive experience with using the DET3D codes for detonation propulsion, we will continue to use them as a benchmark for comparison with the JENRE® code. JENRE® is a new code utilizing unstructured meshes and both continuous- and discontinuous-Galerkin-FEM techniques to solve a wide variety of complex fluid dynamical phenomena. It has been built from the ground up at NRL to make efficient use of CUDA, Thread-Building-Blocks, OpenMP, and MPI through the use of the Thrust library. By utilizing unstructured meshes, the solver can be coupled easily to solid structural models and can provide a pathway for doing fluid-structure-interaction. Both gas-phase and multiphase models from our DET3D codes have been incorporated into the JENRE® code.

Results: Because detonation engines are a radical departure from the constant-combustion processes in current engines and power-generation devices, integration of the combustion chamber into those devices requires special care and investigation. Centerbodyless rotating detonation engines (RDEs) are interesting because removal of the wall has several advantages, assuming similar efficiency and stability can be demonstrated. Three different RDEs were investigated to better understand the impact of removing the centerbody on performance under realistic operating conditions. The baseline configuration is taken from earlier work on an RDE concept at altitude 12,800 m and Mach 2.5. Two annular RDEs were investigated, one with an aerospike nozzle, and one with a convergent-divergent (C-D) nozzle attached behind the combustion chamber. The third RDE was a hollow RDE with a C-D nozzle, with the outer wall profile based on the annular RDE with a C-D nozzle. Manifold conditions were considered that produced perfect expansion for the C-D nozzles given a steady combustion process. Two more sets of simulations were done with off-design conditions above and below the target pressure. These results demonstrate that properly matching the exit areas to the injection flow rates for the hollow RDE should produce similar performance as an annular RDE. Due to the size of the calculations, we used the continuous-Galerkin FEM representation with JENRE® and found that the resultant flow-field from the hollow RDE was very similar to comparable annular RDE configurations and also had similar performance. Further work is currently being done to quantify the performance of the simulations.

DoD Impact/Significance: The physics involved in RDEs and other detonation engines is substantially different from what is in gas-turbine engines, and also is different from more traditional premixed detonation calculations, requiring research into how an RDE can fit into existing frameworks for propulsion and power generation. Our work in computing RDE flow fields has helped us to better understand the physics and to verify our physical models, and our development of JENRE® gives us the capability to explore how best to fit RDEs into these existing frameworks. Through this research, the potential of significant efficiency gains for detonation engines can be realized in propulsion and power-generation devices.

[1] JENRE® is a registered trademark of the Department of the Navy.

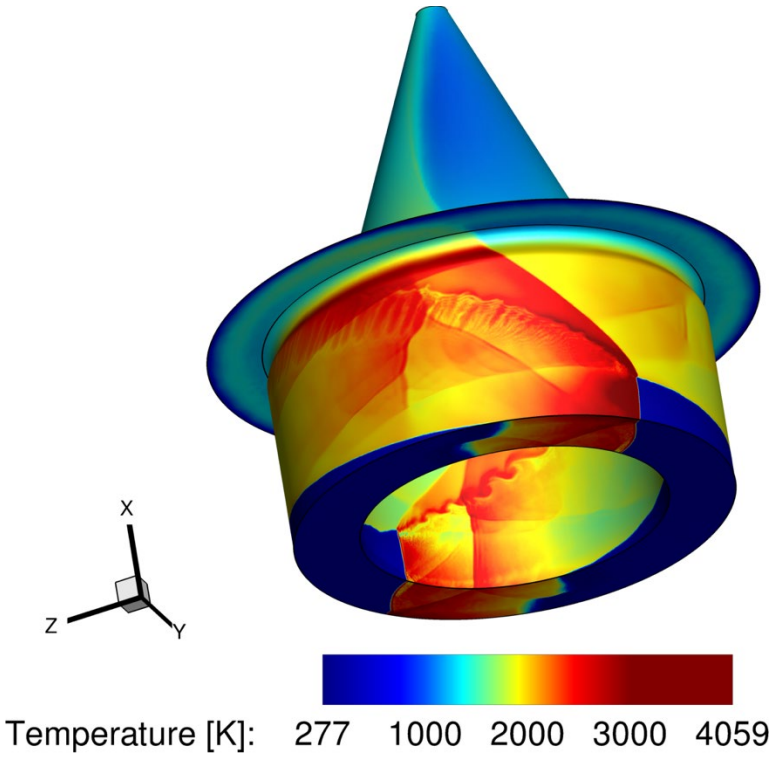

Figure 1. Temperature for an annular-RDE with a back-pressurization nozzle and an aerospike nozzle. Diameter of the combustor is from 0.1067 m (inner) to 0.1524 m (outer), inlet area ratio is 0.6, throat area ratio is 0.8, stoichiometric ethylene/air used for propellant.

Title: Predicting Fluid-Structure Interaction for Military Applications
Author(s): D.R. Mott and Y. Khine
Affiliation(s): Naval Research Laboratory, Washington, DC
CTA: CFD

Computer Resources: SGI ICE X, Cray XC40 [ARL, MD]; Cray XC40/50 [ERDC, MS]

Research Objectives: Create the computational capability to predict the interaction of fluids with complex structures that also can be flexible, including large, high-rate deformations due to blast loading. Flows may include advection and diffusion of multiple materials and may include convective and evaporative heat transfer and species transport at ambient atmospheric conditions. Use the new capability to study other problems with defense relevance, including helmet design and microfluidic transport applied to additive manufacturing.

Methodology: Among the various flows of interest listed above for this project, FY21's focus was the transport phenomena around a warfighter in different ambient wind conditions. A baseline model was considered including a bare head of the warfighter. Two configurations of helmet are investigated in no-wind and crosswind conditions. A developmental version of CFD++ software that could address the physics of the simulations was received from Metacomp Technologies and was installed on an ARL system with the support of HPC Helpdesk. The software was tested before production simulations were performed. The model simulated the sweating of the head due to a higher temperature and a higher relative humidity than the ambient. The results were analyzed in detail to understand the impact of various helmet configurations and the crosswind toward the warfighter.

Results: Figure 1 shows the velocity wake, the transport of water, and the temperature wake for a 5-mph wind into the face of the mannequin for the case with no helmet. Ambient relative humidity (RH) is 50%, and the head surfaces are assumed to be sweating sufficiently to fully saturate (100% RH) the air adjacent to the head. Figure 2 demonstrates the forced convection cases for the 5-pad and 7-pad configurations using snapshots taken at half-second intervals. As flow structures such as unsteady vortices form along the rear brim of the helmet and are shed into the wake and carried away, bursts of moisture-laden air from under the shell are pulled into the wake with them. Table 1 gathers the average rate of transport for each geometry configuration and flow condition and quantifies the advantage of forced convection over natural convection for delivering effective cooling, and also highlights that the 5-pad configuration, with less blockage of the space between head and helmet shell, delivers no advantage over the 7-pad case for natural convection, nor does it improve cooling for this particular forced-convection case.

DoD Impact/Significance: Thermal loading in the field not only undermines concentration and performance of cognitive tasks, it also can result in heat-related injury. A design approach that accurately emphasizes the relative importance of a variety of design factors and threats and can be weighted differently for different scenarios can produce optimal configuration options for targeted theaters and operations.

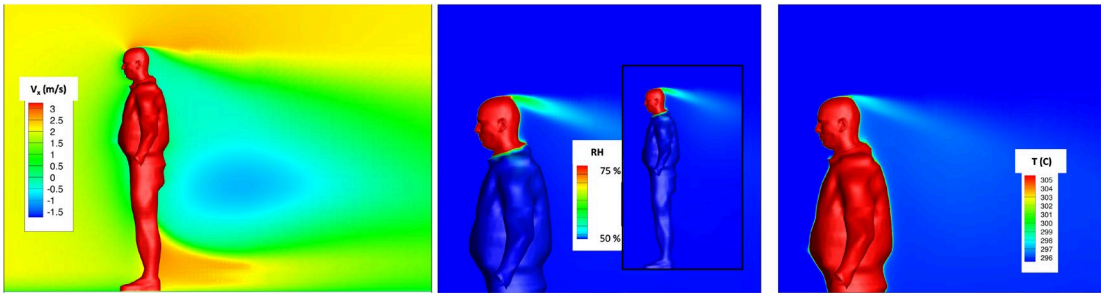

Figure 1. Velocity (left), water vapor (center), and temperature (right) downstream of the mannequin for a 5-mph wind for the case without helmet.

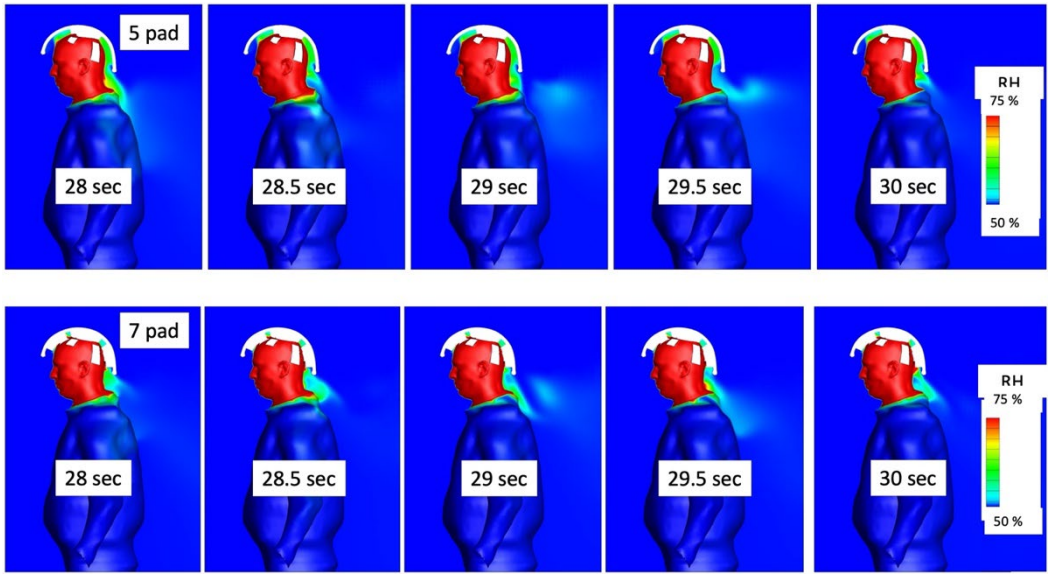

Figure 2. Transport of water vapor by forced convection for the two helmeted configurations. Top: 5 pad; bottom: 7 pad. Contour scale maximum at 75% relative humidity (RH) to highlight distributions; surface boundary condition on head is 100% RH.

Table 1. Collected Vapor Transport and Cooling Capacity Results

	Natural Convection		Forced Convection	
Pad Configuration	**H_2O Vapor Transport [kg/s]**	**Watts**	**H_2O Vapor Transport [kg/s]**	**Watts**
no helmet	**7.57E-06**	**18.37**	**2.13E-05**	**51.70**
5 pad	**4.88E-06**	**11.84**	**2.12E-05**	**51.45**
7 pad	**4.72E-06**	**11.46**	**1.93E-05**	**46.84**

Title: Dynamics of Multi-dimensional Detonations in Ethylene-Air Mixtures
Author(s): V.N. Gamezo[1] and A.Y. Poludnenko[2]
Affiliation(s): [1] Naval Research Laboratory, Washington, DC; [2] University of Connecticut, Storrs, CT
CTA: CFD

Computer Resources: SGI ICE X [ARL, MD]; Cray XC40/50 [ERDC, MS]; Cray Shasta [NAVY, MS]

Research Objectives: Multidimensional gas-phase detonations play a central role in a wide variety of practical combustion systems, including novel propulsion designs such as rotating detonation engines (RDEs). In recent years, there has been an increasing interest in using ethylene as a fuel in detonation engines, in particular in air-breathing RDEs, due to its higher reactivity and better detonability compared to other hydrocarbons. Ethylene is also formed as a main species during pyrolysis of real liquid fuels (such as Jet A and JP8). For these reasons, a systematic study of the dynamics of multidimensional detonations in ethylene-air mixtures is beneficial to a fundamental understanding of fuel-dependent detonation chemistry and detonation dynamics as well as to practical RDE design.

Methodology: We carry out both 2D and 3D simulations of ethylene-air detonation in channels using realistic no-slip, isothermal wall boundary conditions, and complex, finite-rate, multistep chemical kinetics that include 30 species and 231 reactions. The unsteady, reactive, compressible Navier-Stokes equations are solved on a uniform grid using the fully compressible reactive flow solver Athena-RFX. The solver uses a directionally unsplit corner transport upwind (CTU) integrator with the piecewise-linear method (PLM) for spatial reconstruction. The interface fluxes are computed using the HLLC-ADC Riemann solver, which avoids the carbuncle phenomenon in the presence of strong shocks. The stiff system of ODEs that represent the chemical kinetics is solved using YASS ODE integrator. The chemical reactions are coupled to the flow equations using Strang splitting providing the overall second-order accuracy in both space and time. Numerical soot foils based on maximum pressure histories are used to compare the cellular detonation structures. The computational cell size is set to 12 μm, which gives 20 cells per induction length and 3 cells per exothermic pulse width. This results in 2.8 billion computational cells for the 3D case and 3.5 million cells for the 2D case. Resolution was limited to reduce the high computational cost of the 3D calculation, which still required ≈15 million CPU hours on a Cray XC40/50.

Results: The simulations show that 2D detonations are significantly less stable, with the front being much more irregular than for 3D detonations. Most notably, the detonations in 2D undergo periodic failure/re-ignition events, which cause a periodic formation of transverse detonation waves propagating in extended regions of the compressed unburnt mixture. This leads to a hierarchy of detonation cell sizes with pronounced cell irregularity. In 3D channels, detonations do not exhibit such behavior, and the failure/re-ignition events do not occur. The soot foils resulting from 3D simulations show more uniform, though still irregular cell patterns that qualitatively look very similar to experimental soot foils produced by detonations in hydrocarbon-air mixtures. The detonations in 3D channels also produce more extreme pressures and temperatures than in 2D channels. In particular, in 3D, static pressures reach values over 3,000 atm, while the temperature in the triple point collisions exceed 5,000 K. This is in contrast with maximum pressures of ~800 atm and temperatures of ~3,800 K in 2D under comparable conditions. These differences indicate that the structure and dynamics of 2D detonations do not approximate the structure and dynamics of 3D detonations well, either qualitatively or quantitatively. The physical mechanisms that make 3D detonations more stable than 2D are still unclear and require further studies.

DoD Impact/Significance: Understanding the dynamics of unstable gas-phase detonations and how they are affected by the kinetics of energy release provides insights for further development of chemical models suitable for detonation simulations. In particular, the comparison of numerical and experimental cellular structures produced by unstable detonations provides an important way to validate chemical models. This improves our abilities to predict the behavior of detonations for the next-generation propulsion and energy-conversion systems such as RDEs.

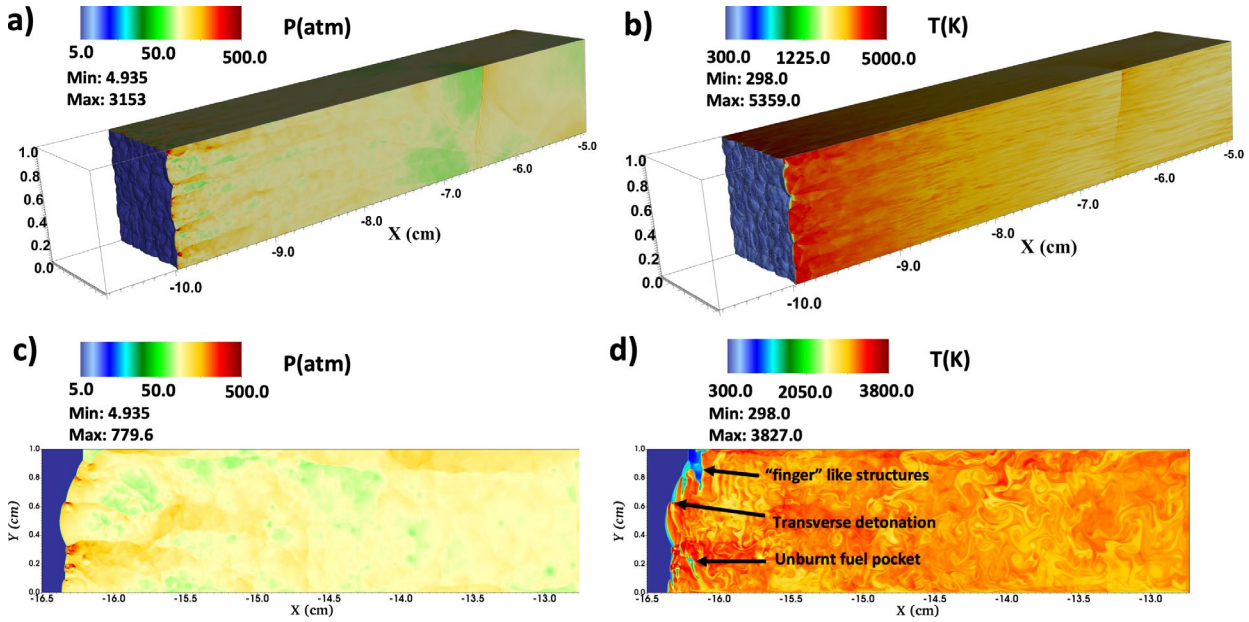

Figure 1. Pressure (a, c) and temperature (b, d) fields resulting from 3D (a, b) and 2D (c, d) simulations of detonations in a stoichiometric ethylene-air mixture at 298 K and 5 bar.

Title: Direct Numerical Simulation of Fluid-Sediment Wave Bottom Boundary Layer
Author(s): A.M. Penko,[1] W.S. Kearney,[2] C. Walker,[1] J.A. Simeonov,[1] S.P. Bateman,[1] J. Calantoni,[1] J. Veeramony,[1] and I. Adams[3]
Affiliation(s): [1]Naval Research Laboratory, Stennis Space Center, MS, [2]ASEE Postdoctoral Fellow, Naval Research Laboratory, Washington, DC, [3]National Research Council Postdoctoral Research Associate, Naval Research Laboratory, Stennis Space Center, MS
CTA: CFD

Computer Resources: Cray XC40 [ARL, MD]; Cray XC40/50 [ERDC, MS]; HPE SGI 8600, Cray Shasta [NAVY, MS]

Research Objectives: Predictive models for nearshore bathymetric evolution require a complete understanding of the physics of fluid-sediment interactions in the wave-bottom boundary layer (WBBL). Since such processes are difficult, if not impossible, to measure in situ, we performed coupled fluid-sediment numerical simulations to increase our understanding of the sediment and hydrodynamics in the WBBL. Fundamental concepts used in describing the phenomena of sediment transport such as particle size and shape, mixture viscosity and diffusivity, hindered settling, bed failure criterion, bedform evolution, and the concept of acceleration-induced transport are addressed with our models. The models produce high-resolution results necessary to gain insight into the small-scale boundary-layer processes and clarify new directions for measurement techniques needed to improve predictive capabilities.

Methodology: Utilization and development of a suite of discrete and continuum WBBL multiphase models for simulating sediment transport in the near-shore environment from the microscale (cm to m) to the mesoscale (km) is ongoing. At the microscale (<10 cm), the three-dimensional sediment phase is simulated with discrete element method (DEM) that allows individual grains and their interactions to be uniquely specified. The multiphase models vary in complexity from a simple one-dimensional eddy viscosity with one-way fluid-particle coupling to fully coupled fluid-particle models in three-dimensional direct numerical simulation (DNS). Between the micro- and mesoscale (1-50 m), a spectral seafloor model simulates the equilibrium seafloor roughness for given wave conditions and probabilistic models were developed in FY21 to forecast ripple evolution. Additionally, we developed a new multiphase model for DEM simulations of irregularly shaped particles where the flow is not explicitly resolved at the scale of individual particles and hydrodynamic forces are parameterized as a function of the Reynolds number Re, the object orientation, and its Corey shape factor.

Results: CFD simulations of Reynolds-averaged Navier-Stokes (RANS) flow over shell objects (e.g., Fig. 1) were used to evaluate the hydrodynamic forces of lift and drag acting on irregular particles. The RANS simulations were carried out with OpenFoam and use the shear stress transport k-omega model to simulate bulk properties of turbulence such as the turbulent kinetic energy (TKE). TKE gradients in turbulent boundary layers were resolved by constructing meshes with O ($y+ = 1$) grid size near boundaries. Force estimates were obtained for seven different shape factors and seven different flows with $104 < Re < 106$, and for each shell object, 103 different meshes were created by rotating the object in 45-degree steps of pitch, roll, and yaw with respect to the main flow direction.

DoD Impact/Significance: Ultimately, all process-based models for near-shore bathymetric evolution are limited by shortcomings in fundamental knowledge of multiphase boundary-layer physics. The microscale simulations provide an unprecedented level of detail for the study of fluid-sediment interactions that is impossible to obtain with available measuring technologies in the field or laboratory. These results are utilized to improve parameterizations of small-scale processes in larger-scale models. At the mesoscale, our models are highly efficient and well suited for coupling to regional operational hydrodynamic models. The computational resources consumed were in direct support of NRL base programs “Observations and modeling of biological cohesion on seafloor evolution time scales" and "Modeling sediment sorting in sand-shell environments.”

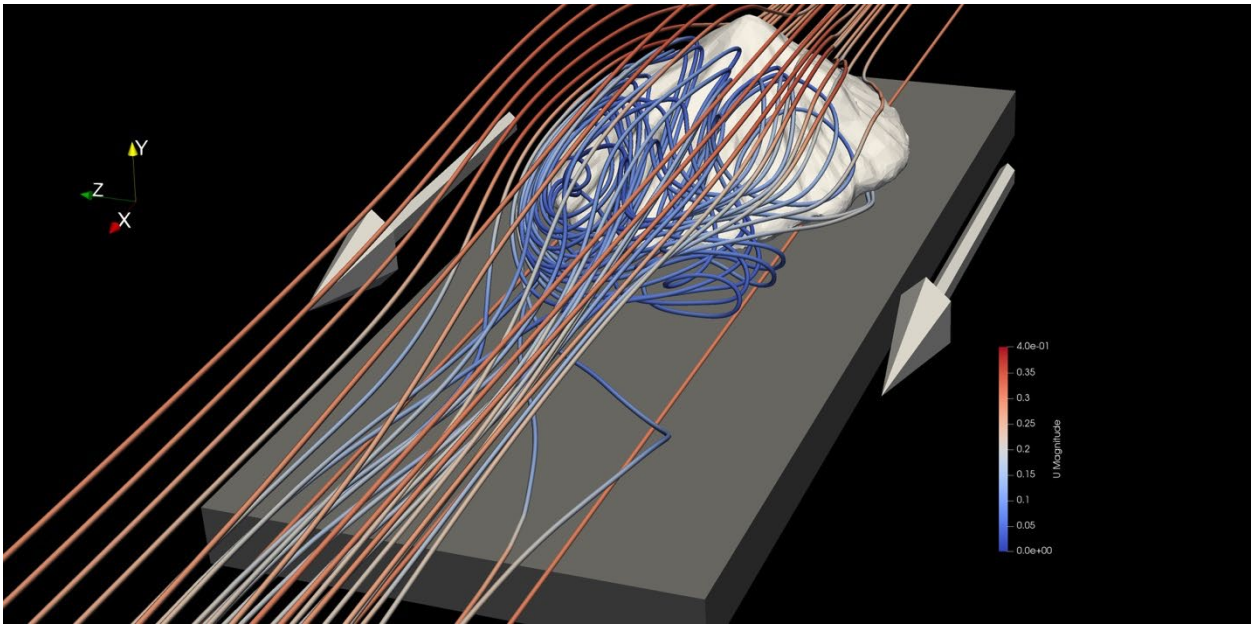

Figure 1. Streamlines (colored by velocity magnitude in m/s) in a fully developed Reynolds-averaged flow over an 8-cm-long Limpet shell (white surface). A steady logarithmic boundary layer flow is imposed at the inlet with velocity of 0.30 m/s at the level of the shell center, corresponding to a Reynolds number of 24,103; the flow direction is indicated by the white arrows. The shell was resting 2 mm above the bottom wall and 15 cm from the inlet of a computational domain with a height of 40 cm, a length of 72 cm, and a width of 56 cm; only a small portion of the domain is shown. In this example, the shell anterior side was facing the inlet and two quasi-steady recirculation cells (blue streamlines) are evident in the wake of the shell.

Title: High-Fidelity CFD Simulations of High-Speed Flows in Realistic Atmospheric Conditions
Author(s): D.A. Kessler, R.F. Johnson, A.M. Hess, B.T. Bojko
Affiliation(s): Naval Research Laboratory, Washington, DC
CTA: CFD

Computer Resources: HPE SGI 8600 [AFRL, OH], [NAVY, MS]; SGI ICE X, Power 9 [ARL, MD]; Cray XC40/50 [ERDC, MS]; Cray Shasta [NAVY, MS]

Research Objectives: (1) Develop an improved physical understanding of how the aerodynamic performance of hypersonic vehicles changes when encountering multiphase flow environments. (2) Characterize the high-speed reacting-flow environment and flame-holding potential within a solid-fuel ramjet propulsion device.

Methodology: We are using NRL's JENRE®[1] multiphysics framework to perform high-fidelity and high-resolution simulations of the chemically reacting, two-phase flows associated with high-Mach-number hypersonic flight and thrust generation within an air-breathing engine.

Results: Air-breathing propulsion systems represent one possible path toward achieving efficient and sustained hypersonic flight. The primary advantage over conventional rocket-based techniques is the weight savings gained by harvesting oxygen from the natural flight environment instead of carrying it aboard. Solid-fuel systems are particularly attractive due to their high energy density and simplified combustor design requirements. The basic physics associated with a solid-fuel ramjet combustor can be described using the generic backward-facing step combustor geometry shown in the top panel of Fig. 1. In this configuration, compressed air flows into the system from the left and is rapidly expanded into a wider combustion chamber bounded on the top and the bottom by slabs of solid fuel. Just downstream of the backward-facing step at the transition between the inlet and the combustion chamber, a recirculation zone forms that serves to anchor the flame. The flow then reattaches to the fuel surface just downstream and a boundary layer forms. Upon ignition, hot product gases in the recirculation zone cause the solid fuel to thermally decompose (or pyrolyze), and, if conditions are favorable, to burn in a stable, turbulent, diffusion-flame configuration. In practice, the operation of this type of combustor is more complex; flow instabilities give rise to periodic vortex shedding from the backward-facing step that drive unsteadiness in the downstream diffusion flame. Likewise, the heat flux to the solid-fuel grain varies along the gas-solid interface, which leads to nonuniform gaseous fuel production and surface regression rates, further amplifying the unsteadiness in the combustor. Exploratory two- and three-dimensional simulations of a model solid-fuel slab burner facility were performed using the JENRE® multiphysics framework. Figures 1a–d show a sequence of temperature contours taken at discrete time intervals over the course of several vortex-shedding events. For rapid identification, several of these vortices are labeled A, B, and C in the figure. These vortices disturb the recirculation zone and boundary layers and ultimately break down into smaller-scale structures as they move downstream. The unsteadiness causes the formation of a complex flame structure that extends into the center of the combustion cavity. The results of these simulations are used to evaluate the impact of flame unsteadiness on the flame-holding potential of a combustor geometry over a range of flow conditions.

DoD Impact/Significance: Achieving a global prompt-strike capability and countermeasures for similar technologies under development by our adversaries are critical for protecting our fleet and maintaining naval superiority. This work will provide an improved understanding of parameters critical to solid-fuel ramjet engine performance under a variety of operating conditions.

[1] JENRE® is a registered trademark of the Department of the Navy.

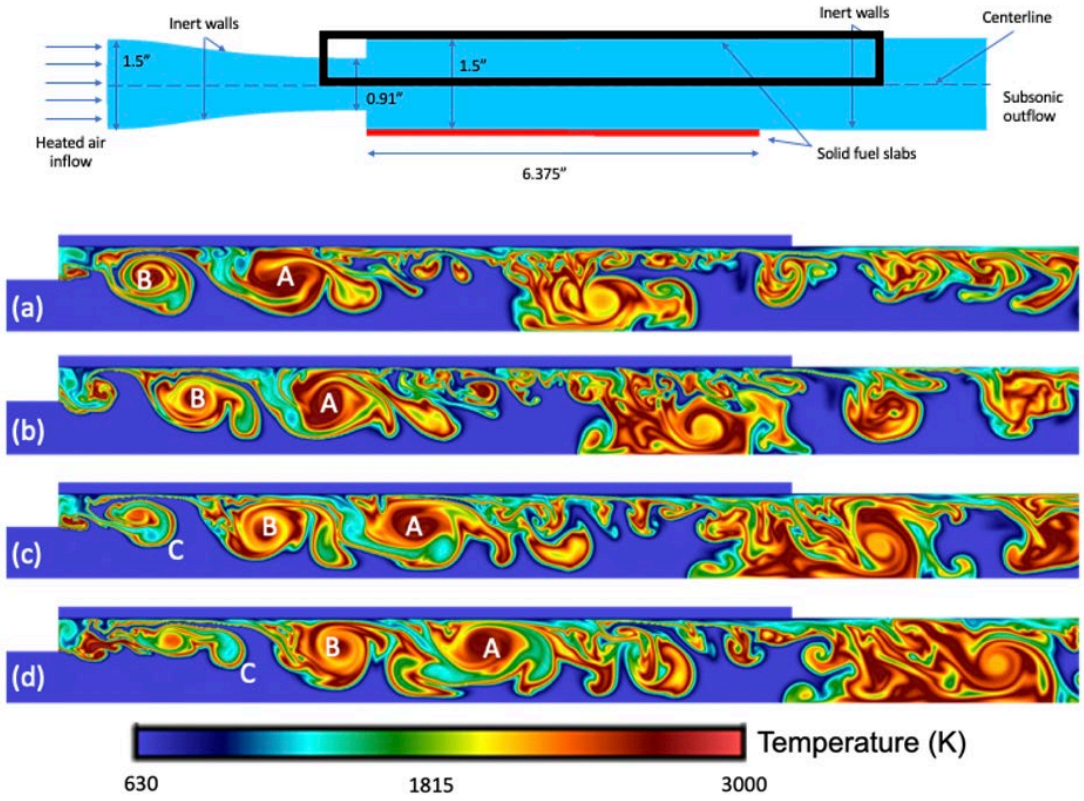

Figure 1. Diagram of a two-dimensional model solid-fuel slab burner facility (top), and (a)–(d) time sequence of the evolution of the temperature field in the channel over the course of several vortex-shedding events. Time increases from top to bottom in the figure at a constant interval of 0.4335 ms. Black frame on the diagram indicates spatial extent of temperature fields shown in (a)–(d).

Title: Aircraft Engine Noise Reduction Technology
Author(s): J. Liu and Y. Khine
Affiliation(s): Naval Research Laboratory, Washington, DC
CTA: CFD

Computer Resources: Cray Shasta [NAVY, MS]

Research Objectives: Use HPC computational resources to predict details of turbulent flow structures and noise generation in supersonic exhaust jets from representative military aircraft jet engine nozzles and use this information to investigate and assess promising jet noise-reduction concepts in support of the ongoing jet noise-reduction programs.

Methodology: The flow solver is JENRE®[1], a Navy-based and NRL-developed nodal finite-element code. JENRE® can take structured meshes and unstructured meshes with arbitrary cell types and has multiple levels of parallelism: multicore CPUs or multicore GPUs, and MPI for inter-processor communication. JENRE® has achieved an exceptional computational performance and scalability. Since using large-eddy simulations (LES) to fully resolve wall-bounded flows at high Reynolds numbers is computationally prohibitive due to the limitations of the available numerical methods and computational resources, the wall-layer-model approach is used to simulate the boundary-layer effect of the wall-bounded flows. The far-field noise prediction is based on the Ffowcs Williams & Hawkings (FW-H) surface integral method. To simulate the high-temperature effect observed in realistic jet engine exhausts, a temperature dependent function of the specific heat ratio is developed and implemented in JENRE®.

Results: LES has become an important tool in developing and optimizing the jet noise-reduction technologies. LES has been used to develop and optimize the noise-reduction technology of micro-vortex generators (MVGs) implemented on a model-scale F404 nozzle, which is a faceted biconic convergent and divergent nozzle made of 12 seals and flaps. An extensive parametric study of MVGs has been conducted to explore the potential of this technology. The information provided by the large-eddy simulations is very helpful to understand the impact of MVGs on the shock-cell structure, the jet plume turbulence and the noise generation. This greatly speeds the process of obtaining the optimal MVGs that provide promising noise-reduction performance. Chevron technology is one of the most investigated and tested noise-reduction technologies to reduce the aircraft engine noise. It has reached a TRL of 6. Therefore, the thrust-based noise-reduction performance of MVGs has been compared with the state-of-the-art performance of chevrons. Two MVGs and two chevron nozzles are shown in Figure 1. These four nozzles have a comparable thrust performance at the cruise condition. Figure 2 shows the comparison of the noise-reduction performance at a takeoff condition. It can be seen that MVG nozzles reduce much more noise in both the upstream and downstream directions. MVGs can reduce more noise by up to 50%, comparing to the state-of-the-art noise reduction by chevrons. In addition, the thrust performance of MVGs is relatively stable, but that of chevrons increases with the nozzle pressure ratio. That means the thrust penalty induced by chevrons is higher at the cruise conditions than at the takeoff conditions.

DoD Impact/Significance: There is a growing need to significantly reduce the noise generated by high-performance, supersonic military aircraft. The noise generated during takeoffs and landings on aircraft carriers has a direct impact on shipboard health and safety issues. It is estimated that the US Veterans Administration pays $4.2 billion or more for hearing-disability claims each year. The results of our work will provide better understanding of the noise production for both industrial and military aircraft, and will aid the current effort of noise reduction, especially for supersonic aircraft.

[1] JENRE® is a registered trademark of the Department of the Navy.

(a) (b) (c) (d)

Figure 1. Two MVGs and two chevron implementations in a model-scale F404 nozzle. Patent pending. (a) MVG-P nozzle where 12 pairs of MVGs are implemented (b) MVG-N-Alt nozzle where azimuthally alternating arranged MVGs are implemented. (c) Nozzle with 12 chevrons (P06L20W100) attached to the nozzle lip. (d) Nozzle with azimuthally alternating arranged chevrons (P10L20W100_Alt) attached to the nozzle lip. Chevron parameter's definition of P10L20W100_Alt: Penetration: 10%D, Length: 20%D, Width: 100% of the nozzle seal width. Alt: alternating arrangement. D: equivalent nozzle-exit diameter.

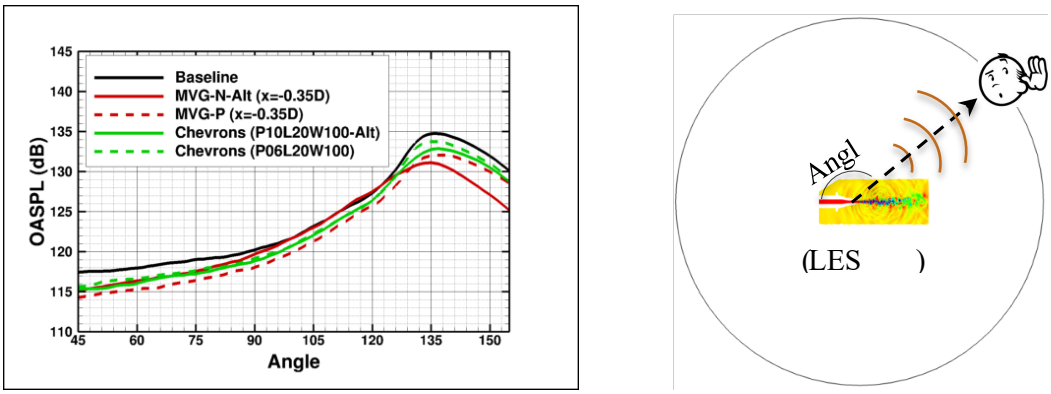

Figure 2. Far-field noise intensity distributions. The distance is roughly 90 ft away from the aircraft. Black lines are baseline noise intensity. The image at right is the description of the noise radiation direction.

Title: Multidimensional Chemically Reacting Fluid Dynamics with Application to Flameless Combustors
Author(s): R.F. Johnson
Affiliation(s): Naval Research Laboratory, Washington, DC
CTA: CFD

Computer Resources: HPE SGI 8600 [AFRL, OH]

Research Objectives: Use the HPC computational resources to simulate the computationally expensive chemically reacting fluid dynamics in various multidimensional configurations with the goal of better understanding various complex, multiscale, combustion phenomenon.

Methodology: The codes currently in use at The Laboratories for Computational Physics and Fluid Dynamics can accurately predict the flow field in many configurations. These codes employ high-order methods, which are capable of simulating unsteady flows with strong shocks, chemical reactions, and other complex features. This work focuses on developments that are currently underway that will allow for the simulation of high-speed and low-speed reacting flows using state-of-the-art numerical methods. This year, we produced several important results that demonstrate the superiority of our methods for simulating chemically reacting flows.

Results: This year, we employed the previously produced methodology that is able to resolve the mixing of multicomponent chemically reacting flows without the need for legacy stabilization methods. In the past, simulating just the pure mixing of two species, such as hydrogen and oxygen, would result in failure without the use of expensive stabilization methods. The Laboratories for Computational Physics and Fluid Dynamics have developed a novel method for simulating multicomponent flows that utilizes the properties of the discontinuous Galerkin method (DG) and correct thermodynamics to simulate propulsion problems. With our method, we are able to run this problem with detailed thermodynamics, transport, and chemical kinetics without any issues of stability. This year, we aimed not only to increase stability, but also to produce results for larger-scale hydrocarbons.

An appealing property of the DG method is resolving structures with high-order accuracy without the need for mesh refinement. Instead, the DG method's cell accuracies can be increased arbitrarily to resolve flows within the computational cells. A critical issue that was encountered was that shock capturing still required some stabilization at areas near the discontinuity in order to utilize the power of DG. Without these methods, the shock capturing would be too diffuse and the resulting flow structures would not improve when increasing the order of accuracy for a given mesh. This year, we developed new entropy-preserving limiters that prevent oscillations at high order that were causing the need for extra artificial viscosity. This, therefore, improved upon our methods to simulate chemically reacting flows as it unlocked the full potential of DG. Figure 1 shows detonation structures for one mesh but at two different accuracies. These cases were run on HPCMP systems and demonstrate that resolving structures improved via increasing the order (DG(p=1) to DG(p=2)) on the same mesh.

DoD Impact/Significance: The research in producing better numerical techniques for simulating propulsion devices will yield better understanding and predictive capability for Navy/DoD aircraft.

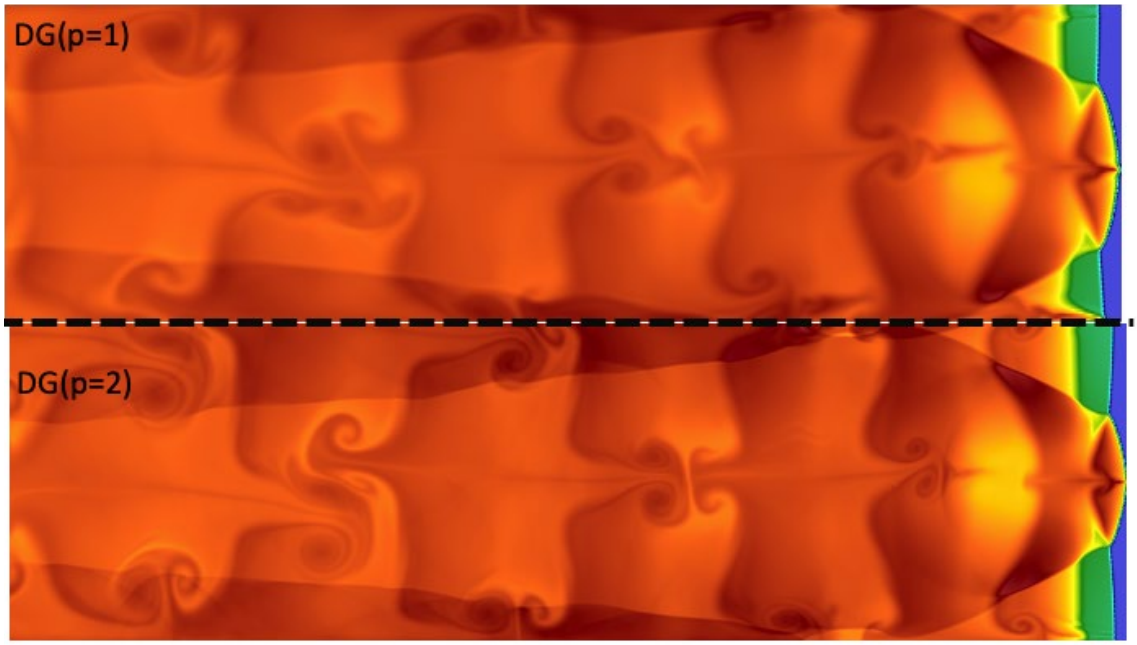

Figure 1. Canonical detonation case run on the same mesh but with different levels of accuracy; The top is low order (DG(p=1)) and the bottom is high order (DG(p=2)). The higher-order simulations are better at resolving structures.

Title: Numerical Investigation of Advanced Military Aircraft Noise Reduction Concepts
Author(s): J. Liu and Y. Khine
Affiliation(s): Naval Research Laboratory, Washington, DC
CTA: CFD

Computer Resources: HPE SGI 8600 [AFRL, OH]; SGI ICE X, Cray XC40 [ARL, MD]; Cray XC40/50 [ERDC, MS], Cray Shasta [NAVY, MS]

Research Objectives: To predict details of turbulent flow structures and noise generation in supersonic exhaust jets from representative military aircraft jet engine nozzles and to use this information to investigate and assess promising jet noise-reduction concepts in support of ongoing jet noise-reduction programs.

Methodology: The flow solver is JENRE®[1], a Navy-based and NRL-developed nodal finite-element code. JENRE® can take structured meshes and unstructured meshes with arbitrary cell types and has multiple levels of parallelism: multicore CPUs or multicore GPUs, and MPI for inter-processor communication. JENRE® has achieved exceptional computational performance and scalability. Since using large-eddy simulations (LES) to fully resolve wall-bounded flows at high Reynolds numbers is computationally prohibitive due to the limitations of the available numerical methods and computational resources, the wall-layer-model approach is used to simulate the boundary-layer effect of the wall-bounded flows. The far-field noise prediction is based on the Ffowcs Williams & Hawkings (FW-H) surface integral method. To simulate the high-temperature effect observed in realistic jet engine exhausts, a temperature dependent function of the specific heat ratio is developed and implemented in JENRE®.

Results: LES has become an important tool in developing and optimizing jet noise-reduction technologies. LES has been used to develop and optimize the noise-reduction technology of microvortex generators (MVGs) implemented on a model-scale F404 nozzle, which is a faceted biconic convergent and divergent nozzle made of 12 seals and flaps. An extensive parametric study of MVGs has been conducted to explore the potential of this technology. The information provided by LES is very helpful to understand the impact of MVGs on the shock-cell structure, the jet plume turbulence and the noise generation. This greatly speeds the process of obtaining the optimal MVGs that provide promising noise-reduction performance. Since MVGs are implemented inside the nozzle, the axial location of the implementation is a critical parameter in this optimization process. Two MVG nozzles with MVGs implemented at two axial locations are shown in Fig. 1. The MVG impact of these MVG nozzles on the shock-cell structure is shown in Fig. 2, where two takeoff nozzle-pressure ratios are presented. The noise-reduction performance is presented in Fig. 3. It can be seen that the axial location of MVGs greatly affects the shock-cell structure and the noise-reduction performance. It is found that the most optimized axial location is found around 0.65D upstream of the nozzle exit at the nozzle pressure ratio of 2.7, but a further upstream location of 0.35D is better for the higher nozzle-pressure ratio. (D is the equivalent nozzle exit diameter). The latter location provides more consistent noise-reduction performance when all takeoff nozzle-pressure ratios are considered. The peak noise reduction of ~4dB–5dB in the peak radiation direction (135°) is observed.

DoD Impact/Significance: There is a growing need to significantly reduce the noise generated by high-performance, supersonic, military aircraft. The noise generated during takeoffs and landings on aircraft carriers has a direct impact on shipboard health and safety issues. It is estimated that the US Veterans Administration pays $4.2B or more for hearing-disability claims each year. The results of our work will provide better understanding of the noise production for both industrial and military aircraft, and will aid the current effort of noise reduction, especially for supersonic aircraft.

[1] JENRE® is a registered trademark of the Department of the Navy.

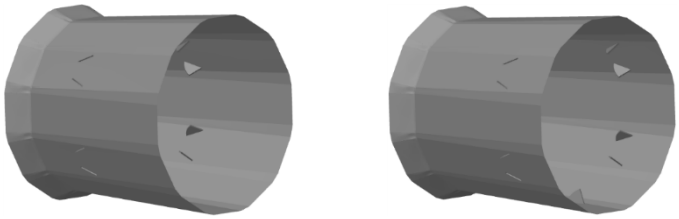

(a) (b)

Figure 1. Two MVG implementations in a model-scale F404 nozzle. *Patent pending*. (a) MVGs implemented at 0.65D upstream of the nozzle exit. (b) MVGs implemented at 0.35D upstream of the nozzle exit. D is the equivalent nozzle-exit diameter.

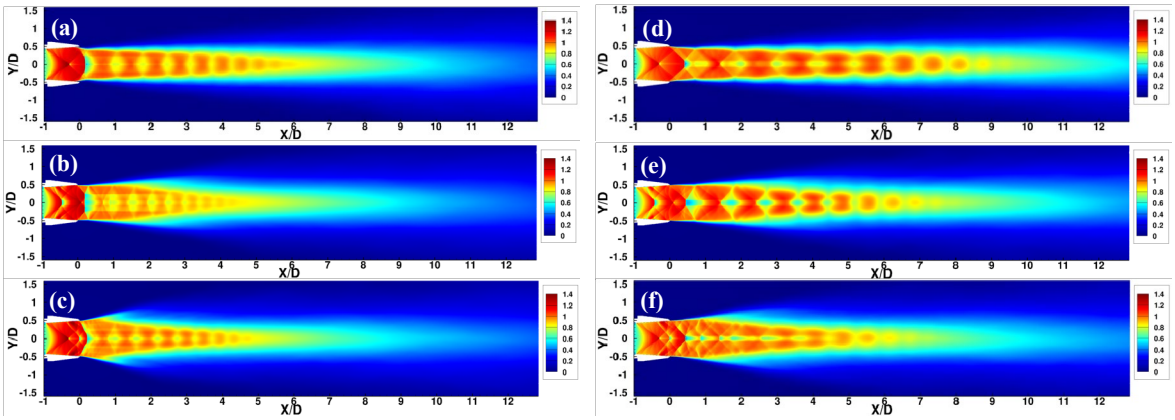

Figure 2. MVG impact on the shock-cell structure. (a–c) Nozzle pressure ratio is 2.7. (d–f) Nozzle pressure ratio is 3.5. Nozzle pressure ratio is the ratio between the nozzle total pressure and the ambient pressure. (a, d) Baseline nozzles. (b, e) MVG implementation shown in Fig. 1(a). (c–f). MVG implementation shown in Fig. 1(b).

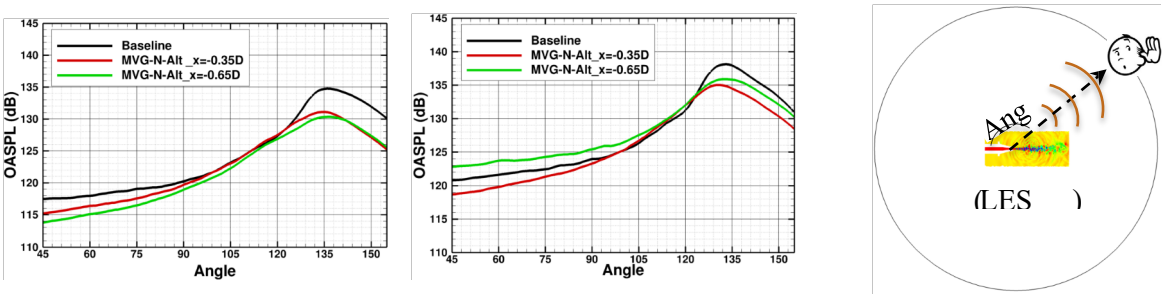

Figure 3. Far-field noise-intensity distributions. The distance is roughly 90 ft away from the aircraft. Black lines are baseline noise intensities. Green lines: nozzle implemented with MVGs shown in Fig. 1(a). Red lines: nozzle implemented with MVGs shown in Fig. 1(b). (a) Nozzle pressure ratio is 2.7. (b) Nozzle pressure ratio is 3.5. (c) Description of the noise radiation direction.

Title: Advanced Computational Models that Exploit Emerging Computer Architectures
Author(s): K. Obenschain and A. Moses
Affiliation(s): Naval Research Laboratory, Washington, DC
CTA: CFD

Computer Resources: HPE SGI 8600 [AFRL, OH]; Cray XC40/50 [ERDC, MS]; Cray XC40 [ARL, MD]

Research Objectives: This project aims to expand the use of many-core devices in high-performance computing environments while creating specific needed research capabilities that these devices enable. Specifically, 1) Develop methodologies to enable existing codes to exploit the performance of rapidly evolving many-core devices (MCD) to solve current roadblock problems. 2) Develop approaches to exploit the improved high-bandwidth communication architectures that are becoming available currently. This project is also used to evaluate and advise how emerging architectures impact HPCMP and the wider HPC community.

Methodology: HPCMP's resources are utilized to define a baseline for performance comparisons with exploratory architectures. The 6.1 project this effort supports in turn looks at different approaches such as algorithm improvements and tactics to allow legacy codes to exploit the additional computing power on leading-edge hardware. Simulations of high-speed flows were run on HPCMP machines to evaluate and define software and hardware requirements for future detailed simulations.

Results: Figure 1 depicts an example of an evaluation performed with a result from the code FDL3DI. CFD simulations and underlying implementations of algorithms were run on Mustang to generate a performance baseline for evaluating emerging architectures. This year, architectures from AMD Rome, AMD GPUs, and NEC Vector engines were evaluated with a focus on scaling. With some refactoring, the emerging architectures proved to have significant performance advantages for their respective problems.

DoD Impact/Significance: The proposed work and applications proposed above are relevant to: expeditionary and irregular warfare (counter-IED, sensors, lethality, and survivability), computational environment architecture (open architecture) platform design and survivability (advances platform design, survivability, unmanned vehicles, high-speed platforms), power and energy (energy security, power systems), computational materials science, and fluid dynamics.

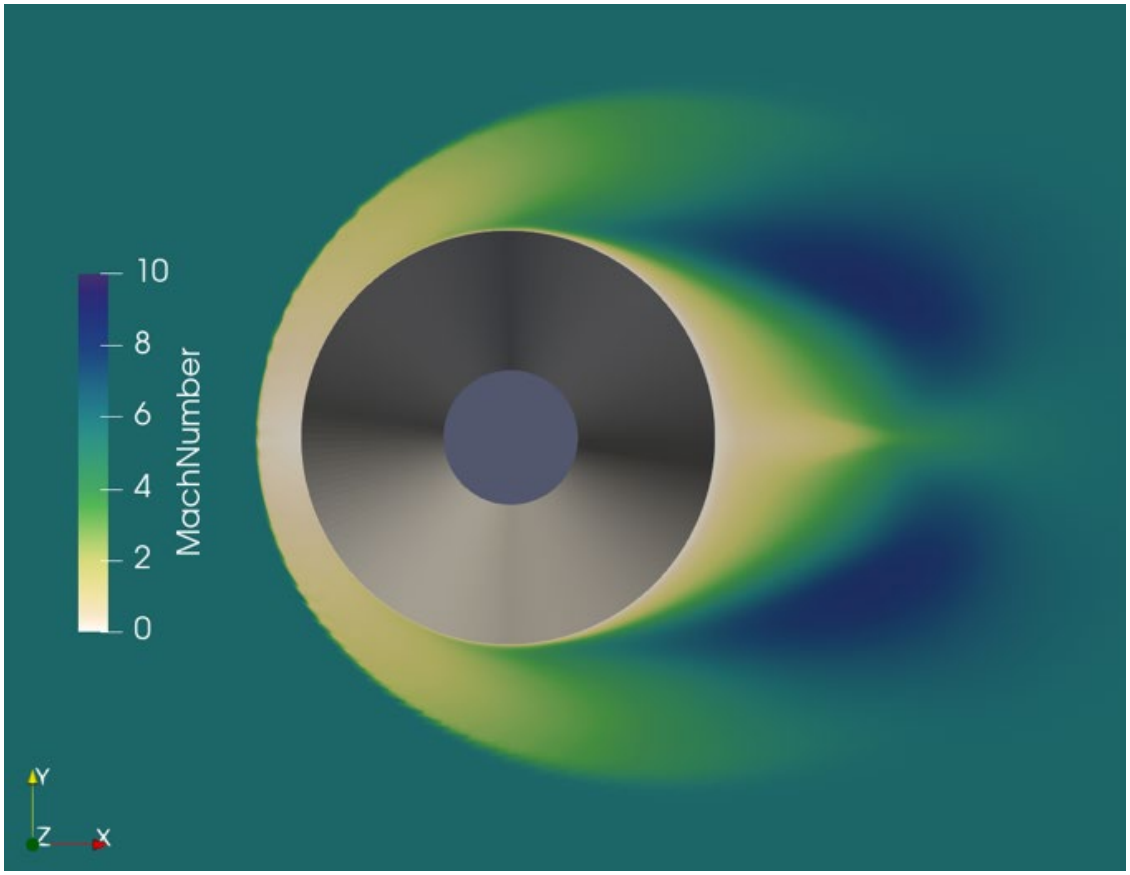

Figure 1. Simulation from FDL3DI

Title: Simulations of the Ionosphere/Plasmasphere/Thermosphere System
Author(s): J. Krall[1] and J.D. Huba[2]
Affiliation(s): [1]Naval Research Laboratory, Washington DC; [2]Syntek Technologies, Fairfax VA
CTA: CFD

Computer Resources: HPE SGI 8600 [AFRL, OH]; Cray XC40/50 [ERDC, MS]; Cray Shasta [NAVY, MS]

Research Objectives: Predict the dynamics of the ionosphere/magnetosphere environment as it relates to operational communications and navigation systems used by the warfighter. Develop a first-principles physics-based model of near-Earth space based on the NRL code SAMI3 to obtain an understanding of equatorial spread F disturbances and plasmasphere dynamics.

Methodology: The research uses the NRL SAMI3 code, a comprehensive 3D simulation model of Earth's ionosphere/plasmasphere system, coupled to a thermosphere model (e.g., TIE-GCM, GITM, WACCM-X) and an inner magnetosphere model (e.g., RCM, CIMI) to self-consistently describe geospace. SAMI3 can include metal ions, Fe+ and Mg+, that form low-altitude ionosphere layers. These simulations use solar wind and irradiance data to drive the system.

Results: Last year, we reported a breakthrough in modeling plasma bubbles in the equatorial ionosphere. With the first-principles whole atmosphere model WACCM-X coupled to the SAMI3 global ionosphere model, self-consistently generated atmospheric gravity waves acted as seeds to trigger the equatorial spread *F* (ESF) instability. Because a high-resolution grid ($\lesssim$70 km) was used, ESF-related structures were resolved in the ionosphere and in the plasmasphere, the extension of the ionosphere into the inner magnetosphere. This is pictured in Fig. 1 (a, b), where we show isosurfaces of the electron density (10^3 cm^{-3} and 10^4 cm^{-3}) from a high-resolution SAMI3 simulation using the empirical models NRLMSISE00 and HWM14 (a) and WACCM-X (b) to specify the thermosphere. The isosurfaces using the empirical models are smooth, as anticipated. Isosurfaces using the WACCM-X model thermosphere are structured, showing corrugations and ducts (tube-like electron density features aligned with the geomagnetic field).

While these low-density ducts and irregularities have been observed in increasing detail over the years, this is the first self-consistent global simulation study showing this dynamic plasmasphere behavior. It is well-known that plasmasphere ducts and irregularities affect whistler wave propagation in the plasmasphere and radiation belts. Whistler waves strongly affect the population of satellite-damaging radiation belt particles. This plasma-wave interaction process also affects man-made radiation belts.

We continued the above research using the high-resolution HIAMCM atmosphere model in lieu of WACCM-X. Here the grid spacing was decreased to 0.5° or ($\lesssim$50 km). Results for June 6, 7, and 8, 2008, are shown in Fig. 1 (c-e). All three days had virtually the same geophysical conditions, but differed in the development of equatorial plasma bubbles, the blue striations in Fig. 1 (c-e) at longitude 150°–160°. This variation, attributed to the atmospheric waves captured in HIAMCM on these 3 days, sheds light on the day-to-day variability of the ionosphere. The above studies were supported by additional SAMI3 simulations of wind-driven ESF [Krall et al., 2021], SAMI3 simulations of ionosphere outflows [Krall & Huba, 2021b] and, along with the CIMI inner magnetosphere model, SAMI3 simulations of inner magnetosphere H+ and O+ ion outflows [Krall & Huba, 2021a].

DoD Impact/Significance: Potential protection of communication satellites and the power grid. Support of ongoing experiments in remote sensing of the space environment. Provide input to ionospheric and thermospheric models.

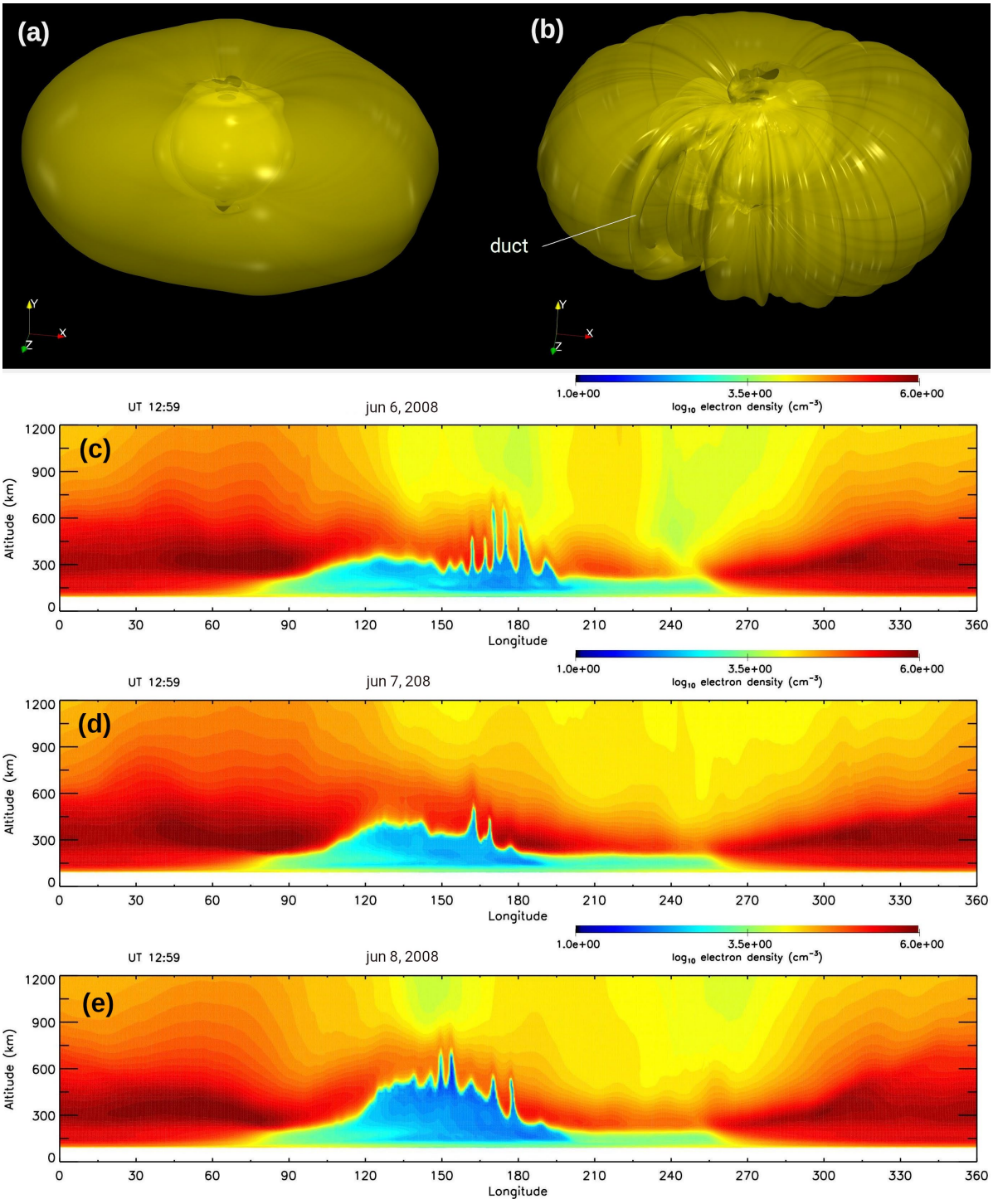

Figure 1. Related plasma structures are shown in the plasmasphere (a, b) and the ionosphere (c-e). Isosurfaces of electron density are pictured for SAMI3 coupled to (a) empirical atmosphere models NRLMSISE00 and HWM14 and (b) the first-principles model WACCM-X. The latter simulation shows high-altitude ducts. Contours of the electron density (log 10) as a function of longitude and altitude at time ~01:00 UT for three consecutive days (c-e) in June 2008 at ~ 01:00 UT show ESF "bubbles" from a SAMI3/HIAMCM simulation. The dynamics that produce bubbles in the ionosphere also produce ducts in the plasmasphere.

Title: Applications of FEFLO Incompressible Flow Solver
Author(s): R. Ramamurti
Affiliation(s): Naval Research Laboratory, Washington, DC
CTA: CFD

Computer Resources: SGI ICE X [ARL, MD]

Research Objective: Perform three-dimensional (3D) numerical simulations of flow past complex configurations. The proposed studies will investigate the use of bio-inspired fins for propulsion and to characterize the thrust generated by these propulsive flapping surfaces.

Methodology: A finite-element solver, called FEFLO, for 3D incompressible flows based on unstructured grids is used. The flow solver is combined with adaptive remeshing techniques for transient problems with moving grids and is also integrated with the rigid body motion in a self-consistent manner that allows the simulation of fully coupled fluid-rigid body interaction problems of arbitrary geometric complexity in three dimensions. NRL has developed a flapping-fin UUV for effective low-speed operations. Three-dimensional unsteady flow simulations past passively deforming flapping pectoral fins in tandem configuration are performed. Limited parametric studies are conducted varying the stiffness of the material, phasing between the front and rear fins, and the pitch amplitude of the fin.

Results: Our previous results with rigidly flapping bio-inspired trapezoidal fins in tandem showed that the rear fin produced higher thrust compared to the front fin. Depending on the spacing between the fins, there is an optimal phasing between the front and rear fins where the rear fin achieved a maximum thrust. With the recently developed coupled fluid-structure-interaction capability, we are able to simulate the effect of passively deforming fins on the thrust production. The flexible fin consists of a rigid leading-edge region made out of nylon and a flexible region made out of PDMS. Results from the simulation show that the flexible fin produces higher thrust compared to the rigid fin for some of the kinematics studied. The shape of the flexible fin was also compared to that obtained from planar laser-induced fluorescence imaging from the experiments. Expanding these parametric studies for different materials and kinematics will lead to the development of reduced models for the thrust production.

DoD Impact/Significance: Simulations have enabled characterization of the thrust generation mechanisms in flapping-foil propulsion and the interactions of the flow between these propulsors for use in unmanned underwater vehicles. This will provide the next steps toward development of a comprehensive analytical tool for bio-inspired fin and vehicle design.

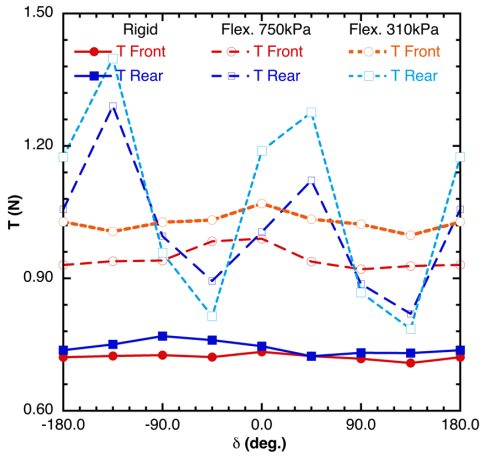

Figure 1. Effect of phasing and material stiffness on tandem flapping fins at 1 Hz

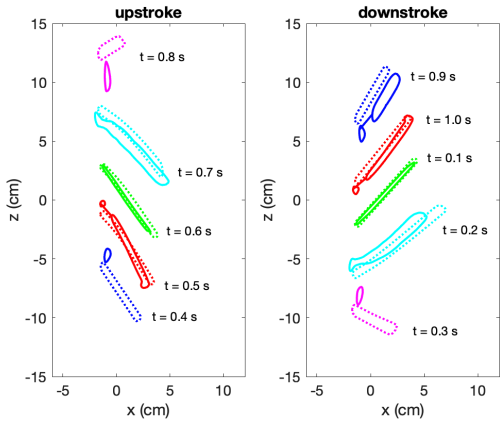

Figure 2. Comparison of the passively deforming fin shape flapping at 1 Hz, CFD (dotted) and experiments (solid)

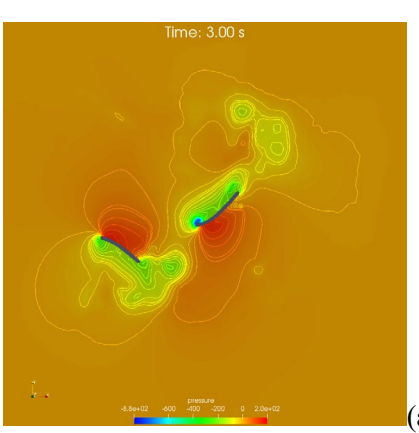

(a)

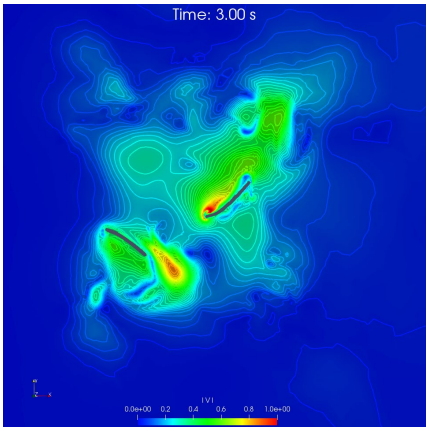

(b)

Figure 3. (a) Pressure and (b) velocity distribution on the plane cut for a passively deforming tandem fins

Title: High-Temperature and Rarefied Gas Dynamics in Hypersonic Flows
Author(s): E.W. Hyde, J.R. Maxwell, R.E. Rogers, C. Aguilera, and J. Sosa
Affiliation(s): Naval Research Laboratory, Washington, DC
CTA: CFD

Computer Resources: SGI ICE X [ARL, MD]; Cray Shasta [NAVY, MS]

Research Objectives: Two CFD codes, ANSYS Fluent and JENRE®[1], the latter developed at NRL, were used to perform high-fidelity simulations of the United States Naval Academy's supersonic wind tunnel. These simulations accompanied experimental data that used CO_2 Rayleigh scattering to visualize the boundary layer in the wind tunnel. The combined work was presented in a conference paper at the 2021 AIAA Propulsion and Energy Forum. Additionally, JENRE® was used to study boundary layer thickness and startup criteria for a series of continuous-operation, vacuum-driven wind tunnels.

Methodology: This research utilized the CFD codes ANSYS Fluent and JENRE®, which employ significant parallel computing to achieve high-fidelity results. Several 3D geometries were created for the variable-speed wind tunnel at different Mach number configurations ranging from 2 to 4. The present CFD effort focused on capturing the boundary layer thickness to evaluate the agreement between experimental visualization techniques and the simulated velocity and thermal boundary layers. Additional simulations were performed on a scaled-down, vacuum-driven wind tunnel and will be compared with data from ongoing experimental efforts that are currently underway.

Results: High-fidelity LES simulations, along with RANS simulations, were compared with the experimental dataset obtained in the Naval Academy's supersonic wind tunnel. The CO_2 Rayleigh scattering images show very good agreement with the simulation results depicting the thermal boundary layer. In the Naval Academy's wind tunnel, the thermal boundary layer is much thicker than the velocity boundary layer. It was therefore impossible to interrogate the velocity boundary layer in the facility using this technique as the CO_2 crystals vaporized near the wall. Future efforts aim to perform high-fidelity simulations of wind tunnels where this technique can be used to capture turbulent structures, turbulence intensity, and boundary layer thickness.

DoD Impact/Significance: This research has contributed to a better understanding of nonintrusive, high-speed-flow visualization methods that are applicable to supersonic combustion and chemically reacting hypersonic flow applications.

[1] JENRE® is a registered trademark of the Department of the Navy.

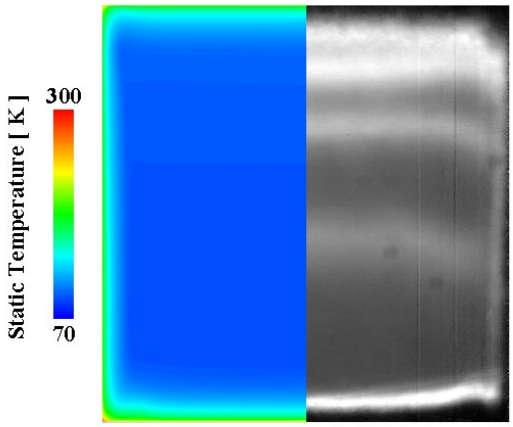

Figure 1. Comparison of simulated temperature contour and Rayleigh scattered image of the test section normal to the direction of flow

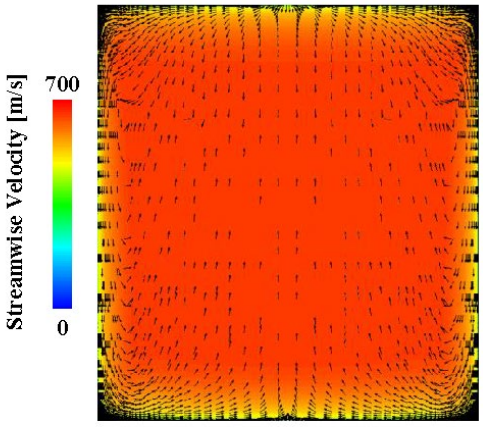

Figure 2. Streamwise velocity contour with vectors overlaid depicting the in plane velocity, highlighting greater vorticity in the corners

Figure 3. Mach contour of a small-scale, continuous-flow, vacuum-driven wind tunnel

Title: Simulations of Laser-plasma Interactions and the Radiation Hydrodynamics of High-velocity Laser-accelerated Matter
Author(s): J.W. Bates, A.J. Schmitt, and K. Obenschain
Affiliation(s): Naval Research Laboratory, Washington, DC
CTA: CFD

Computer Resources: HPE SGI 8600 [AFRL, OH], Cray XC40 [ARL, MD], Cray XC40/50 [ERDC, MS]

Research Objectives: The two principal obstacles to thermonuclear fusion with laser-driven implosions are hydrodynamic and laser-plasma instabilities. The objective of this research is to gain a better understanding of the physics underlying these phenomena and also to develop practical strategies for their mitigation using the numerical codes LPSE, FastRad3D, and ASTER.

Methodology: LPSE is a wave-based, massively parallel computer code designed to model laser-plasma instabilities, which can scatter laser light away from inertial-confinement-fusion (ICF) targets before its energy gets absorbed and also can generate suprathermal electrons, which can preheat the thermonuclear fuel and can spoil high fusion gains. The most significant varieties of laser-plasma instabilities for ICF today are two-plasmon decay (TPD), stimulated Raman scattering (SRS), stimulated Brillouin scattering (SBS), and cross-beam energy transfer (CBET), all of which can be modeled with the LPSE code. The level of physical detail in LPSE is intended to lie between more fundamental particle-in-cell codes and full-scale radiation-hydrodynamic codes such as FastRad3D and ASTER, which are used to simulate full ICF implosions. Like LPSE, FastRad3D and ASTER are massively parallel codes, and while they do not account for laser-plasma instabilities, they do model a variety of other complex physical processes important for laser fusion such as laser absorption, radiation transport, thermonuclear burn and hydrodynamic instabilities. We are using all three of these codes in an effort to improve our understanding of the physics of ICF implosions and to develop target designs that are less susceptible to the deleterious effects of both hydrodynamic and laser-plasma instabilities.

Results: Our principal results for FY2021 address the efficacy of a short laser wavelength and a broad laser bandwidth for suppressing the TPD and SRS-backscatter instabilities, both of which limit the performance of ICF targets by scattering laser light and generating suprathermal electrons. Using the LPSE code, numerous three-dimensional simulations were performed this year to estimate laser intensity thresholds for these instabilities under conditions relevant to ICF implosions (see Fig. 1). Our simulations demonstrate that an argon fluoride (ArF) laser with its combination of a broad native bandwidth (5 to 10 THz) and the shortest wavelength that is practical for ICF (193 nm) has significantly greater TPD and SRS-backscatter thresholds than the industry-standard, third-micron, Nd:glass laser. (Note that the latter has a native fractional bandwidth less than 0.1%, and achieving a degree of mitigation comparable to the ArF laser would require the use of an auxiliary optical process at the end of the laser propagation train, e.g., an optical parametric amplifier to enhance the effective bandwidth, which greatly increases the cost and complexity of the laser drive.) Results of this work have helped to advance efforts by researchers in the Laser Plasma Branch at NRL who are advocating for the development of an ArF laser as a next-generation driver for ICF.

DoD Impact/Significance: Suppression of hydrodynamic and laser-plasma instabilities will expand the design space available for viable ICF target designs, which will benefit the National ICF program and auxiliary research efforts related to stockpile stewardship.

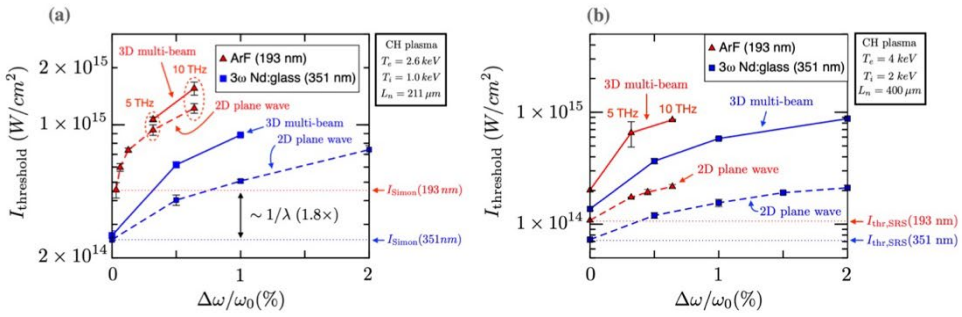

Figure 1. Laser intensity thresholds for: (a) the absolute TPD instability (for plasma conditions similar to those found on the OMEGA laser); and (b) the absolute SRS-backscatter instability (for NIF-like plasma conditions), as a function of laser driver ad bandwidth. Note that the results for 351-nm laser light assume that some sort of auxiliary, nonlinear optical process has been utilized to enhance the laser bandwidth to large values. Also note that two sets of thresholds results are shown for each laser driver; one set shows the thresholds for a single, two-dimensional, p-polarized beam and the other depicts threshold values resulting from six overlapped laser beams in three spatial dimensions including the effects of collisional and Landau damping. The dotted, horizontal lines are predictions from linearized theoretical models that agree well with the two-dimensional plane-wave results in the monochromatic limit, thus providing a useful benchmark for the LPSE code. We see the shorter wavelength of ArF yields higher instability thresholds for both the TPD and SRS-backscatter instabilities, with further enhancement resulting from its large native bandwidth between 5 and 10 THz.

THIS PAGE INTENTIONALLY LEFT BLANK

CCM

Computational Biology, Chemistry, and Materials Science

CCM covers computational tools used to predict basic properties of chemicals and materials, including nano- and biomaterials. Properties such as molecular geometries and energies, spectroscopic parameters, intermolecular forces, reaction potential energy surfaces, and mechanical properties are being addressed. Within the DoD, quantum chemistry, molecular dynamics, statistical mechanics, and multiscale methods are used to design new chemical, polymer, nanomolecular, and biomolecular systems for fuel, lubrication, laser protection, explosives, rocket propulsion, catalysis, structural applications, fuel cells, and chemical defense. Solid-state modeling techniques are employed in the development of new high-performance materials for electronics, optical computing, advanced sensors, aircraft engines and structures, semiconductor lasers, advanced rocket engine components, and biomedical applications. Of recent emerging interest in the Computational Biology, Chemistry, and Materials Science (CCM) CTA are methodologies that cover bioinformatics tools, computational biology, and related areas, such as cellular modeling.

Title: Multiple Length and Time Scale Simulations of Material Properties
Author(s): N. Bernstein
Affiliation(s): Naval Research Laboratory, Washington, DC
CTA: CCM

Computer Resources: HPE SGI 8600 [AFRL, OH]; SGI ICE X [ARL, MD]; Cray XC40/50 [ERDC, MS]

Research Objectives: To understand and predict mechanical, structural, and energetic material properties.

Methodology: Molecular dynamics (MD) and Monte Carlo (MC) are used for the time evolution and sampling of atomic configurations. Trajectories use energies and forces from density functional theory (DFT) and interatomic potentials. Nested sampling is used for calculating thermodynamic quantities and phase diagrams. Gaussian approximation potential (GAP) method is used for developing single- and multispecies interatomic potentials. The software implementing these methods included Vienna Ab initio Simulation Package (VASP) for DFT simulations, LAMMPS for interatomic potential MD, ASE and libAtoms/QUIP for GAP development and interfacing between various programs, and pymatnest for nested sampling.

Results: Simulations of paramagnetic steels continued using the previously developed workflows to use DFT to calculate structural properties. These include elastic constants, stacking faults, and point-defect formation energies and volumes. Chemical and magnetic disorder were both included, making the computational demands large. A paper presenting these results is currently under review. DFT was also used to calculate similar properties for insulating ceramics, which undergo very rapid densifiction and strengthening during flash sintering. Results for vacancies in ZrO_2 and their effect on the stability of various phases have been published, and new calculations for vacancy-stacking fault interactions in Al_2O_3 are ongoing. DFT calculations were also used to calculate the large number of reference values needed to fit a machine-learning potential that can describe structural phase transitions of the inorganic lead-halide perovskite material $CsPbBr_3$.

A simple interatomic potential was used within LAMMPS to describe anharmonic vibrations in various skutterudite crystals based on Fe or $CoSb_3$, some filled with La or Yb. The simulations are used to predict lattice thermal conductivity for these materials, which is crucial to their performance as thermoelectrics and how it depends on chemistry and interatomic interactions. Finally, a paper reviewing previous work on nested sampling was published, summarizing various previously generated results on various materials including model systems and chemically realistic metals and alloys.

DoD Impact/Significance: Atomic-scale simulations provide explanations and mechanistic understanding of microscopic processes that govern useful material properties, whether structural or functional. First-principles methods provide the state-of-the-art description of interatomic interactions. Simulations of structural materials such as steels will help design new alloy compositions with low magnetic response and good mechanical properties for maritime hull applications. Ceramics are used for their mechanical properties and corrosion resistance, and flash sintering of ceramics greatly reduces the time and energy cost for their fabrication and leads to greatly enhanced toughness, which is facilitated by the defects simulated here. Functional materials such as inorganic halide perovskites are a promising material for light-emitting and photovoltaic applications with high brightness and efficiency, which quickly rose to rival traditional materials that have been refined for decades. Skutterudites are promising thermoelectric materials for power harvesting applications.

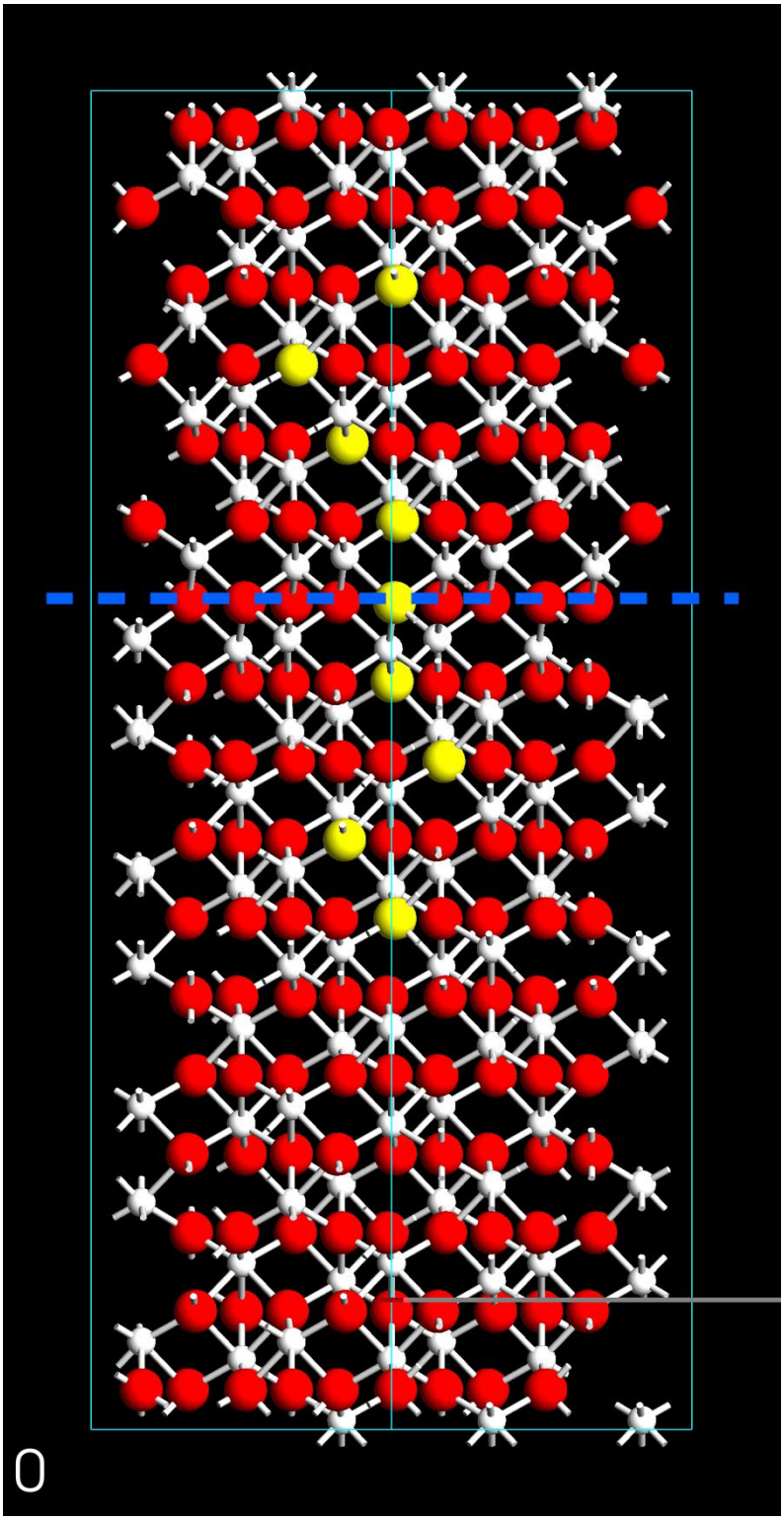

Figure 1. Visualization of an $\alpha - Al_2O_3$ unit cell containing a stacking fault (horizontal, dashed line), with sites for possible O vacancies at various distances from the plane highlighted as yellow spheres

Title: Materials for Energy Storage and Generation
Author(s): M. Johannes
Affiliation(s): Naval Research Laboratory, Washington, DC
CTA: CCM

Computer Resources: HPE SGI 8600 [AFRL, OH]; SGI ICE X [ARL, MD]

Research Objectives: The objectives of this program are to use density functional theory (DFT) and its extensions, including molecular dynamics, to understand the materials properties that drive functionality in materials relevant to energy storage and generation, including new materials for low-power electronics and topological materials suitable for switching and spintronics.

Methodology: First-principles pseudopotential methods are employed to calculate the quantities of interest. The majority of the work was done using the Vienna Ab initio Simulation Package (VASP), but a substantial minority was done using the FPLO (Full Potential Local Orbital) code. Postprocessing is done using personal codes. Both standard (static)T=0 DFT calculations and temperature-dependent molecular dynamics (MD) calculations were used.

Results: In FY21, the project's focus was on analyzing strain effects in topological materials for switching. In materials where band crossings are "protected" due to the symmetry of the bands, cone-like Dirac states form and surface metallicity occurs. Symmetry-breaking strain removes the symmetry protection and gaps out the band crossings. Interestingly, in orthorhombic Cd3As2, uniform tensile strain applied by epitaxial growth on a suitable substrate preserves the relevant symmetries to maintain the materials' topological nature, as is expected. However, uniform compressive strain subtly changes the energy of the vacancy ordering that defines the crystal structure, removing the inversion symmetry and changing the topological ordering of the bands. This is rather unexpected, since the compressive strain fully preserves the glide plane symmetry that is known to be the relevant topological characteristic. We have also calculated the origin of the extreme magnetocaloric effect in MnAs. This effect stems from the removal of entropy via application of an external field that polarizes formerly disordered spins. A subsequent magnetostriction in this material also occurs. Our calculations accurately reproduce experimentally observed crystal structures in the ordered and disordered phases and uncover a competition between bonding and Pauli repulsion as the underlying mechanism driving the phase transition.

DoD Impact/Significance: Topological materials have incredible potential for electronics usage, since the metallic surface states that characterize them are 100% spin polarized and impervious to the scattering effects of normal spintronics materials. Furthermore, due to symmetry-protected properties that diminish decoherence, these materials may be the future of quantum computing. Magnetocalorics are an exciting possibility for refrigeration, especially computer cooling.

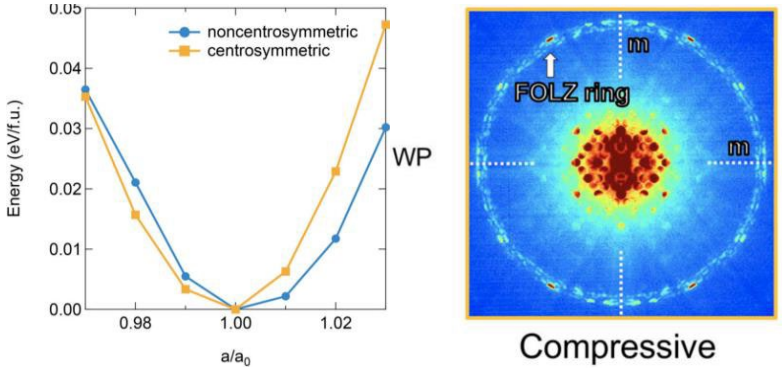

Figure. (left): Density functional theory calculation of the ground state structure of Cd_3As_2 as a function of tensile and compressive strain. (right): Experimental convergent beam electron diffraction pattern along $[110]_T$ for a compressively strained (001)001 Cd_3As_2 film, showing the loss of one mirror plane, indicating lack of inversion (non-centrosymmetric) symmetry.

Title: Marine Biofilm Metaproteomics
Author(s): W.J. Hervey, C.M. Spillmann, and G.J. Vora
Affiliation(s): Naval Research Laboratory, Washington, DC
CTA: CCM

Computer Resources: HPE SGI 8600 [AFRL, OH]; Cray XC40/50 [ERDC, MS]

Research Objectives: To implement, adapt, and maintain a modular workflow of bioinformatics applications capable of leveraging distributed computing on HPC, such as the Message Passing Interface (MPI) or Shared Memory (SHMEM). This effort leverages a previous HPC Application Software Initiative (HASI) awarded for multi *-omics* data analytics of complex biological systems on emerging architectures. Selectively tailoring bioinformatics applications to specific Department of Defense use-cases continues to enable *-omics* characterizations of microbiomes, biofilms, and complex marine eukaryotes. In FY21, our suite of tools was adapted to *-omics* studies of the acorn barnacle, *Amphibalanus amphitrite*.

Methodology: Factors limiting analysis and interpretation of large-scale genomic (DNA), transcriptomic (RNA), proteomic (protein), and metabolomic (metabolite) datasets include a code base of largely serial bioinformatics software tools and an increasing data volume. To alleviate computational bottlenecks among these *-omics* data analyses, the applications DISCO, MetaCarvel, and Sipros Ensemble (SE) are used for metagenome assembly, metagenome scaffolding, and metaproteome identification, respectively. DISCO, ***Dis***tributed ***C***o-assembly of ***O***verlap graphs, assembles genome reads by an overlap-layout-consensus (OLC) approach while using both OpenMPI and distributed memory. DISCO output is passed to the multithreaded MetaCarvel scaffolding application, which joins contiguous DNA segments (or "contigs") into larger genome scaffolds. MetaCarvel output is representative of multiple genomes present in a microbiome, but is also able to retain genome sequence variants among assembly graphs as SPQR trees. SE leverages hybrid OpenMP/MPI capabilities to search tandem mass spectra for potential matches among millions of proteins arising from *in silico* translations of MetaCarvel metagenome scaffolds. SE significantly reduces the false-discovery identification rate in metaproteome profiles by applying a random forest classifier to multiple scoring functions. For each biological system's study and HPC use-case, any combination of these three distributed bioinformatics tools may be applied for *-omics* analyses and analytics.

Results: This subproject contributed to *–omics* data analyses among a range of biological systems. FY21 allocations were specifically leveraged to analyze biomolecular measurements of the acorn barnacle. Allocations enabled identifications of barnacle proteins via targeted proteomics as well as primary sequence analysis of genome and proteome sequences. In FY21, HPC allocations on this subproject yielded contributions to one peer-reviewed publication, one oral presentation, three conference proceedings, and one invitation to participate in an intralab study (one non-peer-reviewed professional society report).

DoD Impact/Significance: This HPC subproject has broad DoD significance. It is directly applicable to "sense and sense-making" from large data, biotechnology, artificial intelligence, machine learning, biologically inspired materials design, biosensing, synthetic biology, systems biology, alternative energy sources, and platform sustainability.

(*a*)

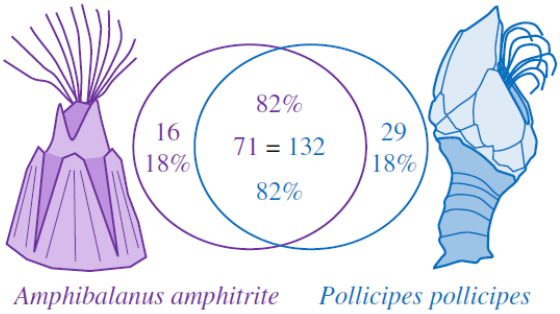

(*b*)

category	*Amphibalanus amphitrite*	*Pollicipes pollicipes*
bulk	43 (15)	42 (13)
pheromones	11	25
enzymes	11	43 (12)
protease inhibitors	11	28 (2)
homologous	13 (1)	23 (3)

Figure 1. Comparison of the proteins identified via mass spectrometry in the adhesive of *A. amphitrite* and *P. pollicipes*. (a) Venn diagram indicating the number and percentage of the total identified proteins that do and do not share homology between the two species. Seventy-one *A. amphitrite* proteins align to 132 *P. pollicipes* proteins. (b) Number of proteins per protein category for each species, with the number of proteins with no homology to the other species in parenthesis. These broad categories are based on the annotation or conserved domains present in the protein sequences or homology to barnacle proteins identified in previous studies. The bulk proteins are predicted to make up the bulk mass of the adhesive and may contribute to adhesion. Pheromones are either α-macroglobulins (settlement inducing or MULTIFUNC in pheromones) or have cupin domains (waterborne settlement pheromones). Enzymes cover a range of potential processes, including oxidation and protease (inhibition) activity. The homologous group includes the remaining proteins with homology to broader taxa. These numbers exclude highly likely intracellular proteins (35 *P. pollicipes*, three *A. amphitrite*), based on annotation and the lack of predicted signal peptides." (Figure shown above is Figure 1, Schultzhaus JN *et al., Open Biology*. 2021. doi: 10.1098/rsob.210142)

Title: Synthetic Biology for Military Environments
Author(s): W.J. Hervey, Z. Wang, and G.J. Vora
Affiliation(s): Naval Research Laboratory, Washington, DC
CTA: CCM

Computer Resources: HPE SGI 8600 [AFRL, OH]; Cray XC40/50 [ERDC, MS]

Research Objectives: To expand molecular genetics tools and host species (or "chassis") for synthetic biology applications. Conventional host chassis, such as *E. coli*, and recombinant expression systems limit *on-demand* production of military-relevant analytes, molecules, or materials. In previous years, NRL has demonstrated synthetic biology applications in two marine microbial species, *Marinobacter atlanticus* and *Vibrio natriegens*. In FY21, HPC allocations were used to test and evaluate the black yeast, *Exophiala dermatitidis*, as a chassis for synthetic biology applications. A prerequisite for engineering synthetic biology platforms is systematic, high-throughput assessment of newly imparted, desired functions and any collateral effects on the host chassis relative to the unaltered version (or "wild-type strain") of the organism. Proteome profiling yields this insight in a single measurement, particularly for characterizing molecular-level responses of *E. dermatitidis* to environmental stimuli. Among DoD Tri-Service labs engaged in biotechnology research, this HPCMP subproject serves an essential role for co-investigators to collaboratively analyze '*-omics*' data and benchmark emerging bioinformatics software applications.

Methodology: An active area of synthetic biology research is engineering desirable, yet controllable, functions into cells. Engineered functions are often modulated by genetic means, ranging from simple antibiotic resistance to encoding elaborate genetic circuits. High-throughput proteome profiling of unaltered (or "wild-type") and engineered systems enables simultaneous measurement of genetic circuit performance, as well as potential collateral effects on microbial physiology. To characterize the response of *E. dermatitidis* to radiation, proteome profile measurements by liquid chromatography tandem mass spectrometry (LC-MS/MS) and other *-omics* measurements were performed on HPCMP systems. Resulting proteome profiles were integrated with *-omics* based measurements (e.g., transcriptomics, genomics) to yield molecular-level snapshots of *E. dermatitidis*.

Results: To identify expressed proteins, the Sipros Ensemble application (SE) applied a random forest classifier to correlate peptide masses and fragmentation patterns to *in silico*-predicted patterns of *E. dermatitidis*. SE, an HPCMP application software initiative (HASI)-sponsored application, leverages OpenMPI to distribute computationally intensive tasks. Integration of *-omics* measurements among wild-type and mutant strains enabled formulation of multiple hypotheses that potentially impart *E. dermatitidis'* ability to repair DNA damage from radiation (Fig. 1). In FY21, HPC allocations contributed to two peer-reviewed publications, one invited oral presentation, and one peer-reviewed conference proceeding.

DoD Impact/Significance: This subproject is a collaborative Tri-Service resource for synthetic biology and biotechnology. It is directly applicable to "sense and sense-making" from large data, biotechnology, artificial intelligence, machine learning, biologically inspired materials design, biosensing, synthetic biology, systems biology, and alternative energy sources.

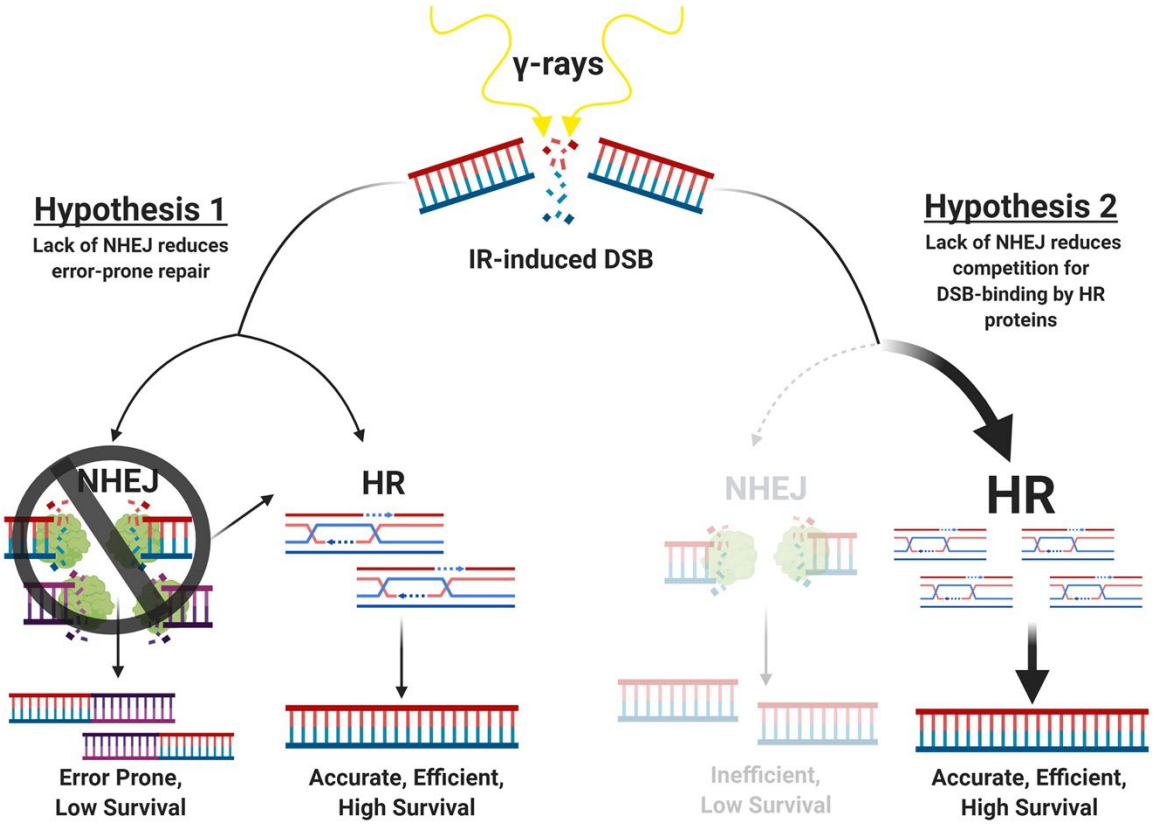

Figure 1. Model demonstrating the two proposed possibilities for increased ionizing radiation (IR) resistance in nonhomologous end-joining (NHEJ) mutants. These two hypotheses include either a lack of error-prone repair, mediated by nonhomologous end-joining (or NHEJ; left), when this pathway is abolished, or reduced competition for homologous recombination (HR)-mediated repair components to work at DNA lesions (right).

Image above is Figure 8 from Romsdahl et al., *Environmental Microbiology*, 2021: https://doi.org/10.1111/1462-2920.15285

Title: Numerical Studies of Semiconductor Nanostructures
Author(s): T.L. Reinecke[1] and I. Welland[2]
Affiliation(s): [1]Naval Research Laboratory, Washington DC; [2]National Research Council Postdoctoral Research Associate at Naval Research Laboratory, Washington DC
CTA: CCM

Computer Resources: HPE SGI 8600 [AFRL, OH]; SGI ICE X [ARL, MD]; Cray XC40/50 [ERDC, MS]

Research Objectives: To make first-principles calculations of the frequencies and lifetimes of phonons in a range of quasi-two-dimensional materials to understand their basic thermal properties and their vibrational quality factors in support of their use in novel high-frequency optomechanical acoustic cavities and potential signal processing.

Methodology: Ab initio density functional methods using Quantum ESPRESSO and Vienna Ab initio Simulation Package (VASP) codes were used to calculate the phonon frequencies and the anharmonic interactions between phonons throughout the Brillouin Zones in a range of two-dimensional materials, including MoS_2, $MoSe_2$, and hBN. Inelastic Boltzmann equation techniques were developed and used to calculate the phonon lifetimes in these materials.

Results: Quasi-two-dimensional layered materials such as the transition metal dichalcogenides are attracting attention for their vibrational properties in addition to their optical and electronic properties. The vibrational properties are of interest for potential optomechanical devices such as ultrafast optomechanical signal processing. Their vibrational quality factors $Q_i = \omega_1/\Delta\omega_1$, where ω_1 is a vibrational frequency and $\Delta\omega_1$ is the linewidth, gives the fundamental limit to the vibrational coherence and is critical to their implementation. In recent experimental work, thin layers of MoS_2, $MoSe_2$, and hBN have been suspended over submicron cavities to explore their vibrational properties. Calculations of the vibrational properties of suspended layers of MoS_2, $MoSe_2$, and hBN have been made using density functional techniques for phonon vibrational frequencies and for the anharmonic interactions between phonons. Inelastic Boltzmann techniques were used to calculate phonon lifetimes through the Brillouin zones and for temperatures up to room temperature for monolayer and bulk systems. The lifetimes of these systems were found to increase by orders of magnitude at low frequencies and to be longer for monolayer systems than for bulk, particularly for MoS_2 and $MoSe_2$. The dependences on frequency and on thickness of the system were found to less dramatic for HBN. Lifetimes decreased substantially, typically by an order of magnitude, for temperatures increasing from zero to room temperature. Q's including both intrinsic losses as well as extrinsic effects from typical surface imperfections were found to be sufficiently high that these materials could provide an important new basis for ultrafast optomechanical technologies.

DoD Impact/Significance: It has been demonstrated that nanoscale cavity structures with thin layers of quasi-two-dimensional materials have vibrational coherences sufficiently high for exploitation in novel ultrahigh-frequency signal-processing technologies.

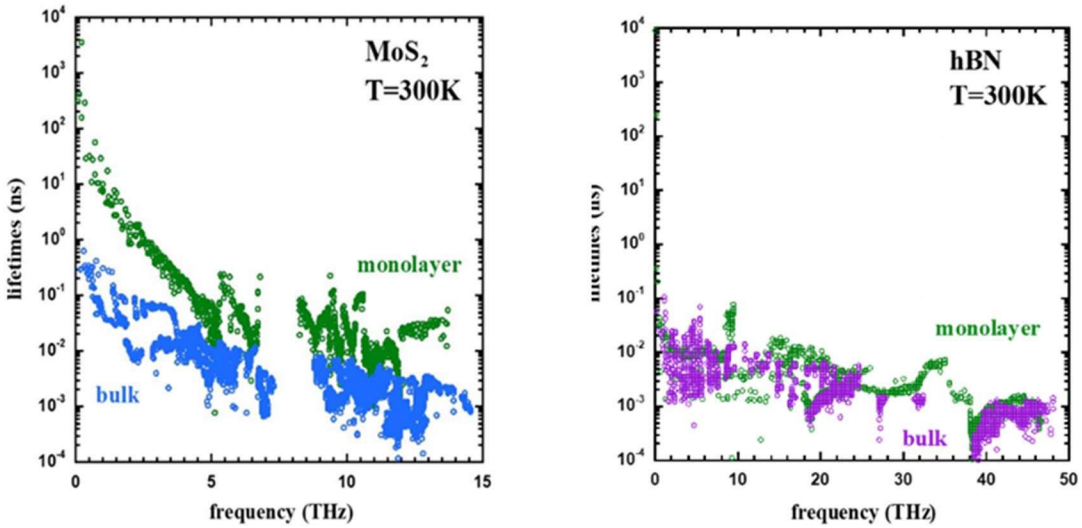

Figure 1. Room temperature phonon lifetimes through the Brillouin Zones for monolayer and bulk MoS_2 and hBN.

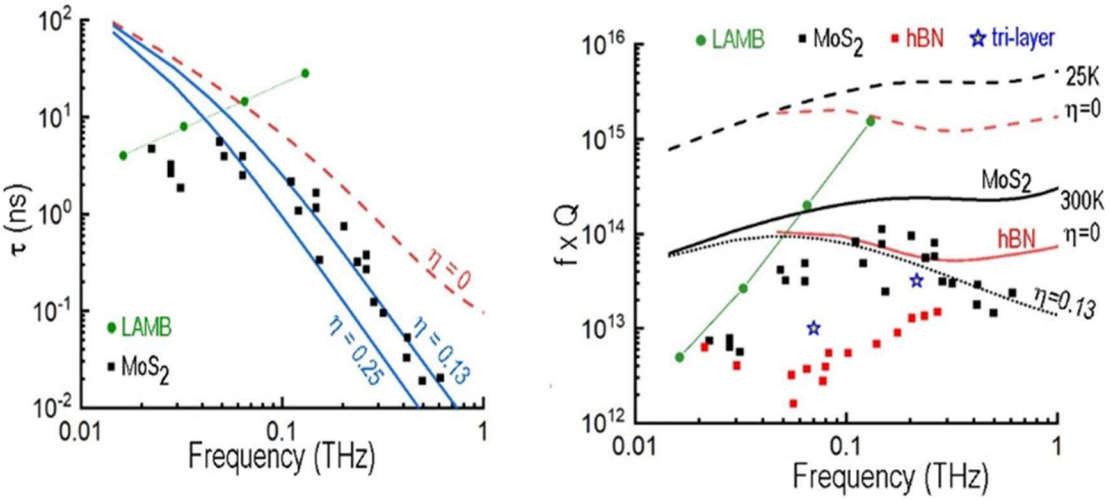

Figure 2. (Left) Lifetimes of LA phonons polarized perpendicular to the surface of MoS_2 for anharmonic phonon scattering alone (dashed curve with surface roughness, $\eta = 0$) and for the sum of anharmonic scattering and surface losses (solid curves with rms surface roughness $\eta > 0$) in nanometers). (Right) Products of calculated and measured frequencies multiplied by phonon quality factors versus frequency. Black lines show MoS_2 and the red lines show hBN at the labeled temperatures and η. Experimental data are given by the square and star symbols.

Title: Calculation of Materials Properties via Density Functional Theory and Its Extensions
Author(s): J.L. Lyons
Affiliation(s): Naval Research Laboratory, Washington, DC
CTA: CCM

Computer Resources: HPE SGI 8600 [AFRL, OH]; SGI ICE X, Cray XC40 [ARL, MD]; Cray XC40/50 [ERDC, MS]; Cray Shasta [NAVY, MS]

Research Objectives: The overall objective is to calculate the electronic structure of wide-band-gap semiconductors (WBGS) such as gallium oxide (Ga_2O_3) and aluminum nitride (AlN) and novel materials such as cesium lead bromide ($CsPbBr_3$) using first-principles approaches including hybrid density functional theory (DFT) that accurately describe the electronic structure and defect properties of WBGS.

Methodology: DFT has long been a proven method for deducing semiconductor electronic structures without the need for experimental input, but when applied to WBGS, the so-called "band-gap problem" makes difficult the quantitative prediction not only of bulk band structures, but also of defect properties. To overcome these issues, we employ hybrid density functional theory. Hybrid functionals mix in a fraction of screened Hartree-Fock exchange into the exchange-correlation functional, and are capable of accurate, quantitative prediction of band gaps and defect transition levels, even in WBGS. Using hybrid DFT, charge-state transition levels, formation energies, and optical transitions associated with defects and impurities in WBGS are calculated. With the same methods, the electrical and structural properties of semiconductor alloys (such as $Al_xGa_{1-x}O_3$) and novel materials (such as lead halide perovskites) are also calculated.

Results: In FY21, resources from this project were utilized to calculate the properties of impurities in GaN, hole-trapping elements in AlN, alloys of Ga_2O_3 with In_2O_3 and Al_2O_3, and dopants, defects, and impurities in lead halide perovskites. For GaN, the properties of multicarbon complexes were investigated and compared with experimental characterization of heavily C-doped samples. Resources were also utilized to perform calculations in support of a review article on defects and impurities in GaN.

Hole trapping in AlN was also studied, since it was discovered that not only acceptor dopants can trap holes, but also that this could be done by isoelectronic elements such as boron. Such species act as hole traps and may also give rise to characteristic optical signals. Because of their usefulness in future device designs, alloys of Ga_2O_3 with In_2O_3 and Al_2O_3 were also under investigation. Using HPC resources, band alignments between these materials and their alloys were calculated.

Also investigated in this FY were native defects, impurities, and dopants in lead halide perovskites. These materials are under development for light-emitting diodes and single-photon emitters, but little is known about how defect centers affect their properties, or whether their electronic conductivity can be controlled via doping. Our calculations find that many stable defects have deep levels in $CsPbBr_3$, in contradiction with commonly held beliefs, and that hydrogen impurities are quite stable. We also investigated donor doping, and found that scandium and yttrium (but not commonly-considered bismuth) were effective donor dopants in the family of lead halide perovskites (see graphic).

DoD Impact/Significance: WBGS such as Ga_2O_3 and AlN are utilized in power electronics that play a crucial role in many Navy-relevant applications, and afford significant SWAP-C savings when replacing components based on traditional semiconductor materials such as silicon or silicon carbide. Optimizing impurity doping to control electrical conductivity, understanding contaminating species to minimize trapping centers, and characterizing unintentionally incorporated defects are crucial steps for improving such materials.

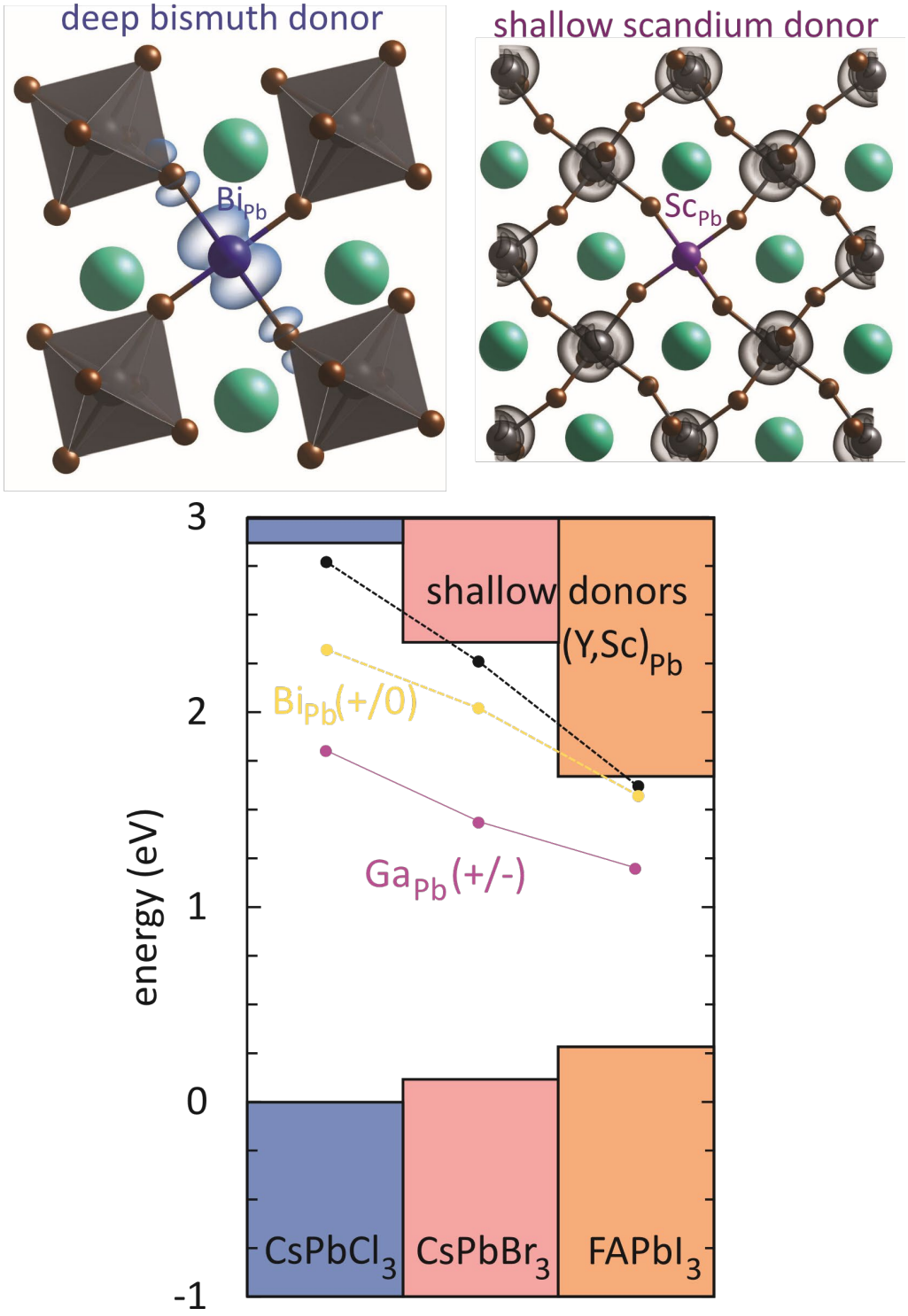

Figure 1. Isosurfaces of donor wavefunctions for the deep bismuth donor (top, left) and shallow scandium donor (top, right) in cesium lead bromide. Lead atoms are in grey, cesium in green, bromine in brown, bismuth in blue and scandium in purple. Donor ionization energies are also shown (bottom subfigure) for bismuth and gallium deep donors as well as yttrium and scandium shallow donors in three perovskites: cesium lead chloride, cesium lead bromide, and formamidinium lead iodide."

Title: Point Defects and Interfaces in Two-Dimensional Materials
Author(s): D. Wickramaratne
Affiliation(s): Naval Research Laboratory, Washington, DC
CTA: CCM

Computer Resources: SGI ICE X, Cray XC40 [ARL, MD]

Research Objective: To understand and predict the electronic, structural and optical properties of point defects, dopants and interfaces in bulk and low dimensional semiconductors.

Methodology: We use density functional theory (DFT) and the projector augmented wave (PAW) method as implemented in the Vienna Ab initio Simulation Package (VASP) code for our calculations. To accurately describe the band gap of semiconductors, we use screened hybrid functional calculations. Accurate forces and total energy calculations are required to identify the most stable configurations of point defects in their various charge states. We use this information to determine the formation energies, charge-state transition levels and optical transitions of various defects.

Results: Using first-principles calculations and an analytical theory for Ising superconductivity, we have systematically investigated proximity-induced effects in $NbSe_2/CrBr_3$ heterostructures. We find $CrBr_3$ leads to a proximity-induced exchange splitting of the $NbSe_2$ states and that the $NbSe_2$ states at G contribute the most to tunneling. We explore the magnitude of the exchange splitting and the tunneling matrix elements as a function of different stacking configurations and number of layers. These parameters obtained from our first-principles calculations were used in an analytical model for tunneling across these heterostructures. A paper on these results was published in Physical Review B as a letter.

DoD Impact/Significance: There are growing experimental efforts to identify new materials for Josephson junctions, which are of potential interest for DoD applications such as single-photon detectors and magnetometers. The interface between 2D superconductors and magnetic insulators will also lead to spins-selective behavior, which can be harnessed for applications in spintronics. Such devices are also being actively pursued within the DoD. This work helped identify a potential combination of superconductor and magnetic insulator materials that can be utilized in such devices and outlines a theoretical framework to analyze tunneling properties across such heterostructures.

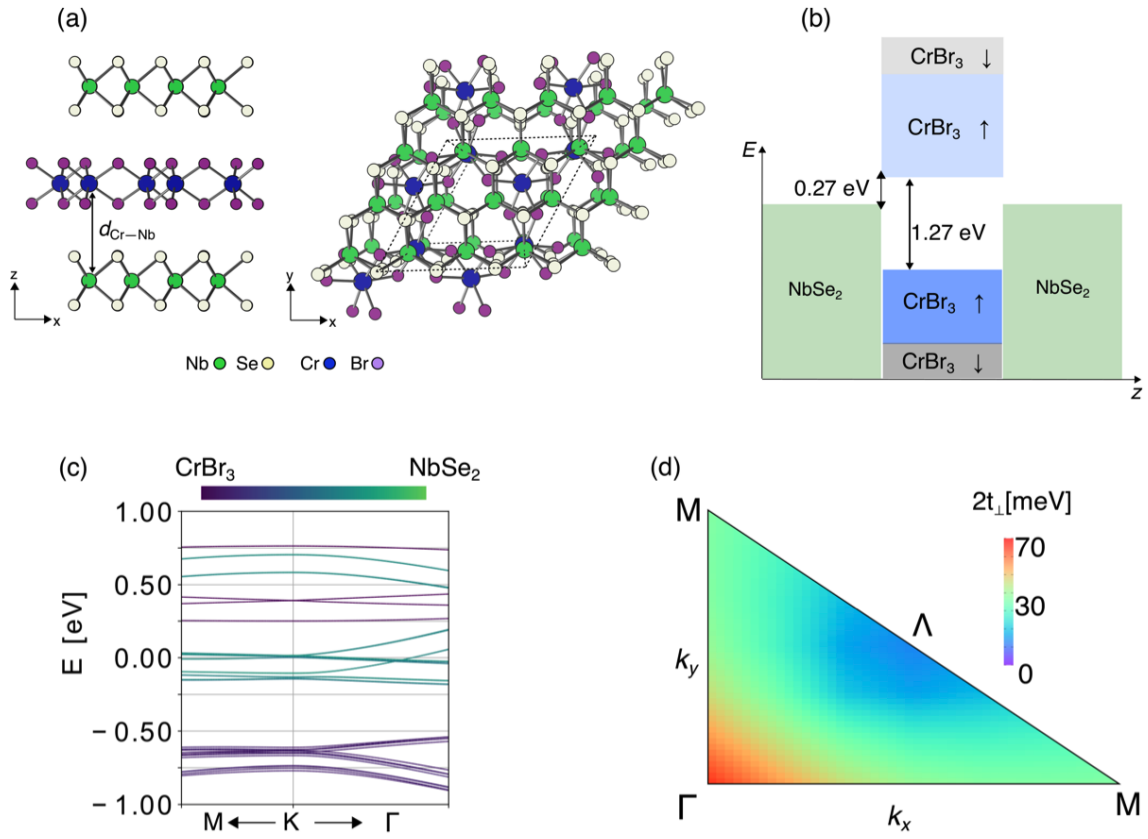

Figure 1. (a) Trilayer heterostructure showing the side view and the top view. (b) Alignment of the energy levels of $NbSe_2$ with respect to monolayer $CrBr_3$ at the K point. (c) Spin-polarized band structure of the trilayer heterostructure around the K point. (d) Interlayer coupling $2t_\perp$ of the $NbSe_2$/ $CrBr_3$/ $NbSe_2$ trilayer heterostructure as a function of momentum.

Title: First-principles Simulations of Condensed-phase Decomposition of Energetic Materials
Author(s): I.V. Schweigert
Affiliation(s): Naval Research Laboratory, Washington, DC
CTA: CCM

Computer Resources: HPE SGI 8600 [AFRL, OH]; SGI ICE X [ARL, MD]; HPE SGI 8600, Cray Shasta [NAVY, MS]

Research Objectives: To predict thermal, mechanical, and chemical properties of explosives subjected to elevated temperatures and pressures.

Methodology: We use crystal structure optimizations and ab initio molecular dynamics (AIMD) simulations to study physical and chemical changes in energetic materials subjected to elevated temperatures and pressures. Structure optimizations use variable-cell optimization algorithms to determine changes in atomic coordinates and lattice constants at elevated pressures. AIMD simulations use constant-pressure, constant-temperature (NPT) integrators combined with multiple replicas to simulate changes in crystal structures at elevated temperatures. Atomic forces needed to perform these simulations are estimated using density functional theory (DFT) and periodic-cell models of crystalline environments. Python and Perl scripts are being developed to facilitate the execution and analysis of these simulations.

Results: This year, we performed AIMD simulations of the anisotropic coefficients of thermal expansion (CTEs) of the HMX explosive. Periodic cells containing four (2 x 1 x 2) primitive unit cells of β-HMX (eight molecules) were used to approximate the ideal (defect-free) crystal structure. Atomic coordinates and lattice parameters were first optimized at 0 K using a variable-cell optimization algorithm, starting with the experimental crystal structure. The optimized structures were simulated at temperatures ranging from 20 to 200 ºC using 12-picosecond-long NPT trajectories. For each temperature, five trajectories were simulated. After a 6-picosecond equilibration period, instantaneous values of temperature, stress tensor, and lattice parameters were recorded every 50 femtoseconds and were averaged over the remaining 6 picoseconds. The trajectory-average values were averaged over ensembles of five trajectories to provide the final estimates for the lattice parameters as functions of temperature. In addition to AIMD simulations, we tested two other MD variants: one based on a self-consistent charge density-functional tight binding (TB-MD) method and one based on an analytical, fixed-charge interatomic potential (MD). The ensemble-averaged lattice parameters and tilt angles for β-HMX extracted from the three types of MD simulations are compared to the available experimental values in Fig. 1. DFT-based AIMD simulations predict the HMX lattice parameters that remain within 2% of the experimental values for all temperatures. MD simulations based on the analytical interatomic potential predict the lattice parameters that deviate by as much as 5% from the experimental values. Interestingly, MD simulations based on the density-functional tight-binding method predict the lattice parameters that approach the accuracy of DFT-based AIMD. We observed similar accuracies for the HMX lattice parameters at cryogenic temperatures discussed in the FY20 report. Because the TB-MD variant is an order of magnitude faster than the AIMD variant, in the future, we plan to use the TB-MD variant for simulations of low-symmetry explosive crystals wherein AIMD simulations are too computationally expensive.

DoD Impact/Significance: Thermomechanical equation of state for β-HMX, including shock Hugoniot relationships, is needed to support physics-based modeling of HMX-based explosives and solid rocket propellants. The simulations completed this year ascertained the accuracy of DFT in application to HMX against available experimental data. Future simulations will focus on the equations of state under elevated temperatures and pressures, for which experimental data is currently unavailable.

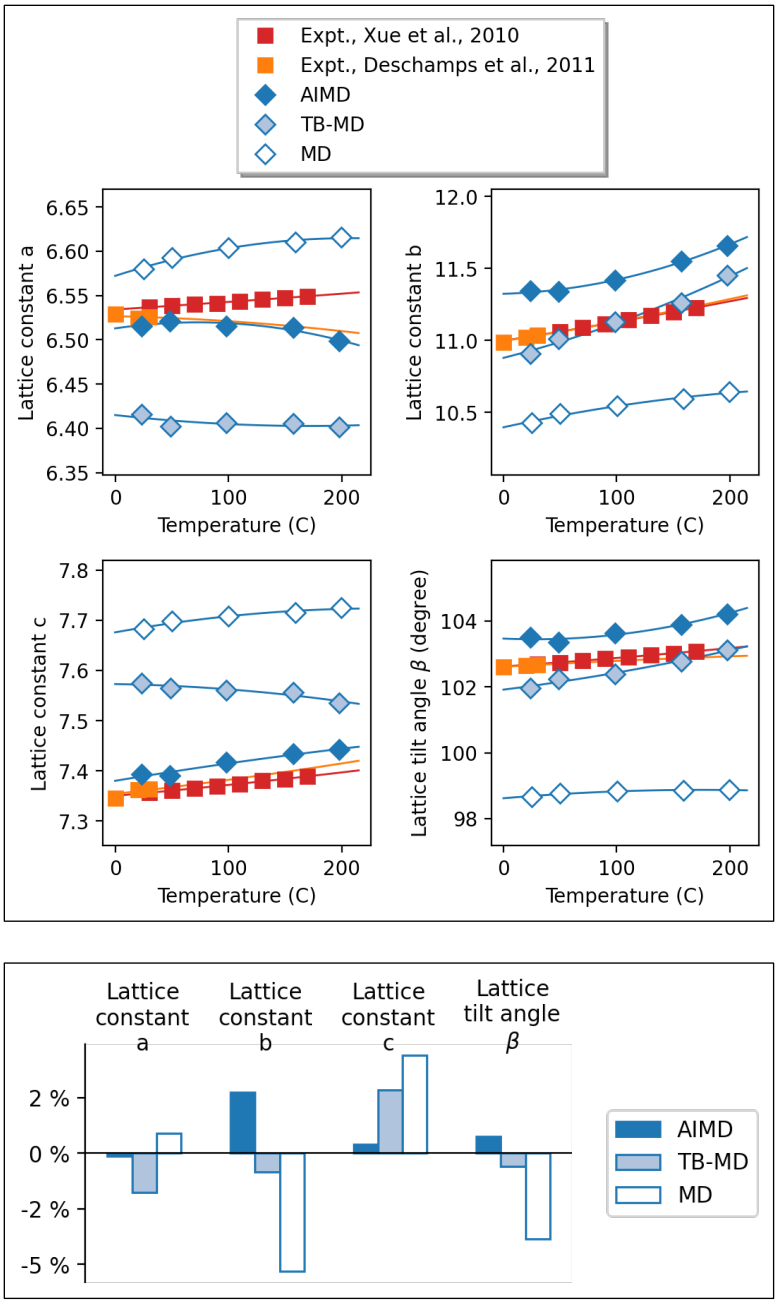

Figure 1. Top panel: Experimental and computed lattice parameters of β-HMX at temperatures ranging from 0 to 200 ºC. Solid lines show quadratic fits to the corresponding values. Bottom panel: Deviations of the computed lattice parameters at 30 ºC from the experimental values.

Title: Ab initio Simulations of Thermal Degradation of Perfluoroalkyl Substances (PFAS)
Author(s): I.V. Schweigert
Affiliation(s): Naval Research Laboratory, Washington, DC
CTA: CCM

Computer Resources: HPE SGI 8600 [AFRL, OH]; SGI ICE X [ARL, MD]

Research Objectives: To determine unimolecular decomposition mechanisms of perfluorooctanesulfonic acid (PFOS) and its decomposition intermediates at temperatures above 1,000 C.

Methodology: We performed ab initio molecular dynamics (AIMD) simulations based on density functional theory (DFT) to study thermal decomposition of PFOS and its decomposition intermediates at temperatures above 1,000 C. All simulations used the PBE functional augmented with the D3 dispersion correction and the double-zeta def2-SVP basis set of Gaussian-type atomic orbitals. AIMD trajectories were calculated using a constant-volume, constant-temperature (NVT) integrator. For each species, 25 replicas of initial atomic coordinates and velocities were prepared using structures optimized at the same level of DFT. Initial atomic velocities were assigned using random sampling from the Boltzmann distribution at 500 C. Each replica was equilibrated using 3-picosecond NVT trajectories at 500 C to ensure the replicas probe different initial conditions. The atomic coordinates and velocities from the equilibration simulations were used in the production simulations at target temperatures ranging from 1,200 to 2,000 C. During the production simulations, atomic coordinates were recorded every 10 femtoseconds to track changes in covalent bonds as thermal motion led to chemical reactions. All simulations were performed with the NWChem software package for computational chemistry. Python scripts were developed to monitor the progress of the AIMD simulations and to analyze the computed trajectories.

Results: Overall, we have simulated decomposition of five species: $C_8F_{17}SO_3H$ (PFOS), $C_8F_{17}OSO_2H$ (perfluorooctyl hydrogen sulfite, i-PFOS), C_8F_{17} (perfluorooctyl radical), $C_8F_{16}O$ (perfluorooctanoyl fluoride), and $C_8F_{17}OH$ (perfluorooctanol). Simulations of PFOS at 1,727 C revealed rapid decomposition at this temperature, with 23 out of 25 trajectories capturing breaking of covalent bonds within the first 20 picoseconds. The majority of the reactive trajectories proceeded via homolytic C-S bond fission and formation of two radicals, C_8F_{17} and $HOSO_2$ (Fig. 1, left panel). While previous theoretical studies did not consider C-S bond fission as a possible decomposition pathway, our simulations indicate its importance at higher temperatures. Several reactive trajectories also captured roaming-radical reactions between C_8F_{17} and $HOSO_2$ (Fig. 1, center panel), wherein an OH moiety was transferred from $HOSO_2$ to C_8F_{17} prior to the radicals' separation. The roaming-radical reaction led to non-radical products $C_8F_{17}OH$ and SO_2. One reactive trajectory showed isomerization to i-PFOS. Simulations of C_8F_{17} at 1,927 C revealed that the radical decomposes via beta-scission of C-C bond, resulting in a smaller perfluoroalkyl radical, C_6F_{13}, and perfluoroethane, C_2F_4. Simulations of i-PFOS at 1,227 C revealed a number of decomposition mechanisms: concerted HF elimination, leading to $C_8F_{16}O$; SO_2 elimination, leading to $C_8F_{16}OH$; O-S bond fission, leading to C_7F_{15} (perfluoroheptyl radical) and CF_2O. Simulations of $C_8F_{16}O$ and $C_8F_{17}OH$ at temperatures up to 2,000 C produced no reactive trajectories within the simulated time of 20 picoseconds, indicating higher thermal stability of these compounds.

DoD Impact/Significance: Our simulations revealed a number of decomposition pathways that have not been considered in previous studies of thermal decomposition of PFOS, including C-S bond fission, roaming-radical reactions, and isomerization. Ongoing DFT studies will provide theoretical estimates for the Arrhenius parameters of these reactions to be included in modeling of thermal incineration of PFOS in commercial incinerators. This Frontier project has also demonstrated the utility of AIMD in studying thermal decomposition of PFAS; AIMD simulations of other PFAS compounds are underway.

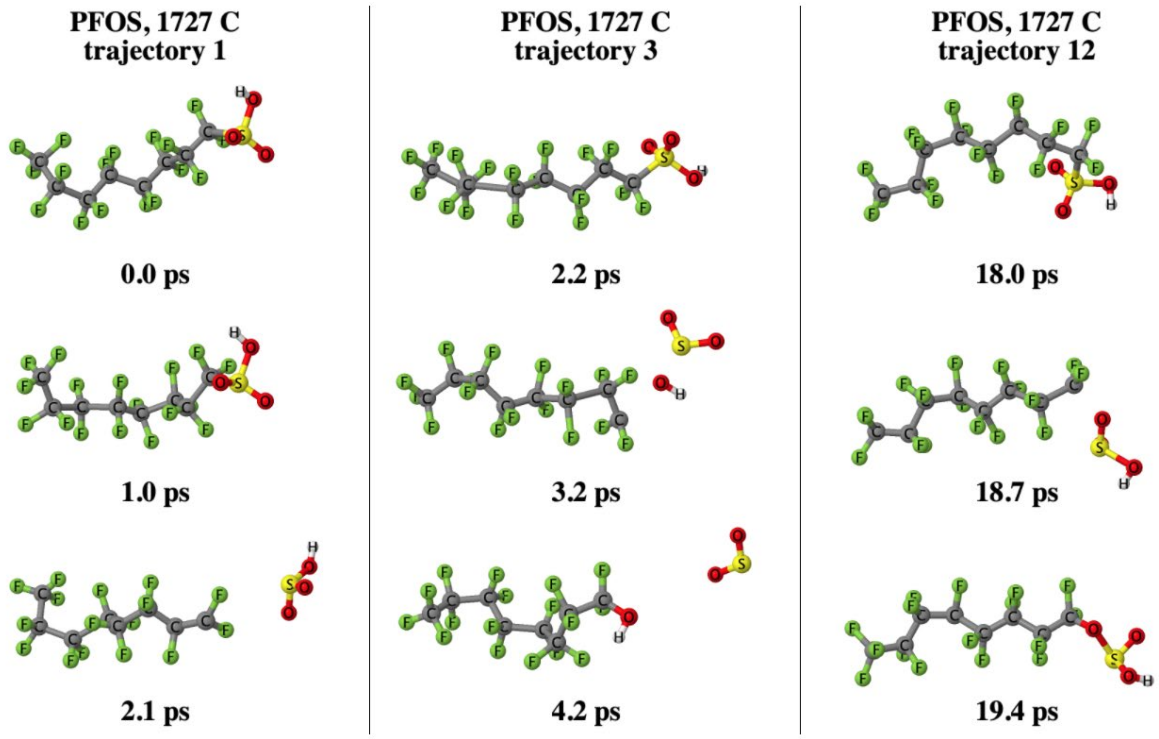

Figure 1. Structures extracted from three representative AIMD trajectories of PFOS at 1,727 C that show decomposition via C-S bond fission (left panel), roaming-radical OH transfer (middle panel), and isomerization (right panel).

Title: IR Absorption Spectra for PFAS Molecules Using Density Functional Theory
Author(s): S. Lambrakos and A. Shabaev
Affiliation(s): Naval Research Laboratory, Washington, DC
CTA: CCM

Computer Resources: HPE SGI 8600 [AFRL, OH]; SGI ICE X [ARL, MD]; Cray XC40/50 [ERDC, MS]

Research Objectives: Calculation of IR Absorption Spectra for PFAS molecules using density functional theory.

Methodology: The present study examines calculation of IR spectra for PFAS molecules using quantum theory-based calculations, i.e., density functional theory (DFT) and associated software technology, which provides complementary information to that obtained from spectroscopic measurements. This complementary information is both spectral features and their physical interpretation with respect to molecular structure, and thus prediction of spectral features that are difficult to measure in the laboratory. The present study adopts the software Gaussian 16 (G16) for the calculation of IR absorption spectra.

Results: The results of our study are relaxed or equilibrium configurations of PFAS molecules, ground-state oscillation frequencies and associated IR intensities for molecular geometries having stable structures, which are calculated by DFT[1,2]. A graphical representation of molecular geometries, and DFT calculated IR intensities as a function of frequency, for the PFAS molecules $C_4H_3F_7O$, C_4ClF_7O and $C_4HF_7O_2$ are shown in Figs. 1-3, respectively. For the calculations described here, geometry energy optimization and vibrational analysis were affected using the computer program G16 with the DFT chemical model B3LYP and basis functions 6- 311++g(3df,3pd). These basis functions designate the 6-311G basis set supplemented by diffuse functions, indicated by the sign ++, and polarization functions (df), having a set of d and f functions on heavy atoms. The details followed by Gaussian for IR analysis are given in [1,2] and references therein.

DoD Impact/Significance: PFAS molecules are chain linked carbon/fluorine atoms widely distributed in the environment, which are dangerously toxic biologically [1,2]. PFAS contamination of U.S. military installations poses a major problem, and thus PFAS detection of significance to the DoD. DFT provides an approach for estimating IR absorption spectra of isolated molecules. Identification of unknown molecules by comparison of spectra is accomplished using signal templates having patterns associated with known materials, which are adopted by different types of filter algorithms. In practice, because spectral features of target molecules are within complex spectral-signature backgrounds, filter algorithms associated with detection require reasonable estimates of target spectral features for construction of comparison templates, e.g., templates for cross-correlation. One would expect small shifts and variation of measured-spectra maxima relative to those of DFT-calculated template spectra due to different types of detector designs and ambient environments, which would result in different levels of coupling between molecular vibration modes and intermolecular interactions. Detecting the presence of target molecules within a complex molecular environment with respect to template spectra defines a problem of spectrum feature extraction, where sets of template spectra within a database are used by feature-extraction algorithms. In this context, DFT-calculated spectra are not only for interpretation of measured spectra, but as spectra from computational experiments, where in many cases, complementary measured spectra are not available.

---

[1]S. Wallace, S.G. Lambrakos, A. Shabaev, L. Massa, "Calculated IR Absorption Spectra for Perfluorroalkyl and polyfluoroalkyl (PFAS) Molecules," Structural Chemistry, (2021), 32, pp. 899-901, DOI 10.1007/s11224-021-01738-6.

[2] S. Wallace, S.G. Lambrakos, A. Shabaev, L. Massa, "On Using DFT to Construct an IR-Spectrum Database for PFAS Molecules," Structural Chemistry, 2021, https://doi.org/10.1007/s11224-021-01844-5.

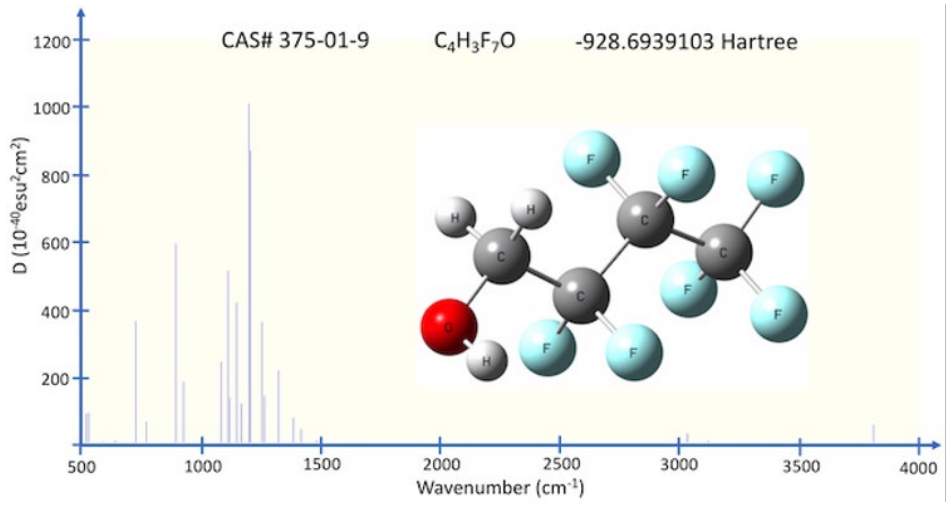

Figure 1. DFT-calculated IR spectra and molecular geometry for CAS# 375-01-9

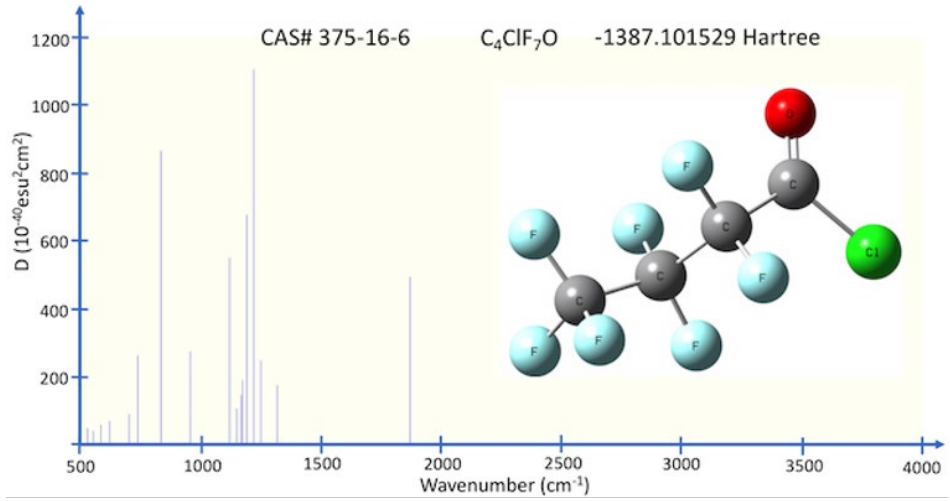

Figure 2. DFT-calculated IR spectra and molecular geometry for CAS# 375-16-6

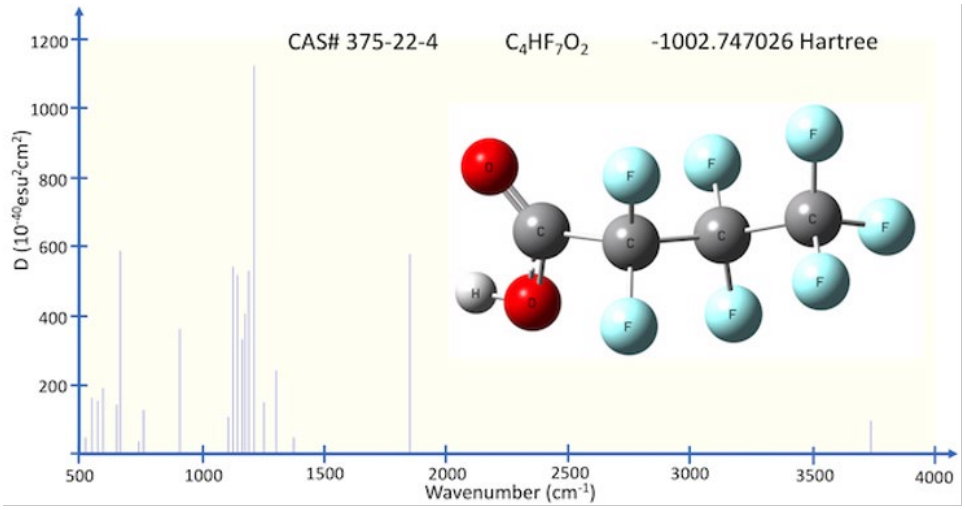

Figure 3. DFT-calculated IR spectra and molecular geometry for CAS# 375-22-4

Title: Quantum-Chemical Simulation of Surface-Science Experiments
Author(s): V.M. Bermudez
Affiliation(s): Naval Research Laboratory, Washington, DC, retired, previously NRL Voluntary Emeritus Program
CTA: CCM

Computer Resources: HPE SGI 8600 [AFRL, OH], [NAVY, MS]

Research Objectives: The objective of this program is to perform quantum chemical calculations as an aid in interpreting surface-science experiments and in understanding the structure and properties of surfaces.

Methodology: The Quantum ESPRESSO (vers. 6.5 and higher) and CRYSTAL (2014) software packages are used for density functional theory (DFT) calculations on periodic structures. The Gaussian 16 program suite is used for DFT calculations on isolated molecules and clusters.

Results: There is presently a critical need for a viable approach to forming ultrathin, high-quality layers of oxides such as Al_2O_3 on MoS_2 and related two-dimensional (2D) transition-metal chalcogenides (WTe_2, WSe_2, etc.). The potential application of such materials in electronic and optoelectronic devices and in chemical sensors is currently of great interest. Although metallic phases are well known, MoS_2 in its most stable form is a semiconductor (band gap = 1.29 eV in the bulk 2H structure), which is an important factor in the design of devices. Many of these applications require the formation of a gate oxide layer that is continuous, free of pinholes, impurities, and other defects, and is at most a few monolayers thick. Atomic layer deposition (ALD) is the most suitable method for preparing such an oxide. For growth on a three-dimensional material, the first step in ALD is to form an OH-terminated surface by reacting H_2O with coordinatively unsaturated surface sites ("dangling bonds"). However, 2D materials, unless defective, do not typically exhibit such sites on the basal plane. Atomic layer deposition has been problematic in this case as a result of the low reactivity of these substrates when free of strain, impurities and defects. Lewis acid-base chemistry provides a possible solution. The work performed during this period employs ab-initio density functional theory to examine the feasibility of adsorbing strongly Lewis-acidic Al reagents on MoS_2. The investigation focuses on small Al precursor molecules that are able to adsorb at high coverage and, therefore, to produce a dense and uniform layer of $Al(OH)_3$ when reacted with H_2O, which is highly desirable for initiating ALD growth. Of those species considered, it is found that $Al(CH_3)_3$, the most widely used reagent for ALD of Al_2O_3, is actually the least favorable in terms of its interaction with the MoS_2 basal plane. Other, more Lewis-acidic reagents, such as Al hydride (AlH_3), are found to adsorb somewhat more strongly in the critical first step of the growth process and, therefore, to be potentially more useful for initiating ALD growth. As a result of its small size, adsorbed AlH_3, when reacted with H_2O in the first ALD cycle, produces a very stable layer of hydrogen-bonded $Al(OH)_3$ (Fig. 1), which is critical in initiating the ALD growth of Al_2O_3. The coverage dependence of the adsorption energy and geometry and the effects of AlH_3 polymerization are also considered, and practical suggestions are given for how such species can be incorporated into an ALD process.

DoD Impact/Significance: The present work contributes toward the goal of developing reliable 2D transition-metal chalcogenide devices for applications in electronic devices and in chemical sensors for toxic and/or hazardous compounds. Different reagents for ALD growth of gate oxides have been evaluated, the chemical considerations have been enumerated and practical suggestions for ALD growth have been proposed. The approach developed here, unlike those put forth previously, does not involve the deliberate introduction of defects and/or impurities in order to overcome the lack of reactivity of these materials.

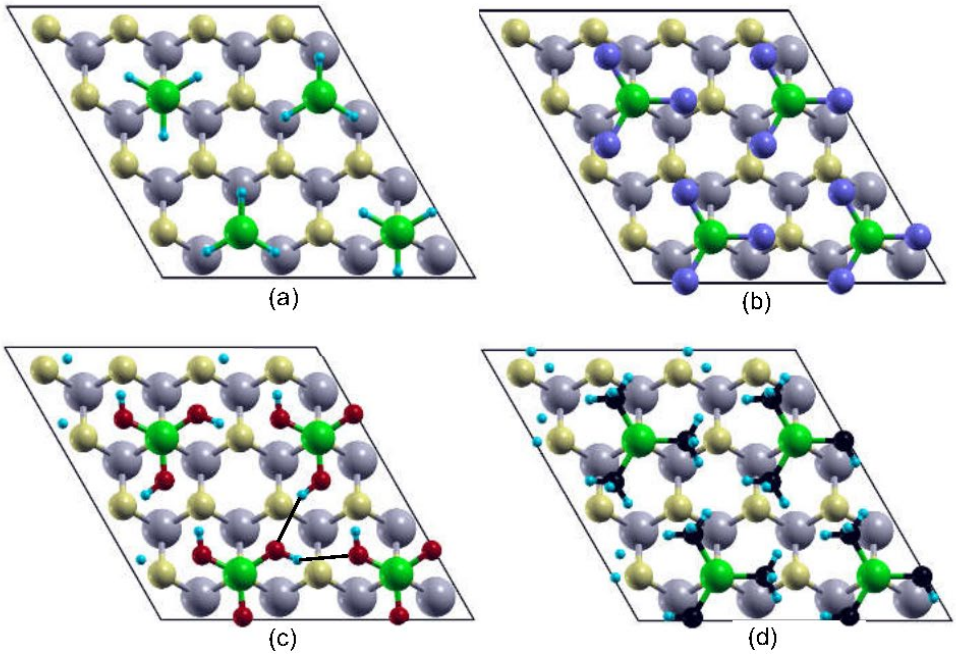

Figure 1. Top-down views of relaxed structures for 1/4 monolayer of (a) AlH_3, (b) $AlCl_3$, (c) $Al(OH)_3$ and (d) $Al(CH_3)_3$ adsorbed on a MoS_2 monolayer. In (c) and (d), some H atoms, which would fall outside the boundaries of the (4x4) supercell, are shown in translationally equivalent positions. The two black lines in (c) indicate weak H-bonds (same for all OH). Gray and yellow spheres represent Mo and S, respectively. Green spheres represent Al. Black, blue, aqua, and red spheres represent C, Cl, H, and O, respectively. The black parallelepipeds indicate the (4x4) supercells used in the calculations.

Title: Surfaces and Interfaces in Oxides and Semiconductors
Author(s): C.S. Hellberg
Affiliation(s): Naval Research Laboratory, Washington, DC
CTA: CCM

Computer Resources: HPE SGI 8600 [AFRL, OH]; SGI ICE X, Cray XC40 [ARL, MD]; Cray XC40/50 [ERDC, MS], Cray Shasta [NAVY, MS]

Research Objectives: Determine the atomic and electronic structure of twisted van der Waals heterostructures.

Methodology: We performed highly converged first-principles density functional calculations of very large supercells containing up to 2,382 atoms of a monolayer of $MoSe_2$ on a monolayer of WSe_2 to determine the electronic structure of the system as a function of twist angle. Larger supercells allow for smaller twist angles, and we are able to compute twist angles as small as 2.88 degrees. The layers are bound to each other via the van der Waals interaction. We used the Vienna Ab initio Simulation Package (VASP) density functional theory (DFT) code at the AFRL, ERDC, and ARL HPC centers. It is important to converge the atomic positions fully, as the structural relaxation provides the confining potential within the layers.

Results: We showed that flat electronic states shift into the electronic band gap at small twist angles. Flat valence band states emerge at twists below 4 degrees. Flat conduction band states emerge below 3.5 degrees, and a second higher-energy flat conduction state emerges at twists smaller than 3.2 degrees. There is significant strain in the moiré structures, both out-of-plane and lateral strain. The electronic band edges vary strongly with strain in dichalcogenides, and these strains are providing the confining potential causing the flat electronic states to form.

DoD Impact/Significance: Twisted dichalcogenide bilayers are candidate materials for hosting strongly correlated carriers, where the interactions between the carriers can be tuned by adjusting the angle of the twist. Our results show that at the band edges, electrons bind to the vertices of the moiré pattern and the domain walls, while holes bind to the "bulk" regions between the vertices and domain walls. Thus, two types of confined carriers will form in the experimental structures: holes in the "bulk" regions and electrons away from the "bulk". Due to their tighter confinement, the Coulomb interaction will be stronger between electrons than between holes. However, the kinetic dispersions for both electrons and holes are small, potentially leading to Mott insulating and superconducting states for both types of carriers, depending on the doping.

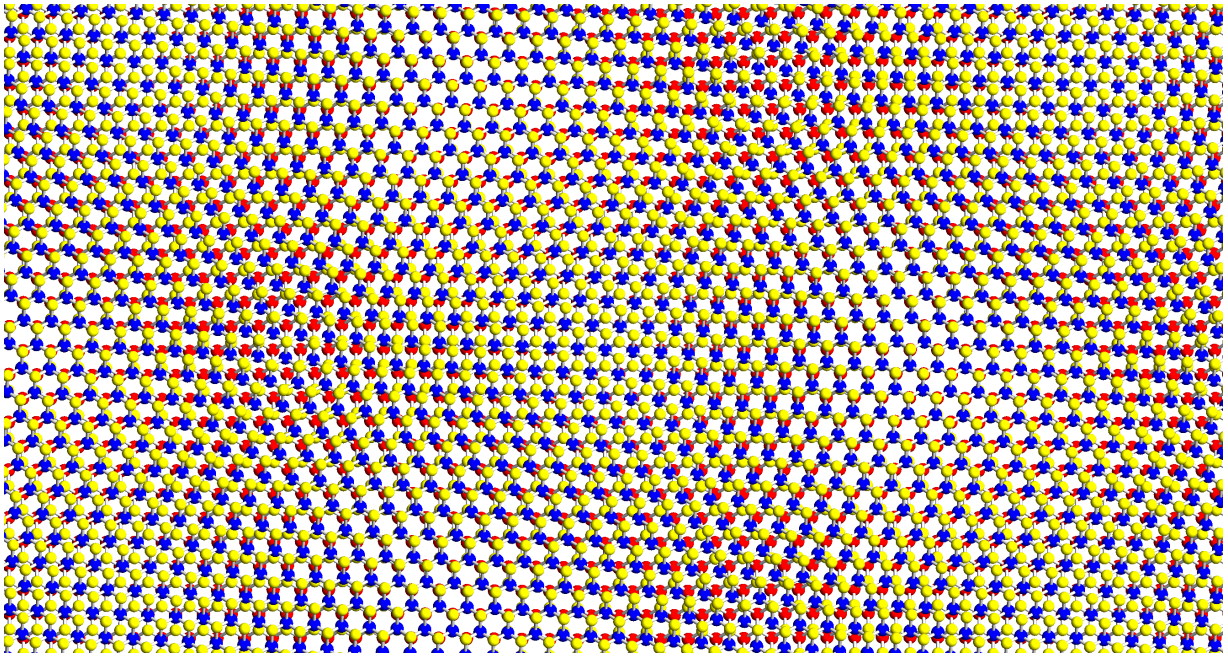

Figure 1. Structure of $MoSe_2/WSe_2$ twisted at 2.88 degrees. Mo atoms are blue, W atoms are red, and Se atoms are yellow. The lowest-energy high-symmetry structure has blue Mo over yellow Se in the lower layer. This region expands by untwisting, concentrating twist in the other higher-energy regions.

Title: Engineering Phase Change Materials for Neuromorphic Photonic Applications
Author(s): J.G. Champlain[1] and K.A. Cooley[2]
Affiliation(s): [1]Naval Research Laboratory, Washington, DC; [2]National Research Council Postdoctoral Research Associate, Naval Research Laboratory, Washington, DC
CTA: CCM

Computer Resources: HPE SGI 8600 [AFRL, OH]; SGI ICE X [ARL, MD]; Cray Shasta [NAVY, MS]

Research Objectives: This program seeks to demonstrate how alloying can be used to modify the structural, optical, and electronic properties of phase change materials for neuromorphic photonic devices. The effect of alloying elements on these properties offers a straightforward way to tune materials to achieve optimum device performance and efficiency for neuromorphic applications, which are of great interest to the Navy and the Department of Defense.

Methodology: Density functional theory (DFT) atomic structure calculations using the Quantum ESPRESSO software suite are used to analyze changes to the crystalline and electronic structure caused by alloying GeTe with elements that include Cu, Bi, and Sn.

Results: Initial results indicate that Bi, Sn, and Cu alloying elements will have varied effects on the crystal structure of GeTe. Bi and Cu are predicted to increase and decrease the cell volume of GeTe, respectively, while Sn is expected to cause the smallest effect on GeTe cell volume and Ge-to-Te bond lengths. This information is important to understanding how alloying could affect the phase-change process of GeTe in a future device, where density changes between crystalline and amorphous phases can induce problematic stresses.

In addition, preliminary calculations of the electronic properties of GeTe alloys predict that Sn is a better choice than Bi and Cu for tailoring the band gap of GeTe for photonics-based neuromorphic computing applications. While increasing amounts of Bi and Cu alloying leads to states within the band gap of GeTe and an ultimate disappearance of that band gap, Sn alloying maintains an electronic and optical band gap in GeTe, even up to 25 at.% Sn alloying (see Fig. 1).

DoD Significance: This work synergistically combines materials computation with materials synthesis and characterization to identify and confirm metal and metalloid alloys that will widen the GeTe optical band gap and reduce free carrier concentration for increased PCM switching contrast and reduced signal losses for neuromorphic photonics and other optical applications. Engineering phase-change materials in this way will not only be significant for the development of neuromorphic photonics platforms that are valuable for Navy, DoD, and commercial computing applications, but also will have far-reaching impact in other PCM-based technologies, such as RF electronics, photonics, and metamaterials.

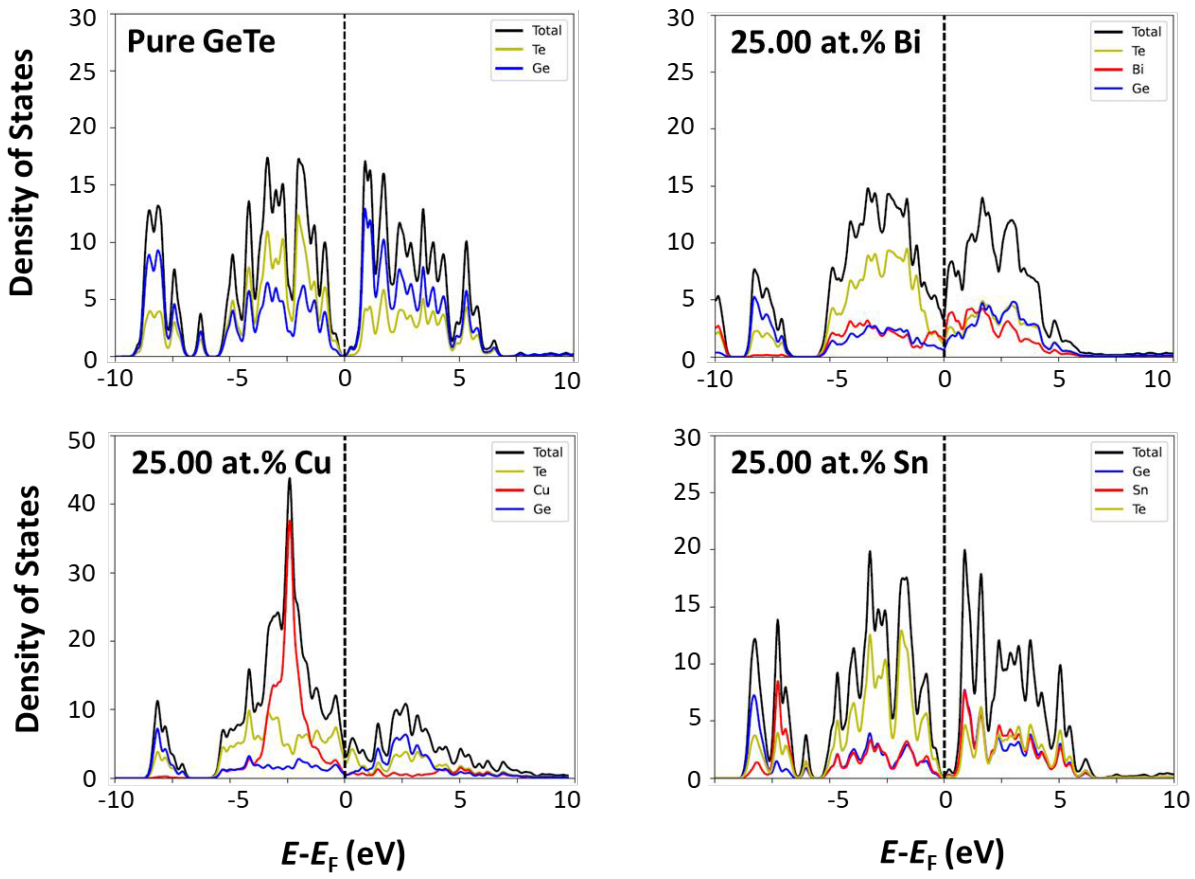

Figure 1. Density of states for GeTe and GeTe alloyed with Cu, Bi, and Sn (25 at.%), as calculated by density functional theory. The Fermi level is represented by a dashed line at $E-E_F=0$. Negative $E-E_F$ values represent the valence band, and positive *E-EF* values represent the conduction band. The total density of states is represented with a black line, while elemental contributions by Ge, Te, and alloy atoms (Cu, Bi, Sn) are represented by blue, yellow, and red lines, respectively. Note that GeTe with Sn is the only alloy which exhibits a band gap at 25 at.%.

Title: Atomistic Simulations of Navy-relevant Materials
Author(s): D. Fragiadakis
Affiliation(s): Naval Research Laboratory, Washington, DC
CTA: CCM

Computer Resources: HPE SGI 8600 [AFRL, OH], [NAVY, MS]; SGI ICE X [ARL, MD]

Research Objectives: The objective of the work conducted was to determine the unimolecular and bimolecular decomposition pathways of two model perfluoroalkyl substances (PFAS) — perfluoromethane sulfonic acid (PFMS) and perfluoroethane sulfonic acid (PFES) — under thermal incineration conditions.

Methodology: Structures of the relevant chemical species and transition states were optimized using density functional theory calculations, at the M06-2XD3/def2-TZVPP level of theory. Reactants and products connected by each transition state were verified using intrinsic reaction coordinate computations. The Gaussian 16 software package was used to conduct the calculations on HPCMP resources, with in-house software for data analysis.

Results: The kinetically favored decomposition pathways of the sulfonic acids PFMS and PFES begin with elimination of HF forming a cyclic intermediate (α-sultone rather than epoxide); free energy barriers are 47.0 and 54.9 kcal mol^{-1} for PFMS and PFES, respectively. The resulting intermediate α-sultones are unstable; the subsequent elimination of sulfur yields the perfluoro carbonyl species $O{=}CF_2$ or $O{=}CF\text{-}CF_3$, but occurs with a smaller barrier of 5.7 and 10.8 kcal mol^{-1}). SO_3 elimination from PFMS and PFES leads to CF_3H and CF_3CF_2H. This pathway is significantly less thermodynamically favorable than the first steps of HF elimination, and the latter is both kinetically and thermodynamically preferred.

The decomposition pathways of PFMS and PFES at incineration temperatures of 600 and 1,200 °C show only minor temperature dependence in the barriers for individual decomposition steps, but large decreases in reaction free energy due to entropic effects. The preferred decomposition routes remain unchanged at these higher temperatures.

A detailed study of bimolecular reactions of PFMS, PFES, and the above reaction intermediates with O_2, H_2, O, H, and OH was performed, and results are currently being analyzed.

DoD Impact/Significance: Reaction rates, calculated from the results of the study, can be incorporated into existing kinetic models and enable accurate prediction of chemical reactions occurring in incinerators utilized for PFAS mitigation. This will enable optimization of incineration conditions to maximize destruction of PFAS and avoid releasing persistent and/or harmful products of intermediate combustion.

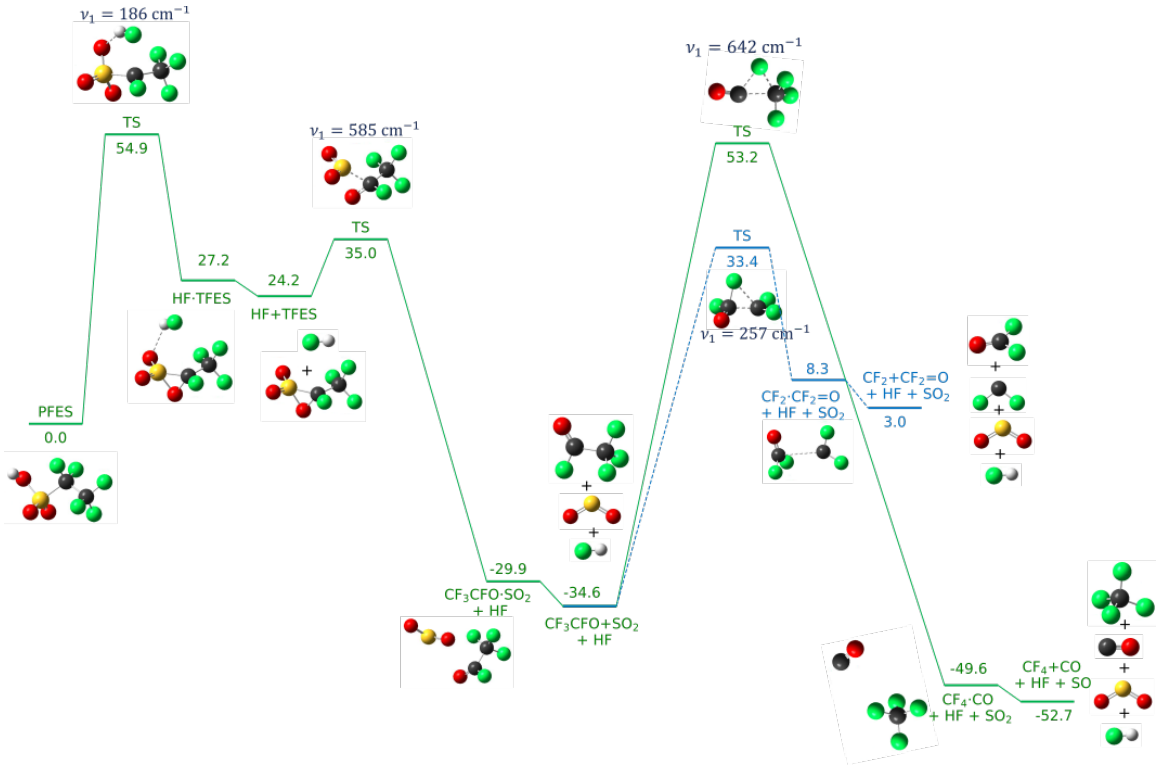

Figure 1. Gibbs free energy PES, drawn to scale, of the kinetically (green) and thermodynamically preferred pathways (blue) for the unimolecular decomposition of perfluoroethane sulfonic acid (PFES) at 298.15 K. Relative free energies are in kcal mol^{-1}. The magnitude of the imaginary vibrational frequency is listed for each transition state.

THIS PAGE INTENTIONALLY LEFT BLANK

CEA

Computational Electromagnetics and Acoustics

CEA covers two primary computational disciplines. Computational electromagnetics covers the high-resolution multidimensional solutions of Maxwell's equations. DoD applications include calculating radiofrequency (RF) sensor performance, radar scattering of tactical ground, air, and sea vehicles, the electromagnetic signature of buried munitions, high-power microwave performance, and the interdisciplinary applications in magnetohydrodynamics and laser systems. The computational acoustics area covers the high-resolution multidimensional solutions of the acoustic wave equations in solids and fluids. DoD applications include the modeling of acoustic fields for surveillance and communication, seismic fields for mine detection, and the acoustic shock waves of explosions for antipersonnel weapons.

Title: Low Grazing Angle Radar Backscatter
Author(s): J.V. Toporkov, J.D. Ouellette, P.A. Hwang, and M.A. Sletten
Affiliation(s): Naval Research Laboratory, Washington, DC
CTA: CEA

Computer Resources: Cray XC40 [ARL, MD]; Cray XC40/50 [ERDC, MS]; Cray Shasta [NAVY, MS]

Research Objectives: Coastal, shipborne, and airborne radar systems routinely encounter signal reflections from the sea surface, frequently under low-grazing-angle (LGA) conditions. Such surface signatures are often perceived as clutter that masks a target echo. On the other hand, they can be a source of information about local ocean conditions. Understanding the properties of sea surface backscatter, their relation to environmental parameters, and their distinctions from those of man-made target echoes is key to improving or even enabling performance of such radar systems and applications. This project investigates detailed characteristics of radar returns from ocean surface under both monostatic and bistatic observation geometries. The task is achieved through simulations that involve both direct numerical solution of the scattering problem and, where appropriate, numerical implementations of approximate scattering models.

Methodology: The approach combines a physics-based model for evolving ocean surfaces with computationally efficient, exact evaluation of the scattered electromagnetic field. A wind-driven surface is represented by realizations of a Gaussian random process defined by a certain wave spectrum. Interactions between surface harmonics are modeled by subsequent application of the Creamer transformation. The introduced hydrodynamic nonlinearities affect shape and motion of smaller ripples that have great impact on scattering of decimeter- and centimeter-scale electromagnetic waves. The field scattered by a "time-frozen" scene at a particular frequency is found by iteratively solving a boundary integral equation for the induced surface current. The formulation is based on first principles and automatically accounts for many phenomena (multiple scattering, shadowing) known to be problematic for analytical treatment. The calculations can be conducted at a number of frequencies covering certain bands to simulate pulse scattering. The procedure is repeated for every surface profile in the sequence representing temporal evolution. The simulations are limited to the two-dimensional (2D) space but have direct relevance to commonly occurring three-dimensional (3D) geometries (e.g., oncoming or receding long-crested waves).

Results: To help evaluate feasibility of passive remote sensing of a sea state utilizing illumination from geostationary communications satellites, we continued time-varying simulations for continuous-wave, time-harmonic, S-band signals with vertical (VV) and horizontal (HH) polarizations. Figure 1 illustrates the setup for the numerical experiment. Ocean-like surfaces were generated according to the advanced wave height spectrum developed by P. A. Hwang that accounts not only for the near-surface wind speed but also for wave age and other parameters. As before, Doppler analysis was employed, with the Doppler spectral width emerging as the most telling indicator of the sea state. In particular, it is sensitive to the so-called wave age, as is demonstrated in Fig. 2. Notably, the normalized radar cross section (NRCS) that the traditional scatterometry relies upon does not display much of a difference for the two cases. The simulations were also used to benchmark an approximate scattering model — the first- and second- order small slope approximation (SSA). Comparisons in Fig. 3 reveal the range of scattering directions where the model predictions are very close to the exact solution. Consequently, under those conditions, this more computationally economical SSA model implementation can be confidently employed to generate data ensembles for analysis.

DoD Impact/Significance: More comprehensive and detailed characterization of sea clutter will help in design and performance assessment of the Navy radar systems, especially those operating in the LGA regime. Bistatic configurations provide covertness for a passive receiver asset and could yield further performance enhancements due to peculiar scattering characteristics of surface and targets that do not emerge in the conventional monostatic case.

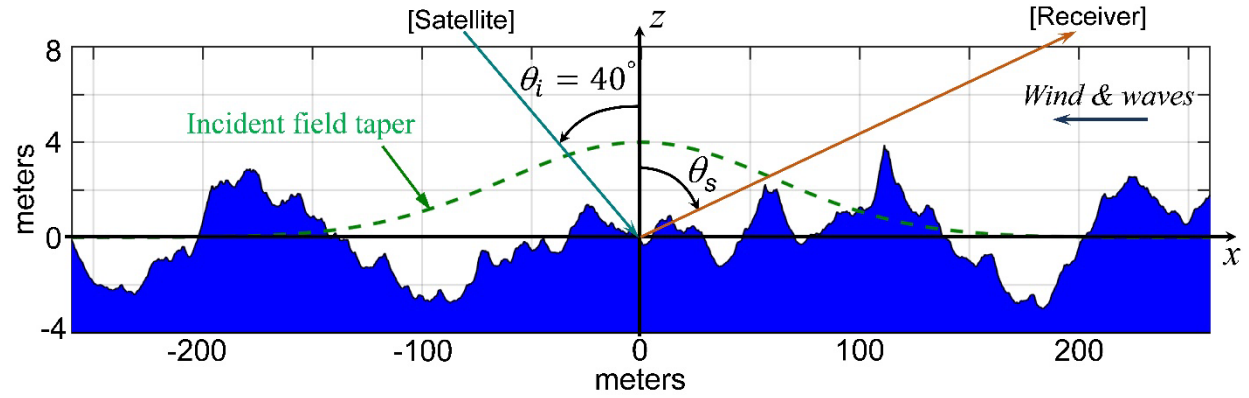

Figure 1. Setup for bistatic scattering simulations from evolving sea surface in the 2D space. All calculations are conducted at S band (2.3 GHz). The incidence angle θ_i is fixed at 40°, while the scatteting angle θ_s varies from -89° to 89°.

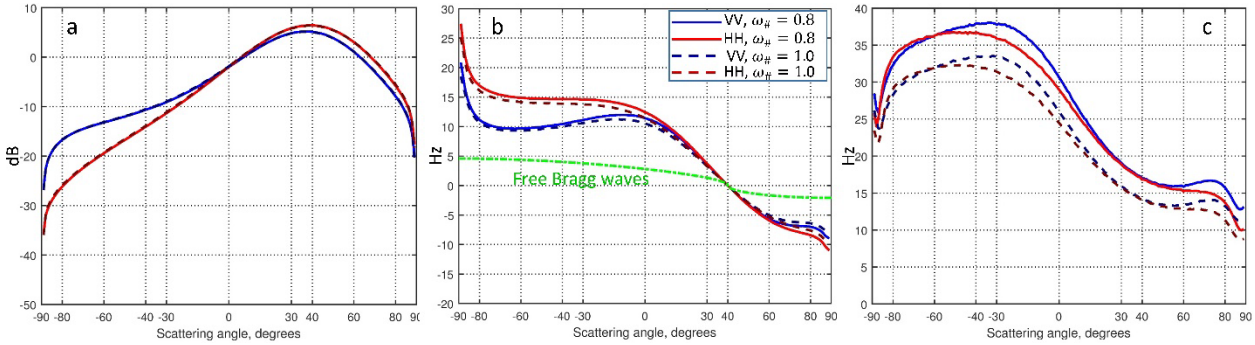

Figure 2. (a) Normalized radar cross section, (b) Doppler shift, and (c) Doppler width resulting from exact electromagnetic calculations for surfaces generated with Paul Hwang's wave spectrum. The wind speed U_{10} is set to 9 m/s, and the impact of inverse wave age $\omega_\#$ is explored. The value $\omega_\# = 0.8$ corresponds to the fully developed wind waves, while larger values describe "young seas". Deep water is assumed.

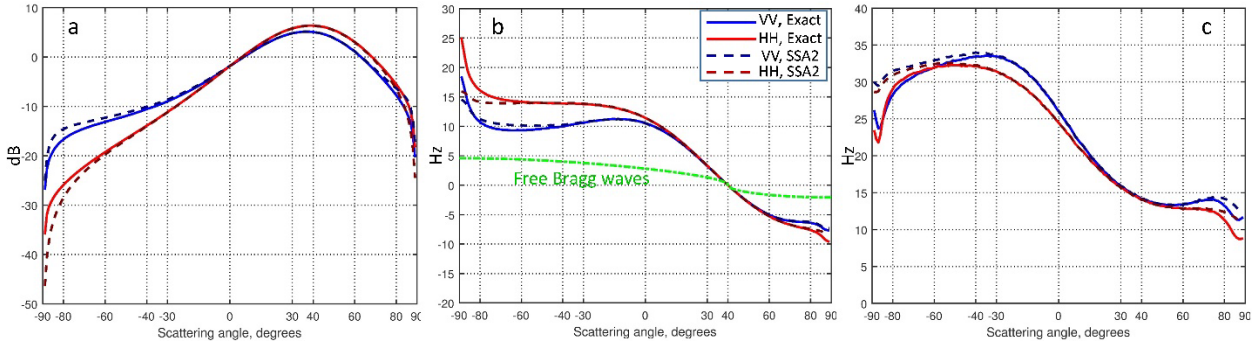

Figure 3. (a) Normalized radar cross section, (b) Doppler shift, and (c) Doppler width for surfaces generated with Paul Hwang's wave spectrum. The results obtained with the exact numerical electromagnetic technique and the second-order small slope approximation are compared. The wind speed equals 9 m/s and the inverse wave age is 0.8 (fully developed wind waves). Deep water is assumed.

Title: Small-Slope Approximation (SSA) Rough-Surface Backscattering Analysis
Author(s): J. Alatishe
Affiliation(s): Naval Research Laboratory, Washington, DC
CTA: CEA

Computer Resources: HPE SGI 8600, Cray Shasta [NAVY, MS]

Research Objectives: To determine and characterize the spatial coherence effects inherent in sea clutter by numerically analyzing the associated response at the antenna port of a monostatic radar. The sea-surface coherence effects are examined with respect to the associated antenna characteristics and the surface properties.

Methodology: The surface model used is based on the linear propagation model for deep-water ocean waves. Once the response from the surface has been computed, the properties of the simulated sea-clutter responses are characterized. The surface scattering amplitude (SA) characterizes the spatial coherence. A version of the small-slope approximation (SSA), which approximates the induced field distribution on the sea surface, is employed in the SA. Once the SA has been computed, the response at the antenna port is determined and the coherence effects due to the surface are examined. Numerical integration is used to determine the antenna response from the rough-surface profile. The sea surface is derived using the Elfouhaily ocean wave-number spectrum for wind speeds at 5 and 10 m/s for an upwind direction. With both the SA and the surface model calculated, the response at the antenna port was computed for each antenna aspect angle. The codes used to execute these steps were first written in MATLAB and then were converted into FORTRAN 90. The codes were then parallelized using the message passing interface (MPI) and were run on 1,024 processors or up to 32 graphics processing units (GPUs) at the Naval Research Laboratory (NRL) High-Performance Computing (HPC) facility. Simulations were conducted at X-band (10 GHz).

Results: Data obtained from published accounts of the simulated response from a sea surface were used as the baseline for comparison. These sea-clutter values were measured at various phase speeds and wind directions for given antenna aspect angles (elevation and azimuth) and polarizations of the antennas. The simulated received sea-clutter responses were computed for elevation angles of 80° and 85° for both vertical and horizontal polarizations. The simulation generated a 4,096-point frequency response of the notional sea surface for a given wind speed for an observed time increment. Fast Fourier transform (FFT) convolution was used to generate the complex time-dependent echo, which is the spectral product of the associated sea-surface frequency response and the transmitted waveform. As a result of the previous step, multiple coherent processing intervals (CPIs) were generated for analysis as depicted in Fig. 1. The number of spatial samples of the sea surface was set to 17,889 in the down-range dimension and 4,095 in the cross-range dimension. The simulation results showed that the range-Doppler properties are similar to real sea clutter in that the roughness scales of the sea surface are present in the spectral structure (no mean current) (see Fig. 2). In addition, some clutter phenomena present in the simulated data and the statistics of the clutter appear to give insight into understanding real sea-clutter data. Further investigation of the simulated data is still required.

DoD Impact/Significance: Understanding the spatial coherence effects in radar sea clutter provides further insight into the phenomenology of backscattering from the ocean. This will be useful in devising new algorithms for detecting threats over the sea.

Example results:

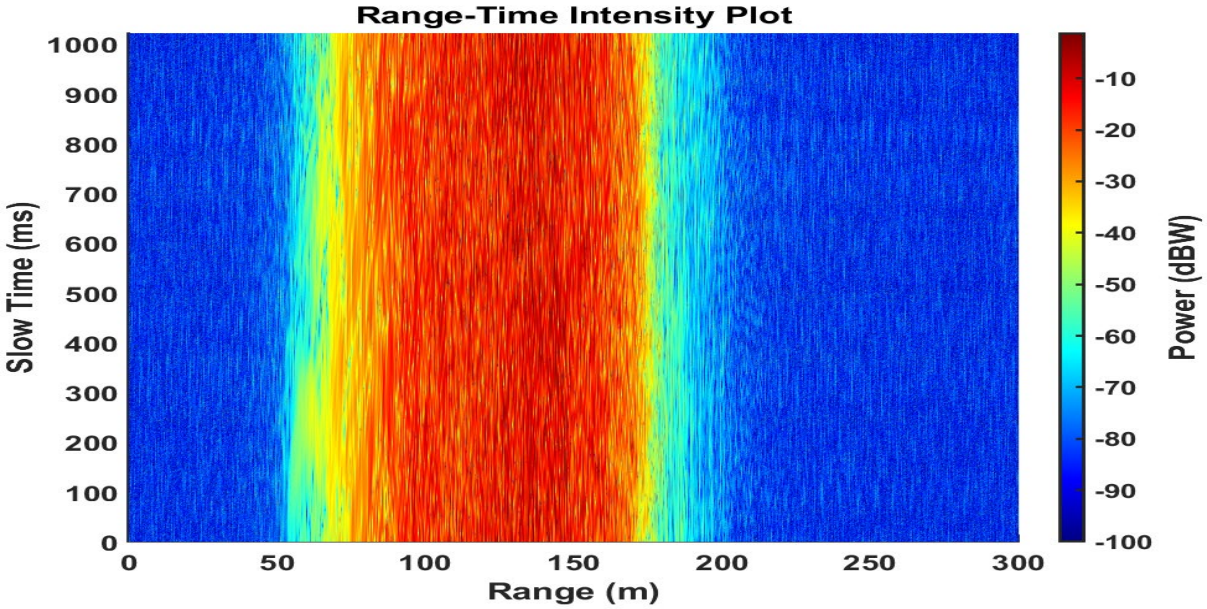

Figure 1. Range-time intensity plot of X-band sea-clutter returns for VV polarization at 85° elevation. Pulsewidth is 0.5 ns, pulse repetition interval (PRI) is 2 ms, and wind speed is 7 m/s toward the radar.

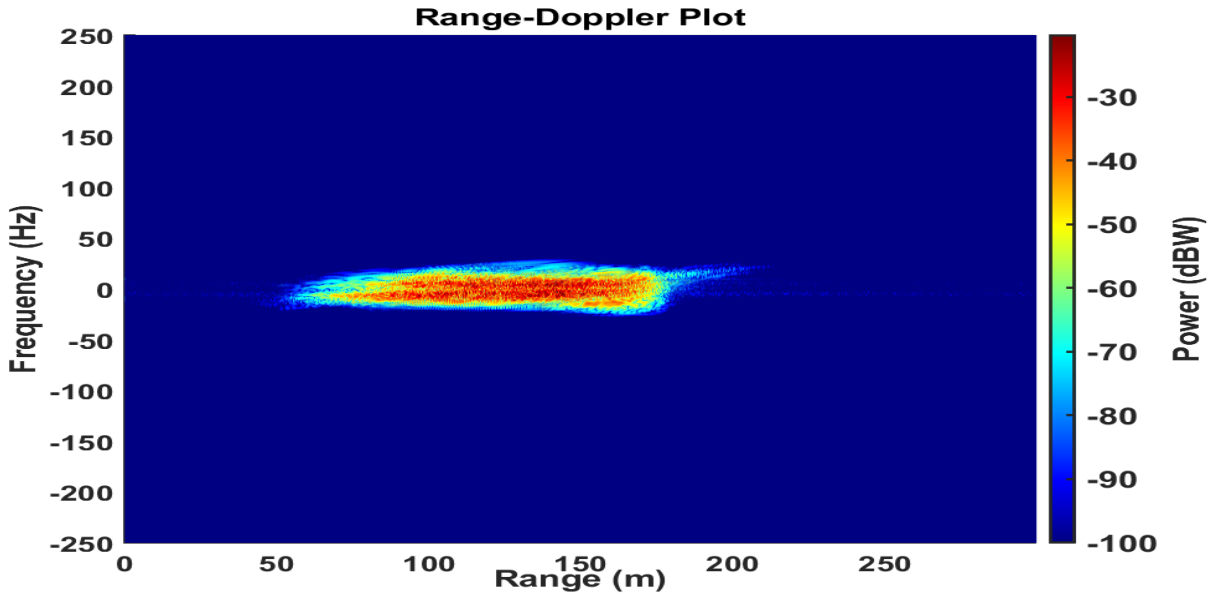

Figure 2. Range-Doppler plot of X-band sea-clutter returns for VV polarization at 85° elevation. Pulsewidth is 0.5 ns, PRI is 2 ms, and wind speed is 7 m/s toward the radar.

Title: Three-Dimensional Acousto-Elastic Modeling
Author(s): S. Dey,[1] M. Villa,[1] D. Hodyss,[1] E.L. Mestreau,[2] R.M. Aubry,[2] M. Williamschen,[2] and W. Szymczak[1]
Affiliation(s): [1]Naval Research Laboratory, Washington, DC, [2]Jacobs, Arlington, VA
CTA: CEA

Computer Resources: HPE SGI 8600 [AFRL, OH], [NAVY, MS]

Research Objectives: Develop and verify the acoustic response of a parametric model for a stiffened elastic cylindrical shell against a semi-analytical axisymmetric formulation. Quantify the impact of uncertainty in the material parameters and variations in structural arrangements on the scattering response of the shell, and develop algorithms for state estimation based on sparse sensor data.

Methodology: We utilized a high-order hp-finite- and infinite-element-based solver (STARS3D) developed at NRL for solving the coupled elasto-acoustics problem. This enables highly accurate solution of the scattering response up to the midfrequency regime. Use of fully three-dimensional elasticity in modeling the structure requires accurate geometric representation of the stiffened shell. In this effort, we used quartic ($p = 4$) basis functions, which require accurate representation of mesh geometry. Both of these requirements were met by using the DoD HPCMP CREATE(TM) Capstone platform for geometry and mesh generation, also developed by a team based at NRL.

For the state estimation and uncertainty quantification, we employed a Bayesian framework where the posterior prediction is based on a prior state and is improved using updates to the prior state from measurements or sensor data. The prior state is also known as the "offline" component and is generated using the computational tools made available by the DoD HPCMP. We have initially formulated the best linear unbiased estimate (BLUE) as the state estimation method to be used for the current problems of interest. The use of the BLUE for state estimation allows for calculation of the posterior error variance, which is interpreted as the expected total squared error of using this estimate and thus allows for the design for optimal sensor placement by applying optimization techniques.

Results: We computed the scattering response for the nominal structure over a distribution of elastic parameter values and plane wave forcing incidence directions in both monostatic and bistatic configurations for frequencies in the range [1kHz, 50kHz]. The computed scattering response for the nominal elastic parameter, an example shown in Fig. 1, was compared and verified against a semi analytical axisymmetric formulation. The ability to estimate quantities of interest (QOI) and to improve the uncertainty of the estimate based on updates to the prior state variables using sensor data and the BLUE methodology is demonstrated in Fig. 2 for the scattering from the same submarine-like target. The uncertainty manifests in the variability of the incidence angle of the plane wave loading. The prior state is generated on high-performance computers and the sparse sensor data is modeled using a leave-one-out analysis. It is demonstrated that the uncertainty associated with the state estimate is significantly reduced with the techniques used to incorporate sparse sensor data.

DoD Impact/Significance: Parametric models like the one developed in this effort help improve the understanding of structure-acoustic response of complex elastic structure and its sensitivity to various design parameters. This is critical to the development of better undersea warfare technologies and to the development of structural-acoustic digital twins that can be used in operational planning as well as condition-based predictive analytics of the real-time, operational state of an individual platform.

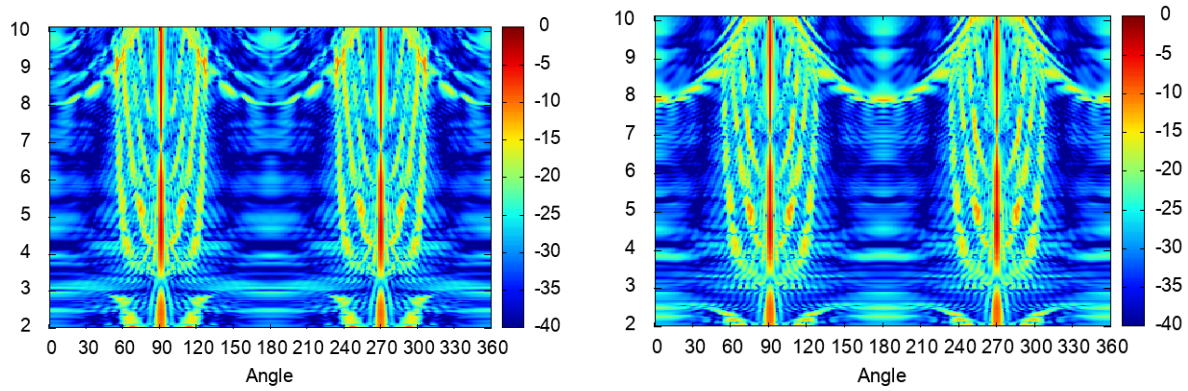

Figure 1. Monostatic free-field scattering target strength versus frequency and aspect angle as predicted with STARS3D (left) and an axisymmetric formulation (right)

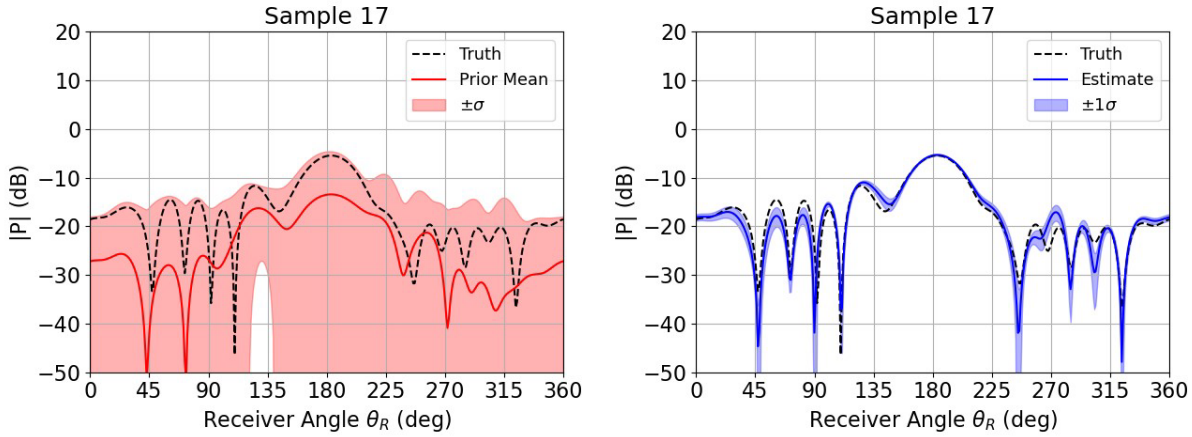

Figure 2. Estimate of the far-field pressure from a submarine-like target for a single sample from a leave-one-out analysis based on (a) the prior state and (b) the prior state updated with sparse sensor data, known as the posterior estimate. The standard deviation associated with the estimate is shaded, and the true far-field pressure is shown with the dotted black curve.

Title: Development of Advanced Pulsed-Power Applications and Modeling a System on Pulsed-Power-Driven Radiation Sources
Author(s): J.C. Foster,[1] S.B. Swanekamp,[2] and P.E. Adamson[2]
Affiliation(s): [1]Air Force Institute of Technology, Wright-Patterson AFB, OH, [2]Naval Research Laboratory, Washington, DC
CTA: CEA

Computer Resources: HPE SGI 8600 [AFRL, OH]; SGI ICE X, Cray XC40 [ARL, MD]; Cray XC40/50 [ERDC, MS]

Research Objectives: In pulsed power generator shots, nonuniform ion beams are experimentally problematic. The purpose of this research is to identify potential sources and to gain understanding of the causes behind ion beam nonuniformities on a target within the Gamble II pulsed power generator.

Methodology: Modeling the ion beams is done through the use of the three-dimensional capable, finite-difference, particle-in-cell (PIC) code Chicago by Voss Scientific. The PIC code employs a user-defined geometry and spatial grid to provide weighting between particles and grid points, and it solves Maxwell's equations to obtain the electric and magnetic fields by moving the particles via the Lorentz equation. Millions of particles are simulated to achieve the resolutions necessary to identify the potential sources of ion beam nonuniformity.

Results: During FY21, we were able to use Chicago simulations to identify potential sources of ion beam nonuniformity from "hot spots" in the geometry of the diode. It is possible that the electrons being admitted from the top of the cathode tips are experiencing a stronger magnetic field than electrons emitted on the face or bottom of the cathode tips. The electrons are also experiencing large swings in the strength of the magnetic field, which affects betatron motion towards the axis. These factors contribute to "hot spot" formation, which appears to be causing ion beam nonuniformity (see Fig. 1 for an example of the "hot spot" effects). Additionally, simulations done using Chicago have provided insight into the ion beam bending angle, which is related to ion beam quality. These simulations call into question previous assumptions that the bending angle is constant from a 1–6 cm radius, but more work is required to reach an explanation for this unusual bending seen in the simulations (see Fig. 2 for an example of the bending angle). Using other analysis and simulation techniques, we were able to take the results from Chicago and to analyze the current enclosed within the diode in an effort to gain insight into how particles from different diode surfaces behave within the diode region. Future work is needed to explain the cathode tip electron flow towards the anode (see Fig. 3 for an example of cathode tip electron flow). In FY22, we plan to further investigate the ion beam bending angle and the cathode tip electron flow, as well as to apply these methods to other diode geometries.

DoD Impact/Significance: The focus of this research is to improve the understanding of sources of nonuniformity in intense ion beams on the Gamble II pulsed power generator. Ion beams on Gamble II are used to perform radiation effects research and testing. This research will potentially lead to improvements to ion beam uniformity, which would increase confidence in nuclear weapon effects simulations for qualifying critical DoD components to operate in nuclear environments.

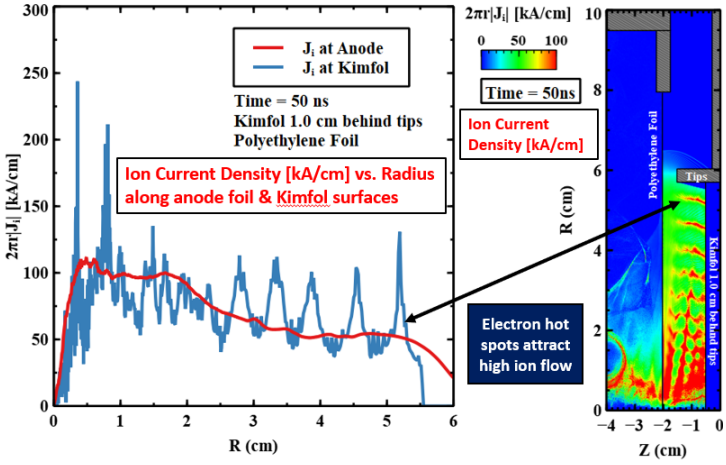

Figure 1. Plot of ion current density at 50 ns within the diode in units of kA/cm. On the left, a plot of the ion current density along the anode foil and Kimfol surfaces in the same units as a function of radius. The figure on the right shows higher ion current density in red. This higher ion current is correlated to the electron "hot spots." The plot on the left illustrates the impact these "hot spots" have on the uniformity of the ion beam. The peaks in blue on the left correspond to the streaks of red on the right. While ion emission appears relatively smooth along the anode foil surface, the ion flow becomes greatly distorted at the Kimfol surface.

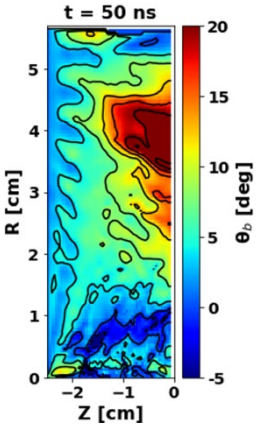

Figure 2. Contour plot of ion beam bending angle at 50 ns. While "hot spot" effects can be seen, high bending angles are observed, which was previously assumed to be constant from 1–6 cm radius. This illustrates that charged-particle dynamics play a role in ion beam uniformity.

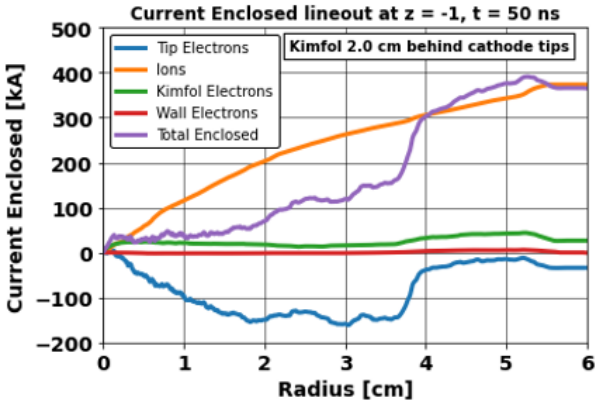

Figure 3. Plot of current enclosed within the diode that shows particle currents originating from different surfaces from within the diode. Painting different particle species within the simulations helps to gain understanding of charged-particle dynamics within the diode.

Title: Modeling Intense Electron Beam Driven Plasmas
Author(s): D.J. Watkins[1] and P.E. Adamson[2]
Affiliation(s): [1]Syntek Technologies, Fairfax, VA, [2]Naval Research Laboratory, Washington, DC
CTA: CEA

Computer Resources: SGI ICE X, Cray XC40 [ARL, MD]; Cray Shasta [NAVY, MS]; HPE SGI 8600 [AFRL, OH]

Research Objectives: In many plasma simulations, a molecule's electronic states are assumed to be in the ground state of the vibrational and rotational modes. In weakly ionized molecular regimes, a more detailed consideration of the molecular processes, including vibrational kinetics, is necessary. The purpose of this research is to compute the vibrationally resolved, inelastic electron scattering cross sections for electron-impact ionization of molecules. Initially, the methods are being applied to the diatomic molecule N_2.

Methodology: In this work, a semi-classical formula is used to compute the electron-impact ionization cross sections. The formula requires the kinetic energy of the participating electron orbital in the target molecule, the threshold energy for the ionization process, the number of effective equivalent orbital electrons, and the Franck-Condon factor (FCF) between the target molecule and the relevant cation. Because we are interested in the vibrationally resolved, state-to-state, ionization cross sections, multireference configuration interaction (MRCI) potential energy curves (PECs) are computed for the ground state and the exited states of interest for the target molecules and the cations. This results in the need for approximately 100 state-averaged MRCI calculations each with 15 to 20 different electronic states. This allows us to compute the vibrational eigenfunctions of each state as well as the vibrationally averaged target electron kinetic energies from the natural orbital kinetic energies and vibrational wave functions.

Results: Molpro was used for the quantum chemistry calculations, and its advanced MRCI methods and program control features provided accurate results for the PECs and natural orbital kinetic energies. A Fourier grid Hamiltonian method was applied to the resulting Molpro PECs to compute vibrational eigenfunctions and energy levels. The vibrational eigenfunctions were used to compute FCFs as the final input to the semi-classical formula to compute the vibrationally resolved, state-to-state, ionization cross sections. In total, we have computed 1000's of vibrationally resolved, partial cross sections, hundreds of lumped cross sections, and hundreds of total cross sections for electronic states of interest (see Figs. 1 and 2 for example results of the cross sections). In FY22, we plan to continue improving the results by establishing uncertainties in our calculations and applying the methods to other molecules.

DoD Impact/Significance: The vibrationally resolved, electron-impact ionization cross sections will support increased resolution of reaction networks for plasma chemistry models, directly leading to improved accuracy of various plasma simulations in many DoD applications. The primary focus of the current research is to improve the accuracy of our intense electron beam driven plasma simulations to validate advanced plasma chemistry models for use in particle-in-cell and fluid simulations.

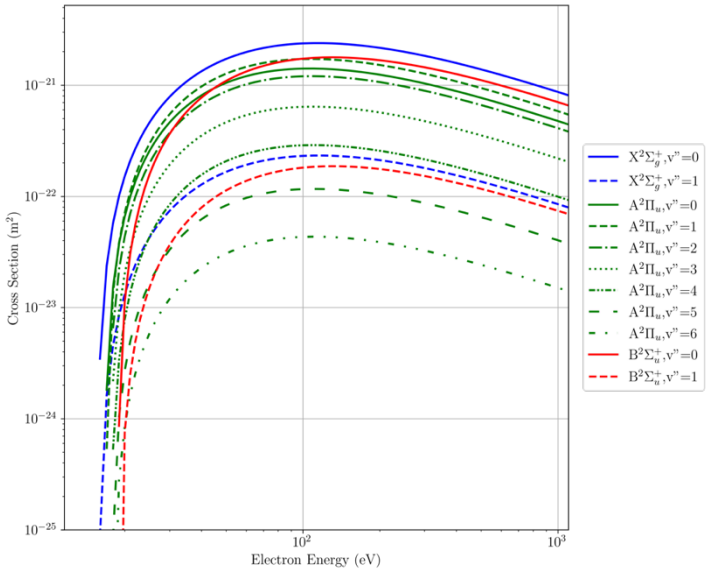

Figure 1. The computed partial electron-impact cross sections for N_2 ($X^1\Sigma_g^+, v'$=0) ionization to N_2^+ ($X^2\Sigma_g^+$, $A^2\Pi_u$, $B^2\Sigma_u^+$) states are plotted for values of v'' that contribute significantly to the total ionization cross section. The magnitudes and shapes of the partial cross-section curves vary as a function of the cation electronic and vibrational state. A family of curves such as these exists for each vibrational state v' of each electronic state of N_2.

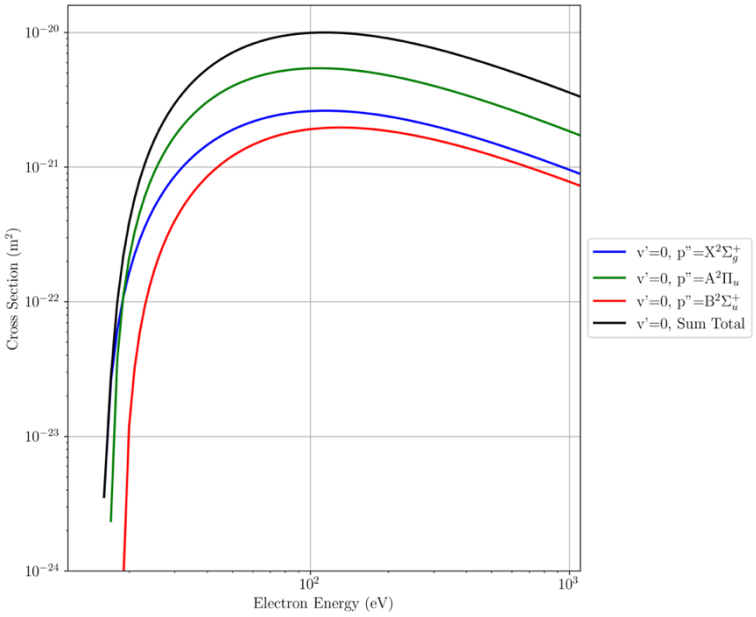

Figure 2. The computed lumped electron-impact cross sections for N_2 ($X^1\Sigma_g^+, v'$=0) ionization to N_2^+ ($X^2\Sigma_g^+$, $A^2\Pi_u$, $B^2\Sigma_u^+$) electronic states are plotted. The total cross section for N_2 ($X^1\Sigma_g^+, v'$=0) to N_2^+ is plotted in black and is the sum of the three lumped cross sections.

Title: Acoustic Parameter Variability over an Ocean Reanalysis (AVORA)
Author(s): J.P. Fabre
Affiliation(s): Naval Research Laboratory, Stennis Space Center, MS
CTA: CEA

Computer Resources: HPE SGI 8600 [NAVY, MS]

Research Objectives: Long-time reanalyses of the ocean are becoming available (e.g., NRL 7300) and are potentially extremely useful for understanding the variability of environmental parameters that impact acoustic sensor performance. The objectives of this effort are to investigate such potential, to provide recommendations for future Navy products to support operations, and to develop prototype products for test and evaluation.

Methodology: Investigate the NRL 25+ year Ocean Reanalysis to quantify and understand the variability over various time frames. Investigate the sensitivity of acoustic propagation and proxy parameters to the environmental variability. Investigate and assess appropriate averaging windows for a number of environments. Develop prototype products and make recommendations based on the results for products that could be derived from the described reanalyses. Such products will facilitate improved understanding of acoustic parameter variability in areas of propagation and ambient noise. Develop prototype products and test various ways of storing and accessing large data sets. NRL has been working extensively in the areas of big data and machine learning. We will include such technologies as part of our analysis, testing, and recommendations, and will incorporate lessons learned into existing products. If successful, these products could become Navy standard

Results: We supported several fleet exercises by analyzing fields from the reanalysis compared to real-world acoustic data to assess ocean acoustics. We also provided some research-based analysis for pre-mission support by analyzing current forecasts and past (reanalysis) trends). We used the transfer queue to cut out (from the global reanalysis) Navy areas of fleet interest and transfer to our local and classified systems for a number of current and future efforts including, but not limited to, premission support, data assimilation, model evaluation, and reconstruction and analysis. We are preparing to support some ONR Task Force Ocean (TFO) initiatives. This year's technical focus was on identifying significant acoustic change and the causal environmental changes, characterizing uncertainty, and compressing large ocean fields. The example figure shows acoustic transmission loss versus range and depth at four snapshots in time, approximately 9 hours apart in the northern Atlantic Ocean. Comparing the snapshots illustrates the variability of acoustic oceanography with time.

DoD Impact/Significance: "In Joint Vision 2020, the Department of Defense's strategic plan to ensure battlespace dominance in the 21st century, a key element is information superiority enabled by emerging technologies...." "An important aspect of information superiority is situational awareness. This implies knowing where you are, where allied and coalition forces are, and where enemy forces are. It means understanding the environment, from the seafloor to the top of the atmosphere." [Heart of ForceNet: Sensor Grid, Advanced Command and Control by RADM STEVEN J. TOMASZESKI]. Our efforts directly inform environmental variability as it applies to acoustics.

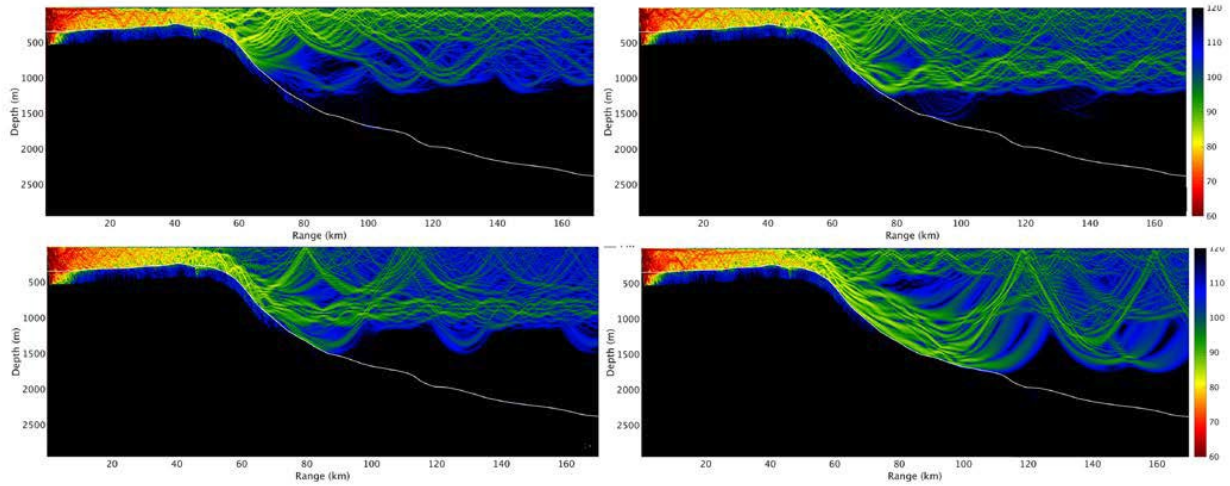

Figure 1. Examples of acoustic transmission loss versus range and depth at four snapshots in time, approximately 9 hours apart in the northern Atlantic Ocean. Comparing the snapshots illustrates the variability of acoustic oceanography with time.

Title: Computer-Aided Design of Vacuum Electronic Devices
Author(s): G. Stantchev,[1] S. Cooke,[1] J. Petillo,[2] A. Jensen,[2] S. Ovtchinnikov[2]
Affiliation(s): [1]Naval Research Laboratory, Washington DC, [2]Leidos, Billerica, MA
CTA: CEA

Computer Resources: Cray XC40 [ARL, MD]; Cray Shasta [NAVY, MS]

Research Objectives: 1) Continue to improve the Leidos MICHELLE charged-particle-beam optics code, the NRL TESLA, NETPUNE and CHRSTINE large-signal codes, and the new Leidos COMPASS design environment that works with the AFRL Galaxy Simulation Builder (GSB) to take advantage of DoD HPC hardware and software, enabling significantly larger high-fidelity simulations, optimizations, and sensitivity studies. 2) Further reduce simulation runtimes and boost user productivity in the design and development of vacuum electronic components and systems of interest to the DoD. 3) Employ the new capability in the design of next-generation vacuum electronic components with optimized performance.

Methodology: The MICHELLE/xVoyager code has been extended to a flexible heterogeneous computing framework that can be deployed on distributed memory HPC clusters, and including support for accelerators such as multicore CPUs and graphics processing units (GPUs). Also developed are several high-level interfaces to existing DoD HPC productivity tools for mesh generation, visualization, simulation environments, including GSB to incorporate other design codes, in addition to MICHELLE, into the pipeline of HPC-based optimizations. Moreover, the new Leidos COMPASS user design environment has been extended to transition the user from the initial design phase of building parametric CAD models and single simulations for early scoping to the optimization phase allowing optimal parameter sets to be derived within the HPC GSB/DAKOTA framework.
These objectives enable the HPCMP objective of exploiting technologies to maintain RDT&E leadership:
I. **Exploitation of Heterogeneous Computing Architectures:** Leveraging existing and emerging DoD HPC architectures to take advantage of distributed-memory HPC clusters and per-node computational accelerators such as multicore CPUs and GPUs.
II. **Integration into the existing DoD HPC ecosystem:** This includes the DoD CAPSTONE CAD/Mesh generator (CREATE-MG), and DoD HPC tools including AFRLs GSB, and Kitware's ParaView visualization software, available and supported through the DAAC.

Results: The focus of the project during FY21 has been on continuing the integration of the HPC version of MICHELLE and the other NRL physics codes as well as the integration with the productivity tools and HPC-enabled codes such as AFRL's ICEPIC and now the COMPASS tool. Figure 1 shows a COMPASS optimization of an electron gun. The beam diameter and current are optimized. The optimization is being used as the initial test case for running COMPASS on the HPC systems. Figure 2 shows the application of the new self-consistent thermal model in MICHELLE, where current through a fiber determines its thermal conductivity and electrical resistivity. The predicted current density includes contributions from both the electric field and temperature factors, and the implementation predicts thermal runaway and fiber failure for large-scale packed arrays. Figure 3 shows predictions of the temperature-limited to space-charge-limited thermionic emission Miram curves that result due to factors such as bitmap-defined surface work function variation. The current density, beam optics and self-consistent 3D space charge from surface band bending fields can be determined. Such scans comprise hundreds of parallel HPC runs per curve. Figure 4 shows hybrid meshing capability used to resolve fine features with unstructured meshing and large open-air regions with structured meshing. Figure 5 shows the hybrid meshing approach from Fig. 4, leveraged to automatically generate a block decomposition of a microstrip structure.

DoD Impact/Significance: This development has impacted several DARPA, ONR, AFRL and NRL programs in vacuum electronics by providing the ability to perform rapid analysis and optimization of mission-critical vacuum electron devices, previously deemed intractable via state-of-the-art methods.

DoD High Performance Computing (HPC) for Vacuum Electronics

Compass graphical user interface for an electron gun simulation

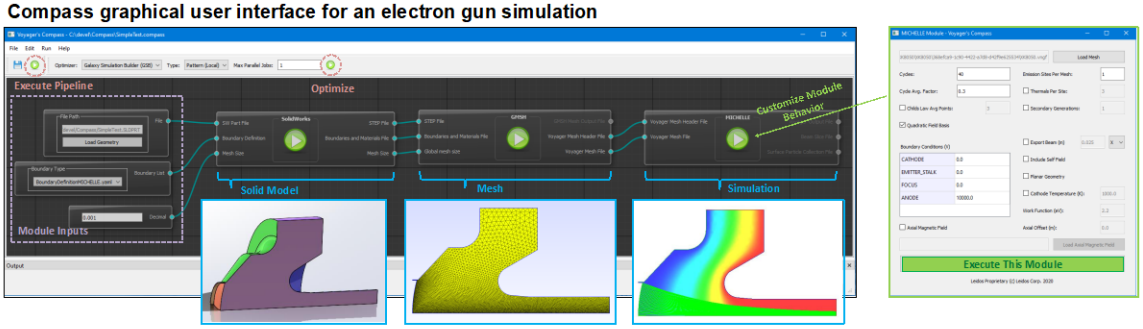

The Compass GUI is used to build a pipeline for generating the geometry, mesh and electron gun simulation. The design is optimized using DAKOTA, and tested on the HPC system.

Figure 1

Self-Consistent Electron Optics, Thermionic Field Emission & Thermal Heating of Fiber Emitters

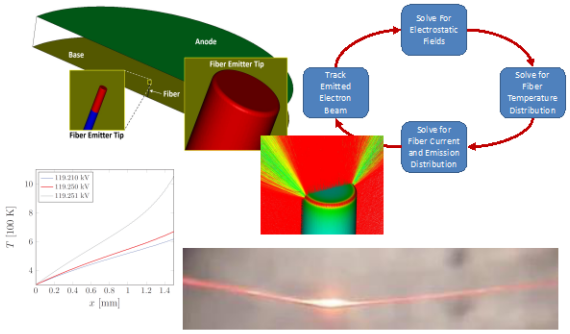

A new model was implemented into the MICHELLE electron beam optics code enabling the self-consistent determination of electron emission, fiber temperature and the prediction of fiber failure.

Figure 2

Microscopic Thermionic Electron Emission from Cathodes

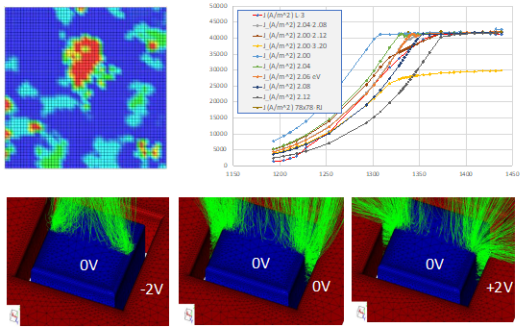

U. Wisconsin production of emission surface work function bitmaps enables the understanding of emission characteristics from the Temperature-Limited regime to the Space Charge-Limited regime.

Figure 3

Hybrid Structured/Unstructured Meshing on the HPC

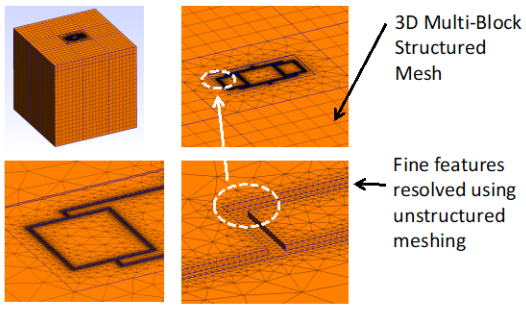

In addition to CAPSTONE, GMSH has been tested as an HPC capable scriptable mesher. GMSH adds the ability to build scripted hybrid meshes.

Figure 4

Automated Hybrid Meshing and Multi-Blocking

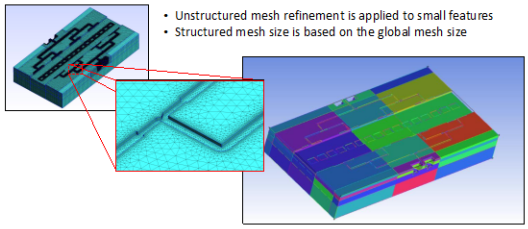

The microstrip geometry is broken into blocks. Blocks with microstrip are automatically tagged for unstructured meshing to resolve fine features while featureless blocks of air are selected for structured meshing.

Figure 5

Title: Intense Laser Physics and Advanced Radiation Sources
Author(s): D.F. Gordon,[1] J. Penano,[1] L. Johnson,[1] J. Isaacs,[1] D. Kaganovich,[1] B. Hafizi,[2] A. Davidson[2]
Affiliation(s): [1]Naval Research Laboratory, Washington, DC, [2]National Research Council Postdoctoral Research Associate, Naval Research Laboratory, Washington, DC
CTA: CEA

Computer Resources: HPE SGI 8600 [AFRL, OH]; Cray XC40/50 [ERDC, MS]

Research Objectives: The primary objectives of this program are to model the propagation of intense, short-pulse lasers in plasmas and other nonlinear media, and to provide computational support for experiments on the NRL MATRIX laser. Current areas of research include nonlinear laser propagation, interaction of short-pulse lasers with materials, plasma-based accelerators, novel sources of short-pulse infrared radiation, and ultrahigh-field physics.

Methodology: We use turboWAVE, an object-oriented framework, which contains modules designed to solve a variety of problems. Both fully explicit and ponderomotive guiding center particle-in-cell (PIC) modules are used to model relativistically intense laser pulses propagating in plasmas. Quantum optics modules are used to describe the interaction of the laser pulse with atoms or ions. Fluid modules are used to describe hypersonic flow and shock propagation in gas targets, as well as interaction of short laser pulses with metals and dielectrics for studying blow-off plasma generation. Optimization requires exploiting three levels of hardware parallelism: vector arithmetic units, shared memory threads, and distributed memory processes. The framework universally supports all of these using a combination of OpenMP directives for vector and loop parallelism, and the message passing interface (MPI) for distributed processes. Some modules support general purpose graphical processing units (GPGPU) via OpenCL. We use HELCAP to solve a paraxial wave equation with a large number of source terms representing atmospheric turbulence, dispersion and various nonlinear processes. HELCAP simulates the propagation of short and high-energy laser pulses, including adaptive optics. It is often useful to run a large statistical ensemble of initial conditions. For this purpose, embarrassingly parallel methodology is effective. Recently, we developed PyCAP, a Python version of HELCAP, which is accelerated using just-in-time compilation, including loop-level parallelism, and takes advantage of the parallel FFTW library.

Results: Significant effort was directed toward improvements to turboWAVE and development of PyCAP. Three-dimensional (3D) runs were made to model backward Raman amplification in the far infrared at wavelengths of a few microns. Extremely high-power long-wavelength lasers are still dominated by CO_2 laser technology, which, due to the limited bandwidth, even at high pressure, produces pulse durations of a few picoseconds at the shortest. Plasma compression overcomes this limitation by increasing the bandwidth via a nonlinear mechanism, while at the same time converting along pump pulse into a shorter and more powerful signal pulse. Transverse instabilities in the plasma lead to filamentation, which required the 3D simulations. Using a combination of fluid and PIC simulations with turboWAVE, we were able to pinpoint parameter regimes where the filamentation is minimized. Another area of active research is laser-material interaction. Absorption of short (femtosecond–picosecond) laser pulses by metals leads to heating and melting of the material surface, followed by the formation of ablated plasma. This phenomena was modeled with turboWAVE, using its unique capabilities as a fully nonlinear hydrodynamic code with a pressure-sourced electrostatic field solver. The calculated ablation depths for two metals, Al and Cu, were benchmarked against experimental measurements.

DoD Impact/Significance: Laser propagation in turbulent atmospheres and high-power pulsed sources of long-wavelength radiation are relevant for directed energy. Laser-driven accelerators and radiation sources have potential applications for ultrafast (femtosecond) imaging of chemical and biological systems. High-energy electron beams might be useful as a gamma ray source for detection of special nuclear materials (SNM). High-energy ions might also be useful for SNM detection, or for cancer therapy.

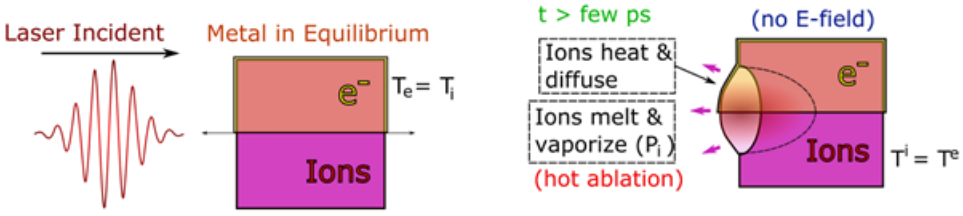

Figure 1. Laser ablation from metal surfaces by short-pulse lasers. Left pane: the laser is incident on a metal surface that is initially in equilibrium. Right panel: the electrons are heated and the resultant electron pressure gradient sources an electrostatic field, pulling ions out (cold ablation). Ions melt and vaporize (hot ablation).

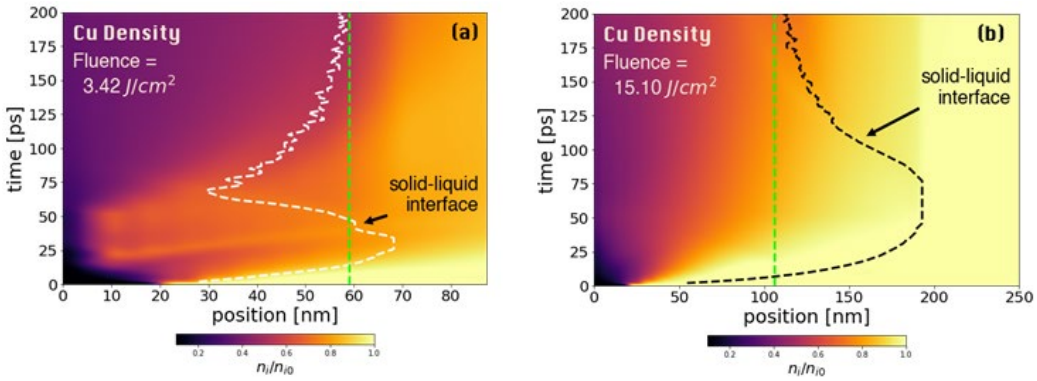

Figure 2. Cu density evolution plotted against the solid-liquid interface of the ablating surface, for $F = 3.42\ J/cm^2$ (a) and $F = 15.10\ J/cm^2$ (b). In both instances, the surface is initialized at $z = 20\ nm$. The vertical, lime-green lines represent the depth at which the solid-liquid interface equilibrates. The laser pulse impinges from right to left.

THIS PAGE INTENTIONALLY LEFT BLANK

CWO

Climate Weather Ocean Modeling

CWO focuses on the accurate numerical simulation of the Earth's atmosphere and oceans on those space and time scales important for both scientific understanding and DoD operational use. This CTA includes the simulation and forecast of atmospheric variability (e.g., temperature, winds, pressure, relative humidity, cloud cover, precipitation, storms, aerosols and trace chemicals, surface fluxes, etc.) and oceanic variability (e.g., temperature, salinity, currents, tides, waves, ice motion and concentration, sediment transport, optical clarity, etc.). Numerical simulations and real-time forecasts are performed from the very top of the atmosphere to the very bottom of the ocean. CWO also includes the development of numerical algorithms and techniques for the assimilation of in situ and remotely sensed observations into numerical prediction systems. CWO has DoD applications on a daily basis for specific warfare areas, mission planning, and execution (air, ground, sea, and space), as well as for flight and sea safety, search and rescue, optimal aircraft and ship routing, and weapon system design. This CTA provides DoD with: (1) real-time, high-resolution weather and oceanographic forecasts leading to incisive decision making and enhanced operational capability in adverse weather and ocean conditions and (2) realistic simulations of the dynamic oceanic and atmospheric environment to permit effective mission planning, rehearsal and training, and materiel acquisition.

Title: Turbulent Mixing in NCOM and HYCOM
Author(s): Y. Fan
Affiliation(s): Naval Research Laboratory, Stennis Space Center, MS
CTA: CWO

Computer Resources: HPE SGI 8600 [NAVY, MS]

Research Objectives: The goal of this project is to provide guidance on the proper setup of ocean boundary layer (OBL) mixing schemes within NCOM and HYCOM, including optimized vertical coordinate systems and resolutions, and to demonstrate the interaction mechanisms between the boundary layer turbulence and the submesoscale processes in the oceanic mixed layer.

Methodology: 1D NCOM, HYCOM, and NCAR large-eddy simulation (LES) experiments were conducted to evaluate the performance of six turbulent mixing schemes implemented in our ocean circulation models through systematically varying the coordinate systems and resolution. Carefully designed idealized 3D HYCOM, NCOM and LES experiments in the presence of moving and stationary submesoscale eddies were conducted to investigate the interaction mechanisms between the boundary layer turbulence and submesoscale processes in the OBL. Combined effects of the dynamical processes on different spatial scales in modulating the upper-ocean density structure were quantified.

Results: A new mixed-layer enhanced vertical grid is developed that outperforms both the uniform and uniform stretched grids currently used in NCOM with significantly fewer vertical layers used. The model accuracy is only strongly dependent on the resolution near the base of the mixed layer regardless of the total number of layers used. In our basin and global models, we often have water depths of several thousand meters and mixed-layer depth (MLD) reaches several hundred meters. Using the old vertical coordinate systems implemented in NCOM and HYCOM, limited by our computational resolutions, we can't afford to have a vertical grid that is fine enough to resolve the sharp layer at the base of the mixed layer needed to represent the physics that is essential to producing realistic upper ocean structure and attaining numerical efficiency. The newly developed mixed-layer enhanced grid through this project can be our pathway to better upper ocean predictions without any increase of computational resources. The effect of submesoscale eddies on oceanic boundary layer turbulence was investigated through controlled numerical experiments conducted using the NCOM, HYCOM and the NCAR LES model with a moving eddy. The mixed-layer dynamics and the variation of the MLD are very different at different locations relative to the eddy and between the HYCOM and LES simulations. Distinct dynamical processes are identified at different locations in the LES simulations. Along the center of the eddy, the turbulent field is dominated by strong shear production due to the geostrophic currents associated with the eddy, and the strong turbulent velocity fluctuations induced by the large horizontal shear brought by the eddy further act on the mean vertical shear to enhance the TKE and vertical mixing. On both sides of the eddy, the mixed-layer dynamics are dominated by the combined effect of Ekman buoyancy flux and geostrophic shear. While Ekman buoyancy flux transports denser/lighter water over less/more dense water on the right/left hand side of the eddy and results in a convectively unstable/stable state and destabilizes/stabilizes the water column, the presence of geostrophic shear that is aligned with/opposed to the wind-driven shear can also augment/reduce the wind-driven TKE generation that occurs through mechanical shear production. Both processes lead to enhanced/reduced turbulence and deepening/shallowing of the mixed layer on the right/left-hand side of the eddy. These mixed-layer behaviors are not observed in the HYCOM simulations because the K-Profile Parameterization (KPP) and the Goddard Institute for Space Studies (GISS) parameterization used in the model cannot represent the effect of horizontal gradients.

DoD Impact/Significance: This study will improve the battlespace environment forecasting accuracy for ocean models with more accurate vertical thermal profiles and better predication of acoustic and optic properties in the upper ocean. Strong scientific foundation and guidelines will be achieved for intelligent ocean forecasts for regional and global tactical planning.

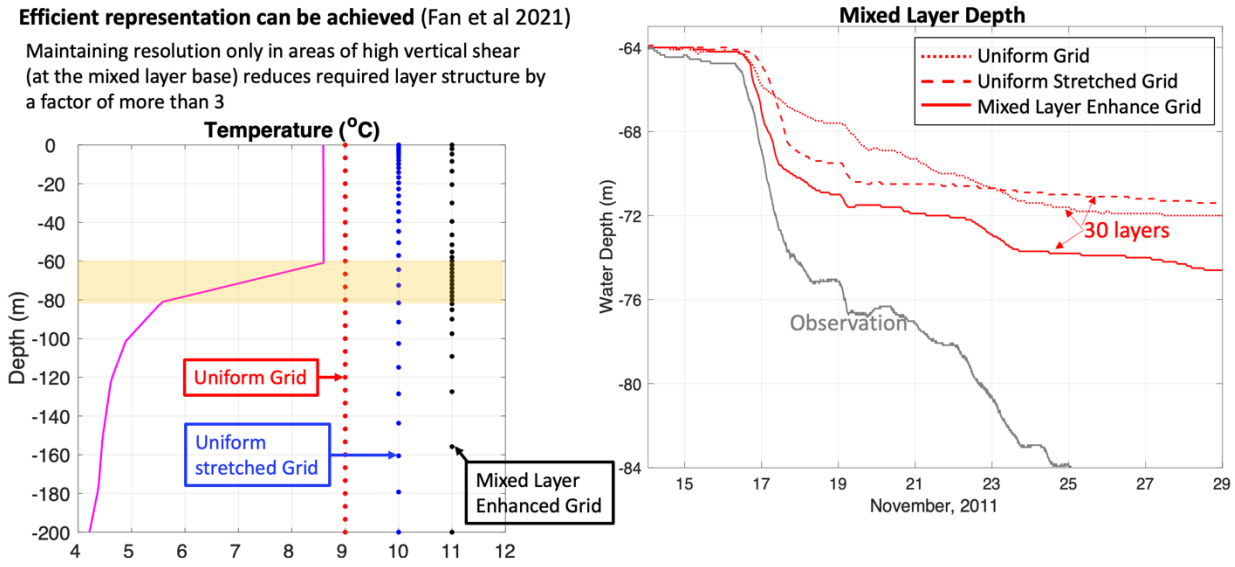

Figure 1. (left) Temperature profile (magenta) at Ocean Station Papa, and the uniform (red dots), uniform stretched (blue dots), and mixed-layer enhanced (black dots) grids used for model simulations (right) Modeled mixed-layer depth comparison using the three types of grids with 30 layers.

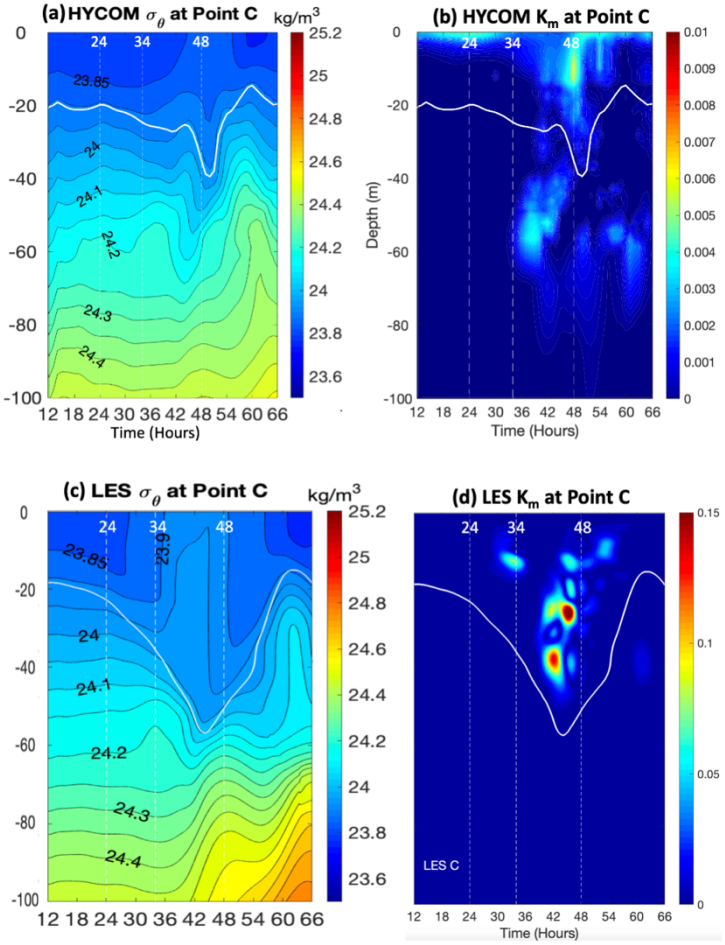

Figure 2. Potential density (σ_θ) and eddy viscosity (K_m) at Point C in the HYCOM simulation with KPP scheme and LES experiment LES_KPP1. The white solid line is the MLD in the experiment, and the white dashed lines indicate simulation hour 24, 34 and 48 respectively as marked.

Title: Data Assimilation Studies Project
Author(s): J. Tsu and W.F. Campbell
Affiliation(s): Naval Research Laboratory, Monterey, CA
CTA: CWO

Computer Resources: HPE SGI 8600 [AFRL, OH], [NAVY, MS]; Cray XC40/50 [ERDC, MS]; Cray Shasta [NAVY, MS]

Research Objectives: Data Assimilation (DA) corrects model analyses of the atmosphere, ocean or surface using a nonhomogenous observations. This project develops, tests, and improves: 1) our 4D-Var assimilation system, which is coupled to the atmospheric global model NAVGEM (Navy Global Environmental Model) and is used by the Navy Earth System Prediction Capability (ESPC), 2) fully ensemble-based DA, now including the ionosphere, 3) hybrid ensemble/4D-Var DA, 4) 4D-Var DA for COAMPS®[1], 5) adjoint, tangent linear, and forecast sensitivity to observations, 6) coupled DA (atmosphere, ocean, sea ice, etc. together), and 7) preparation for and test assimilation of new data types, both satellite and conventional. Our goal is to assimilate traditional data (generally in situ, e.g., weather balloons, ship, aircraft, or buoy reports) as well as data from a variety of new sources (often spaceborne) efficiently and effectively, to provide the best atmospheric analysis and ultimately to improve numerical weather forecast performance.

Methodology: A variety of experimental setups are used to develop and test our global and regional models and DA systems, as well as large datasets of in situ and satellite-based observations for several summer and winter months.

Results: A broad spectrum of research takes place under this project, using the Navy's latest global (NAVGEM 2.0, and Middle Atmospheric NAVGEM (HA-NAVGEM)) and mesoscale (COAMPS®) models, along with our global (NAVDAS-AR, hybrid NAVDAS-AR, and coupled hybrid NAVDAS-AR) and mesoscale (COAMPS-AR) DA systems. Results from FY21 research include: 1) development and testing of all-sky microwave radiance assimilation aboard the NPP and NOAA20 satellite platforms using NAVGEM, 2) measuring the impact of assimilating winds retrieved from HF radar, 3) assimilation of all-sky infrared (IR) radiances from geostationary satellites into COAMPS-TC®[2] to improve tropical cyclone (TC) forecasts, adding a new capability to Navy's battlespace environmental prediction to use satellite observations to predict TCs over oceans where other meteorological data are very limited in TC intensity and track forecasts from the all-sky radiance assimilation, 4) development of the NEPTUNE tangent-linear and adjoint models that provide the foundation for forecast initialization schemes, 5) development of a cycling ensemble Kalman filter (EnKF) DA system for the SAMI3 ionosphere forecast model, 6) testing of NIMO, a 3DVar ionosphere DA system ready for transition to the Fleet Numerical Meteorology and Oceanography Center (FNMOC) for operational evaluation, 7) computation and verification of new meteorological forecast variables required to support the Navy's new UAV, the MQ-4C Triton, and 8) development of machine-learning techniques to dynamically assign observation errors to satellite observations and to improve forecast error.

DoD Impact/Significance: HPCMP computing platforms provide a common environment for collaboration and the rapid development of NRL's multiple DA systems. Large common datasets can be stored and accessed by many researchers. The advancements of NAVDAS-AR, NAVGEM (including hybrid NAVGEM and HA-NAVGEM), and COAMPS-AR systems would not have been possible without the HPCMP systems.

[1]COAMPS® is a registered trademark of the Naval Research Laboratory.
[2]COAMPS-TC® is a registered trademark of the Naval Research Laboratory.

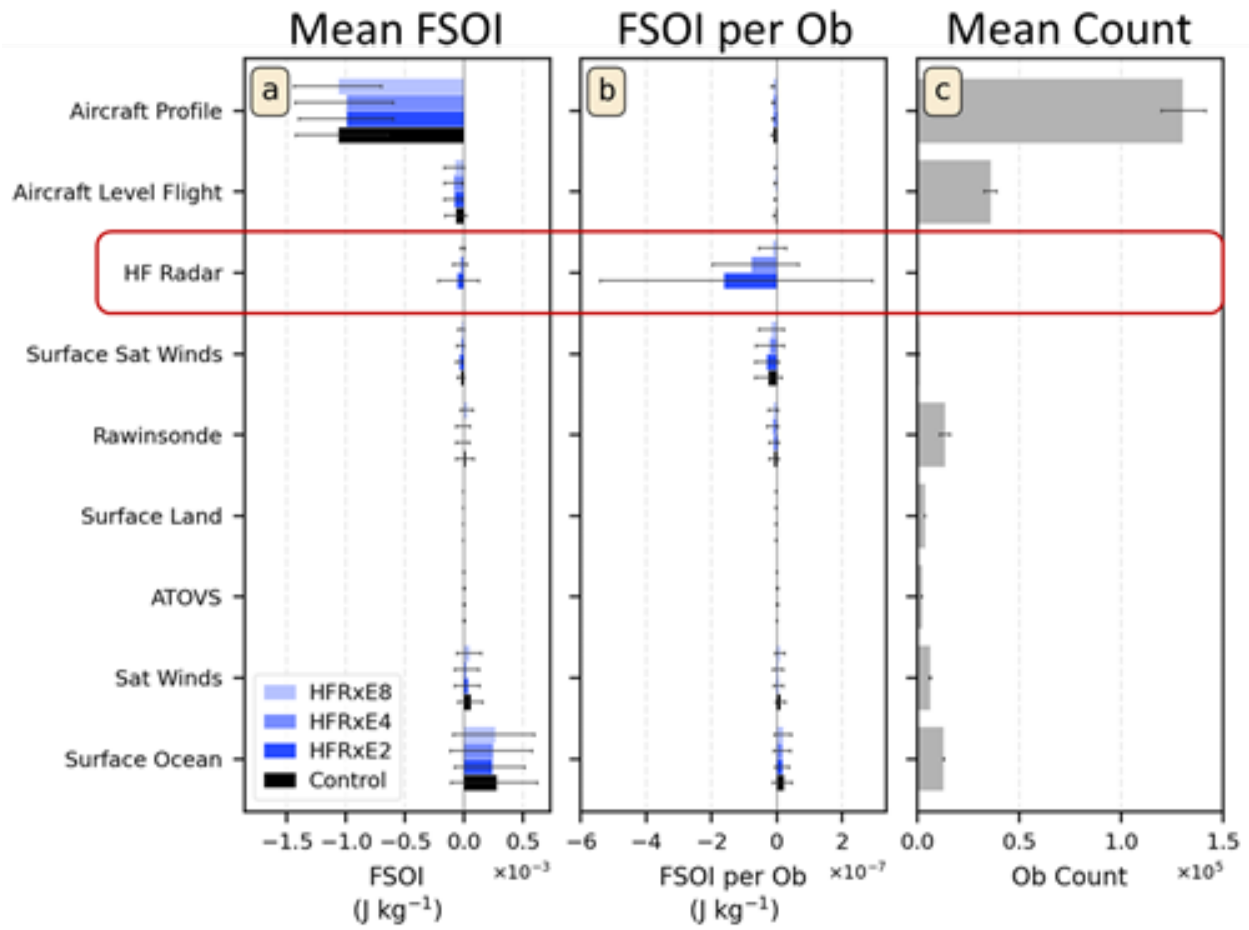

Figure 1. (a) Mean FSOI (b) mean FSOI per observation, and (c) mean observation count for each observation group for the control simulation (black) and high-frequency radar wind-retrieval experiments (shades of blue), using COAMPS®, aggregated over a nearly three-week period in October 2017 in Southern California. Error bars indicate the 95% confidence interval.

Title: Atmospheric Process Studies
Author(s): N. Barton, T. Whitcomb, W. Crawford, J. Ridout, K. Viner, J. McLay, M. Liu, T. Hogan, and C. Reynolds
Affiliation(s): Naval Research Laboratory, Monterey CA
CTA: CWO

Computer Resources: HPE SGI 8600 [AFRL, OH], [NAVY, MS]; Cray XC40/50 [ERDC, MS]; Cray Shasta [NAVY, MS]

Research Objectives: The research objectives of this project are to improve our understanding of the fundamental dynamical and physical processes that operate in the atmosphere and to develop and test a state-of-the-art global atmosphere-prediction system that includes data assimilation and ensembles.

Methodology: Our work focuses on improving the accuracy and efficiency of the Navy Global Environmental Model (NAVGEM). NAVGEM is the Navy's current global atmosphere operational numerical weather-prediction model and is used for basic and applied atmospheric research within this project. NAVGEM is developed in conjunction with its data-assimilation capability, NAVDAS-AR, as initial conditions are very important to numerical systems. In addition, seamless prediction across multiple temporal scales and Earth system components is the next frontier of numerical prediction. NAVGEM is being developed and tested when tightly coupled with the HYbrid Coordinate Ocean Model (HYCOM), the Los Alamos Community sea ICe Code (CICE), and the WAVEWATCH III®[1] wave model using the Earth System Modeling Framework (ESMF) tools under the Earth System Prediction Capability (ESPC) national program. This coupled modeling system is called Navy-ESPC. The focus on seamless prediction across temporal scales requires additional research and development on probabilistic prediction and diagnostics using ensembles.

Results: In FY21, minor upgrades to NAVGEM, the NAVGEM ensemble system, and the Navy-ESPC ensemble system transitioned to our operational partner, the Fleet Numerical Meteorology and Oceanography Center (FNMOC). NAVGEM 2.1 transitioned in December 2020 with updates in the data assimilation and the NAVGEM ensemble system updated to the NAVGEM2.0 code base, and the Navy-ESPC v1.0.1 transition included updates to scripts and code to aid in model debugging. In addition to scheduled upgrades, HPC resources were used to aid FNMOC upon a discovery of an issue in the operational forecasts of NAVGEM. NRL and FNMOC personnel were able to trace the issues to an improperly specified path that led to no satellite observations being assimilated. The issue was fixed and operational NAVGEM forecasts produced more robust results.

Another main result in FY21 was the testing ensemble development. The Navy-ESPC v1 perturbed-observation ensemble-of-data-assimilation (EDA) method does not generate enough spread in the initial conditions of the ensemble. The addition of relaxation to prior perturbations (RTPP) addresses the spread-skill deficiency at initial time by drawing the initial state of the ensemble away from the DA analysis and toward the prior state. The RTPP method has been tested in NAVGEM V1.X and compared to ensemble runs without RTTP. As the system cycles, it draws the spread-skill of the ensemble toward the ideal value of 1 (i.e., the ensemble spread and mean-squared error are perfectly matched) (Fig. 1).

DoD Impact/Significance: The continued development of our global forecast system is making significant positive impacts on the skill of our weather forecasts and DoD predictions dependent on weather forecasting (i.e., ocean modeling, wave modeling, ship routing). Developments in coupled modeling and extended range-probabilistic forecasting increase the utility of the forecast and potential number of users. This development serves to provide an improved modeling system for studying the dynamic and physical processes in the atmospheric system.

[1]WAVEWATCH III® is a registered trademark of the National Oceanic and Atmospheric Administration.

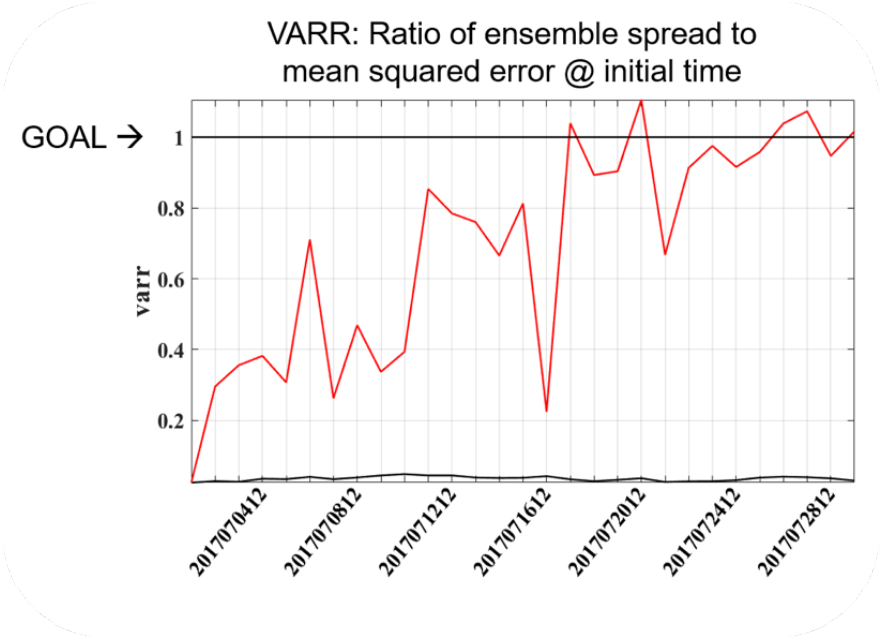

Figure 1. VARR: Ratio of ensemble spread to mean-squared error at initial time for (black) control (without relaxation-to-prior-perturbations (RTPP)) runs and (red) experiment run (with RTPP). The changes in the scorecard are verified against European Center analyses. As the system cycles, it draws the spread-skill of the ensemble toward the ideal value of 1. The control ensemble method does not generate enough spread in the initial conditions of the ensemble. RTPP addresses the spread-skill at initial time by drawing on the initial state of the ensemble away from the DA analysis and toward the prior state.

Title: Coastal Mesoscale Modeling — COAMPS-TC® Tropical Cyclone Rapid Intensification Prediction
Author(s): J.D. Doyle
Affiliation(s): Naval Research Laboratory, Monterey, CA
CTA: CWO

Computer Resources: HPE SGI 8600, Cray Shasta [NAVY, MS]; Cray XC40/50 [ERDC, MS]

Research Objectives: Tropical cyclone (TC) track forecasts have improved in a steady manner during the past several decades, but intensity forecasting has shown a much slower increase in skill during the same time period. This is due, in part, to our limited ability to properly model physical process controlling TC structure and intensity, but also is related to the inherent sensitivity that TC forecasts exhibit to initial conditions. The objective of this project is to advance and test COAMPS-TC®[1], a state-of-the-science numerical weather-prediction system designed for the simulation of TCs in support of Navy and DoD operations, and for civilian applications. The COAMPS-TC® system is operational at the Fleet Numerical Meteorology and Oceanography Center (FNMOC) and has undergone several substantial upgrades recently. The overall goal is to improve the COAMPS-TC® TC intensity predictions through improved vortex initialization and representation of physical processes.

Methodology: There are two types of COAMPS-TC® forecast experiments performed. The first type of application is used to facilitate rapid development and testing of COAMPS-TC®. The prototype testing for COAMPS-TC® needs to be rigorous and involves running approximately hundreds of individual cases in order to assess the performance of the system in a statistically meaningful manner. Each incremental change in the development process, such as an increase in resolution or improved parameterizations, needs to be tested through this procedure. This rapid prototyping is required to develop and evaluate the new version of COAMPS-TC® that will be run operationally at FNMOC. A second type of COAMPS-TC® application involves the near-real-time execution of an experimental version of COAMPS-TC®, which contains more advanced capabilities than the FNMOC operational version. The testing of the experimental COAMPS-TC® system is performed for many tropical cyclones in all basins worldwide.

Results: In the past year, many configurations of COAMPS-TC® were rigorously tested over a suite of storms in the Atlantic Ocean and Pacific Ocean basins based on three previous TC seasons. A new version with significant improvements was transitioned to operations at FNMOC in April 2021. These improvements included the use of high horizontal resolution (4 km), along with upgrades to the physics and model initialization. Figure 1 shows a series of five-day forecasts of the track and intensity for Hurricane Ida in late August and early September 2021. Hurricane Ida was a destructive Category 4 hurricane that severely impacted the U.S. Gulf Coast. As illustrated in Fig. 1, COAMPS-TC® accurately captured Ida's track and landfall location even at longer lead times. COAMPS-TC® also correctly and consistently forecasted the observed rapid intensification of Ida, which is a great challenge for models to capture. COAMPS-TC® continues to be one of the top-performing TC prediction models worldwide for track, intensity, and storm structure (storm size). This new, advanced version of COAMPS-TC® indicates even greater accuracy for improved research and operational TC applications.

DoD Impact/Significance: TCs remain one of the most disruptive and devastating environmental threats that impact U.S. Navy operations. We anticipate that an increase in accuracy of TC forecasts will result in significant cost benefit to the Navy through better sortie decisions and avoidance of hazardous winds and seas. Real-time testing and development of the system have led to significant improvements in the predictive skill of COAMPS-TC® and more rapid transitions to Navy operations at FNMOC. These improvements will inform future directions of TC model development, particularly as computational power increases, allowing for higher-resolution capabilities and increased fidelity in the physical process representations.

[1]COAMPS-TC® is a registered trademark of the Naval Research Laboratory.

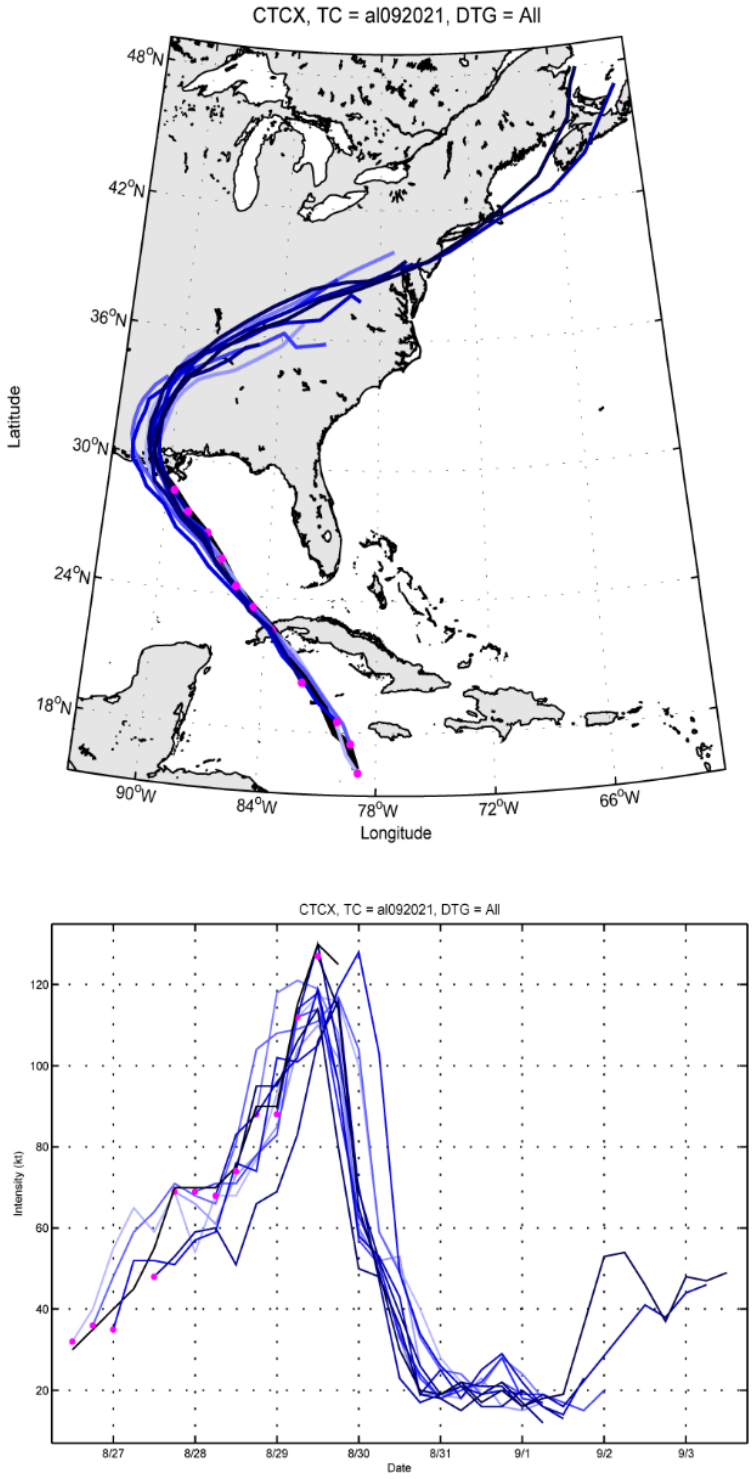

Figure 1. Five-day COAMPS-TC® forecast (blue) and observed (black) tracks for Hurricane Ida for August and September 2021 (top). The magenta dot shows the initial position for each forecast every 6 hrs. Five-day forecast (blue) and observed (black) intensity for Hurricane Ida (bottom). Progressively lighter blue color corresponds to earlier initialization times.

Title: Dynamics of Coupled Models
Author(s): I. Shulman, B. Penta, S. Cayula, and C. Rowley
Affiliation(s): Naval Research Laboratory, Stennis Space Center, MS
CTA: CWO

Computer Resources: HPE SGI 8600 [NAVY, MS]

Research Objectives: Improve our understanding of coupled bio-optical and physical processes in the coastal zone and the variability and predictability of the coastal ocean's optical properties on time scales of 1–5 days. Investigate the coupled dynamics of ocean bio-optical, physical and atmospheric models. Provide a foundation for the development of scientifically valid, dynamically coupled atmosphere-ocean models.

Methodology: The approach is based on using nested, coupled physical-bio-optical models of the coastal region together with bio-optical and physical in situ and remotely sensed observations. Data-assimilation techniques for both physical and bio-optical fields are being used to examine project research issues and objectives. Approach is also based on joint studies of the bioluminescence (BL) potential and inherent optical properties (IOPs) over relevant time and space scales. Dynamical, biochemical, physical and BL potential models are combined into a methodology for estimating BL potential and nighttime water-leaving radiance (BLw).

Results: We submitted a refereed paper, “Modeling studies of the bioluminescence potential dynamics in a high Arctic fjord during polar night”, to the journal *Ocean Dynamics*, Springer. During multiple Polar Nights, we demonstrated that upwelling and advection of deep bioluminescent taxa from offshore areas are dominant factors in observed BL potential dynamics in the top 50 m in the Arctic fjord of Svalbard, Norway. In order to optimize sampling strategies during the planned FY22 and FY23 field programs, we conducted preliminary studies of the origin and pathways (hydrographic history) of water masses circulating to the area of planned field programs (south of Svalbard, Norway).

We have been investigating the location of Iceland Faeroe Front (IFS) in the HYCOM model surface fields, as well as in satellite observations of sea surface temperature (SST) and chlorophyll (Chl). We found good detection and similar representation of the IFS front in SSTs fields as from the HYCOM, as well as from satellite Visible Infrared Imaging Radiometer Suite (VIIRS) (Fig.1). This can be explained first by the fact that the IFS front is considered as a thermal front, and second that satellite SSTs are assimilated into the HYCOM model. We found weak representations of the IFS in the VIIRS Chl fields.

DoD Impact/Significance: Emerging Navy electro-optical (EO) systems under development and special operations missions require an improved understanding of the ocean optical environment. This is critical for operations and weapon deployment, especially in the coastal and littoral zones. Improved basin-scale-to-mesoscale forecast skill is critical to both military and civilian use of the oceans, particularly on the continental margins.

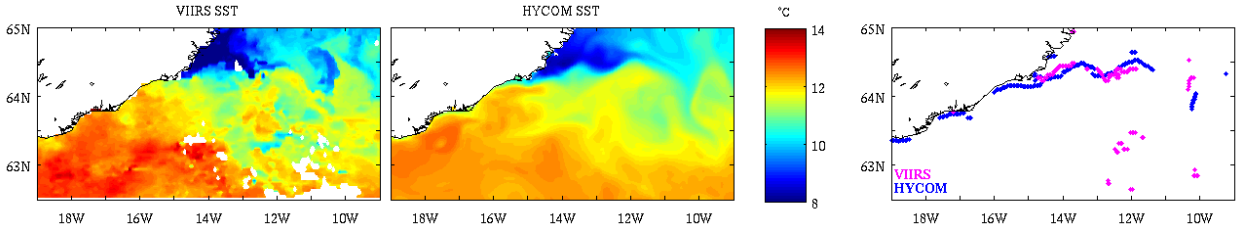

Figure 1. Representation of the Iceland Faroe Front (IFS) in the satellite VIIRS and HYCOM SSTs. Left: panel: VIIRS SSTs. Middle: HYCOM SSTs. Right: locations of IFS front in the HYCOM (blue) and VIIRS SSTs (magenta).

Title: Investigation and Implementation of GPU Capability to Next Generation Weather Prediction Code, NEPTUNE
Author(s): Y. Khine
Affiliation(s): Naval Research Laboratory, Washington, DC
CTA: CWO

Computer Resources: HPE SGI 8600 [AFRL, OH]; SGI ICE X [ARL, MD]; Cray XC40/50 [ERDC, MS]; Cray Shasta [NAVY, MS]

Research Objectives: The goal of this project is to investigate and implement GPU capability to Navy Environmental Prediction sysTem Utilizing the NUMA corE (NEPTUNE) code in order to enhance its performance and to utilize DoD GPU accelerator-based architectures for high-resolution 3D simulations.

Methodology: In FY21, the OpenACC implementation was continued for the standalone diffusion kernel of NEPTUNE code. The profiling of the OpenACC version of a standalone diffusion code resulted in poor performance, so a substantial optimization was performed. The methods used in optimizations included removing extraneous data movement and optimizing the loop structures within the GPU compute regions and collapsing the nested loops. In addition, the object-oriented features of FORTRAN 200X used in the code were not supported by OpenACC. A potential workaround was investigated to overcome the issue. Once the optimized code ran well on a single GPU, the focus turned to improving the performance on multiple GPUs. Tests were performed for a weak scaling study, where the number of processors and the problem size are increased.

Results: The performance of the original OpenACC version of the standalone code was studied and compared with the performance on a single CPU and using 32 CPUs. After optimizations of the OpenACC version, the performance was compared with previous test results. Also, the code was rewritten and optimized and the performance was compared with previous test cases. Figure 1 presents the timings of a standalone diffusion kernel of NEPTUNE code for the same problem size. We can see that the original OpenACC version execution time is higher than a single CPU run. The MPI version of the code performs well when compared with the original OpenACC version run with 32 CPUs. After performing optimizations of the original OpenACC version, the timings in the fourth column on a single GPU is comparable to the 32 CPU run. The rewrite and optimized version in the last column of the figure is close to the optimized OpenACC version. In this project, the groundwork has been laid for the NEPTUNE code to utilize GPUs via OpenACC on DoD DSRCs. The OpenACC implementation effort and converting the OpenACC version of diffusion kernel to OpenMP are currently ongoing in FY22. This work is essential to guide future development of NEPTUNE to utilize a more open programming standard for heterogeneous architectures.

DoD Impact/Significance: Since weather modeling requires a large computational domain on the scale of kilometers and a long enough time period, it is important to achieve results in desired time frame. The GPU implementation to NEPTUNE code will allow users to generate realistic simulations within a reasonable turnaround time while utilizing less HPC resources. Accurate weather forecast is very important to DoD to achieve successful missions and it is also vital in preventing potential natural disasters.

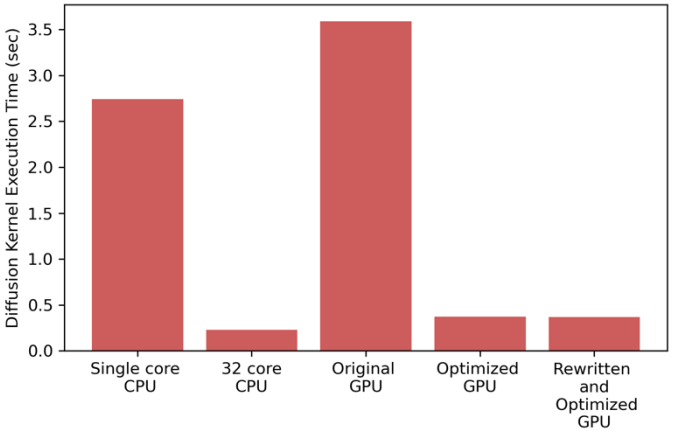

Figure 1. Comparison of original OpenACC, optimized OpenACC, rewrite and optimized OpenACC versions of a standalone NEPTUNE code on CPUs and a GPU. Lower is better.

Title: Rogue Wave Probability Estimator for WAVEWATCH III®
Author(s): M. Orzech and J. Dykes
Affiliation(s): Naval Research Laboratory, Stennis Space Center, MS
CTA: CWO

Computer Resources: HPE SGI 8600 [NAVY, MS]

Research Objectives: Overall objective is to develop and transition an integrated utility enabling WAVEWATCH III®[1] (WW3) to estimate the relative threat of rogue waves throughout the global ocean. The system operates in a broad range of deep-water wave environments and computes a rogue threat index (RTI) to estimate rogue threat as the product of several scalar metrics representing the contributions of selected environmental causal factors. Computations are based on established theory and extensive analysis of representative sea states. The project was moved to 6.4 level in May 2020. Objectives completed during the five-month FY20 period included initiation and partial completion of a 20-year WW3 reanalysis including wave-current interaction, implementation of the rogue threat utility in WW3, and initiation of system calibration. Objectives accomplished in FY21 included completion of system calibration, modification of system to implement RTI via a lookup table, and initiation of system validation. Objectives for FY22 include completion of system validation and transitioning of software to Fleet Numerical Meteorology and Oceanography Center (FNMOC).

Methodology: The WW3 reanalysis was completed in FY21Q1 by J. Dykes for the extended period of 1995–2020 inclusive. The simulations used the 3-grid IRI setup with GOFS3.1 surface currents and CFSR winds. For the system calibration, rogue event data from a large buoy database (Orzech & Wang, 2020) were used together with WW3-generated wave spectra, current fields, and wind fields to determine the RTI values for all identified rogue wave events during the period 2000–2009. We quantified the rogue wave likelihood using the positive predictive value, $PPV = TP/(TP+FP)$, in which TP is the number of correctly identified rogue events ("true positives") and FP is the number of non-events that were incorrectly marked as rogues ("false positives") for over 4,000 combinations of the four causal factors. Note that the PPV likely underestimates the likelihood of a ship encountering a rogue wave, as it is based upon rogue event data from buoys that are much smaller than ships (Fig. 1).

With the calibration completed, we have now begun work on the system validation. The second half of the WW3 reanalysis (2010–2019) is utilized with the RTI lookup table along with available buoy data for the period. In this case, an RTI value is determined for every time step of the reanalysis at the 34 available buoy locations. Each value of RTI (divided into bins of width 0.1) is compared with the rogue occurrence rate, $P/(P+N)$, in the buoy data at each buoy location.

Results: For all time steps of the 10-year calibration, the PPV ranged from approximately 1/100,000 to 1/5. The specificity $(Sp=TN/N)$ values computed for the 10-year dataset ranged between 0 and 1, measuring the consistency of the model in correctly predicting "nonrogue" cases. To minimize "false alarms" by the system, only the PPV values for causal factor combinations resulting in $Sp > 0.99$ were included in the lookup table (PPV was set to zero in the table for cases with $Sp \leq 0.99$). The PPV ratios were then recalibrated to RTI values between 0–10 and were entered into an ASCII-format lookup table, which WW3 was configured to load at run time. Sample plots of RTI were created for selected dates (e.g., Fig. 2).

DoD Impact/Significance: Accurate prediction of environmental hazards is important to tactical and strategic operations in the world's oceans. The results obtained from these simulations will form the core of the configurable WAVEWATCH III® rogue threat utility, which will enhance the safety of Naval missions and will reduce the potential for damage or loss of Navy assets in rogue wave events.

[1]WAVEWATCH III® is a registered trademark of the National Oceanic and Atmospheric Administration.

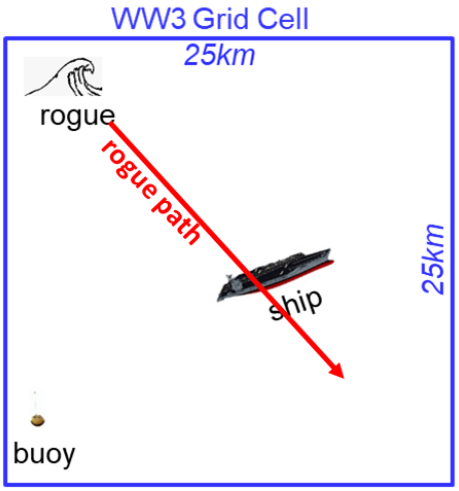

Figure 1. Idealized illustration of rogue wave in WW3 grid cell with ship and buoy. The rogue path will traverse only a small fraction (~ 1/250th) of the grid cell, while the buoy occupies an even smaller area. A ship, occupying much more surface area than a buoy, is more likely to be hit by a rogue wave. Thus, many more rogue waves will appear in a grid cell than are measured by a buoy over any given period, and a ship in the cell will face a greater threat of being hit by a rogue than will a buoy.

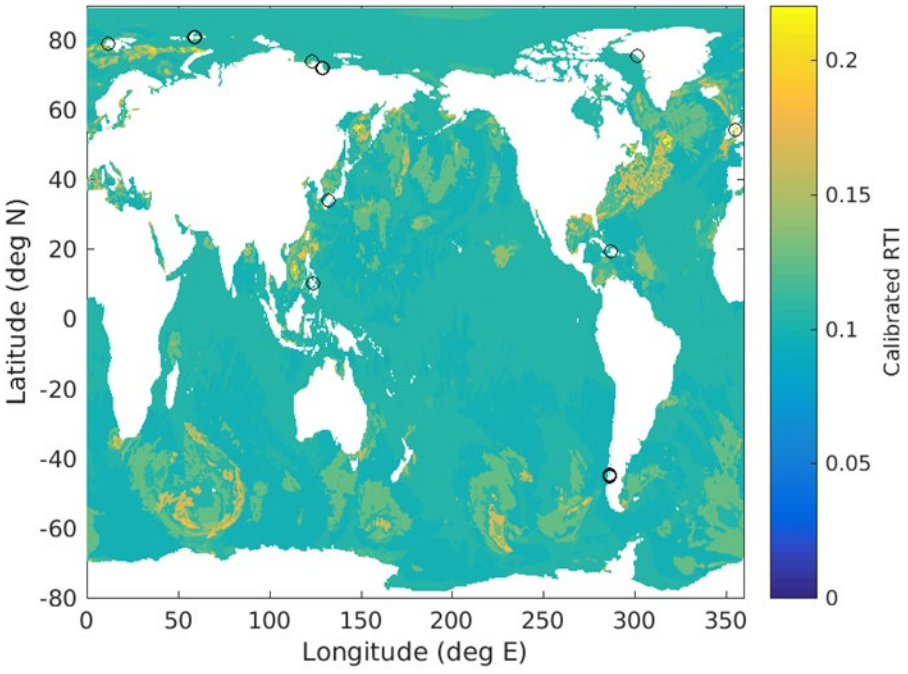

Figure 2. Sample RTI global output (from normalized lookup table) from a single time step of WW3 test case (09 November 2019, 0900 hr). Note that nearly all RTI values for this single time step are small, as would be expected for these rare events. Full range of calibrated RTI is 0–10. Black circles indicate locations with RTI greater than 0.5. The largest RTI value for this case is approximately 1.10 (near the west coast of South America).

Title: Ocean Data Assimilation
Author(s): S. Smith,[1] L. Smedstad,[1] C. Barron,[1] B. Bartels,[2] M. Carrier,[1] J. Crout,[3] J. D'Addezio,[1] C. DeHaan,[2] S. deRada,[1] D. Dobson,[1] R. Helber,[1] Z. Lamb,[2] R. Linzell,[2] B. Maloy,[1] J. May,[1] H. Ngodock,[1] J. Osborne,[1] G. Panteleev,[1] I. Pasmans,[4] M. Phelps,[2] C. Rowley,[1] T. Smith,[1] I. Souopgui,[4] P. Spence,[2] T. Townsend,[1] and K. Weber[1]
Affiliation(s): [1]Naval Research Laboratory, Stennis Space Center, MS, [2] QinetiQ North America, Stennis Space Center, MS, [3]American Society for Engineering Education, Stennis Space Center, MS, [4] University of New Orleans, Stennis Space Center, MS
CTA: CWO

Computer Resources: HPE SGI 8600, Cray Shasta [NAVY, MS]; Cray XC40/50 [ERDC, MS]

Research Objectives: The scope of this project is to advance the analysis and prediction capability of the Navy's environmental modeling and forecasting systems through the improvement of the assimilation software used to merge incoming observations with model forecast fields. Twelve funded NRL projects utilized this subproject in FY21 to perform experiments that went toward either using, adding, improving, or validating various capabilities of ocean data assimilation. A few of these efforts include: 1) further validating the 4DVAR for transition, 2) developing and testing a multiscale capability to better resolve small-scale features, and 3) implementing and testing the capability to assimilate velocity and acoustic observations.

Methodology: The following seven NRL projects used the majority of hours allocated for this HPC subproject to help advance ocean data assimilation in FY21: (1) The 6.4 NCODA-4DVAR project performed additional validation experiments in the northern Atlantic Ocean. (2 & 3) Both the Ocean of Things and the 6.4 ISOP projects performed numerous velocity assimilation tests using both 3DVAR and 4DVAR within COAMPS®[1]. (4) High-resolution 4DVAR OSSEs were performed in the northeastern Atlantic under the Determination of Asset Requirements (EDI) project testing the optimal number and positions of float placement. (5) The Global Heterogeneous Observation System (GHOST) project performed experiments testing new simulation packaging and simulations of new capabilities. (6) The NCODA-NEXT project tested the updated and standardized NCODA software. (7) The 6.2 LATTE project tested the coupled ocean-acoustic 4DVAR assimilation system. There were an additional five NRL projects that minimally used hours under this subproject: (8–12) The Ice DA Development, 6.4 NCODA, Operational Altimeter Processing, 6.2 Smart Gliders 2, and Space METOC projects.

Results: Numerous 3DVAR and 4DVAR experiments were performed using NCODA and COAMPS® under this FY21 HPC subproject with the overall result of improving the analysis accuracy, prediction skill, portability, and robustness of the system. A few of the specific advancements made include standardizing the NCODA software to simplify future updates, coupling the ocean and acoustic assimilation systems, a multiscale assimilation system allowing higher-resolution data assimilation, and the assimilation of velocities (Fig. 1), acoustics, and SWOT observations.

DoD Impact/Significance: The assimilation experiments tested under this project went toward improving the Navy's capability of forecasting the ocean environment and directly address Navy priorities as outlined in the following documents: OPNAVN2N6E FY 2021 RDT&E Priorities Letter 3062, Ser N2N6E/20U119707 (March 26, 2020), and the NRL ocean-modeling road map developed in consultation with the Navy operational modeling centers NAVOCEANO and FNMOC. In addition, the transition of the NCODA-4DVAR and velocity 3DVAR data-assimilation systems made significant progress this fiscal year. Finally, advancements were made to the GHOST system that provides guidance for flight paths of UUV observing platforms.

[1] COAMPS® is a registered trademark of the Naval Research Laboratory.

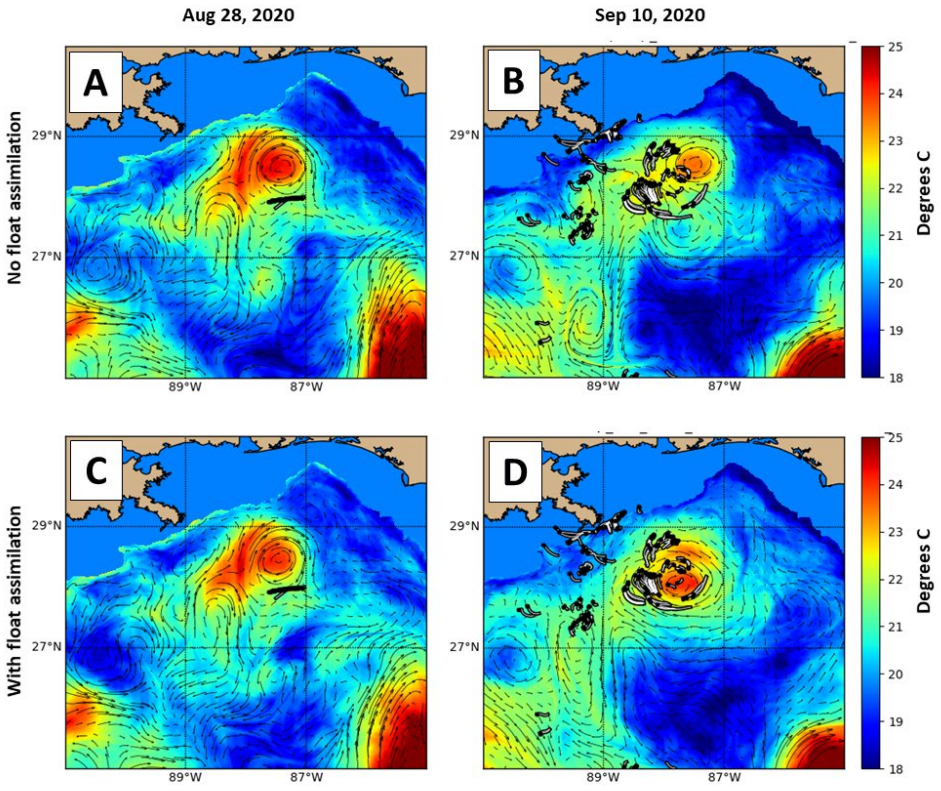

Figure 1. Twin COAMPS® experiments were performed for the Gulf of Mexico, one with velocity assimilation inferred from float trajectories (panels C and D), and the other without (panels A and B). Both experiments assimilated the operational data stream of temperature and salinity observations. The panels show temperatures at 100 m depth (color contours) on Aug. 28, 2020 (panels A and C), and on September 10, 2020 (panels B and D). The overlaid black dots represent the float positions and the white tails are their previous positions for the past day to represent their movement. The deployment of the floats began on August 28, which is why panels (A) and (C) are similar. Panel (D) shows that after two weeks of velocity assimilation, the position of the anticyclonic eddy has been corrected to match the float movement.

Title: Coastal Mesoscale Modeling
Author(s): W.A. Komaromi and P.A. Reinecke
Affiliation(s): Naval Research Laboratory, Monterey, CA
CTA: CWO

Computer Resources: HPE SGI 8600, Cray Shasta [NAVY, MS]; SGI ICE X, Power 9 [ARL, MD]; Cray XC40/50 [ERDC, MS]

Research Objectives: Our objective is to develop and validate a fully coupled coastal/littoral prediction system that can be used to provide high-resolution (< 5 km) data assimilation (DA) and short-term (0–48 h) forecast guidance for tactical-sized areas of the world. This system can also be used for basic and applied research leading to an improvement in our understanding of atmospheric and oceanic processes. Improvements to our mesoscale prediction systems and DA systems will result from this research.

Methodology: The Coupled Ocean/Atmosphere Mesoscale Prediction System (COAMPS®[1]) is being developed further for independent and coupled simulations of the atmosphere and the ocean for the mesoscale. The atmospheric component of COAMPS® is made up of a DA system, an initialization procedure, and a multinested, nonhydrostatic numerical model. This model includes parameterizations for moist processes, surface and boundary-layer effects, and radiation processes. The NRL Coastal Ocean Model (NCOM) is currently being used for the simulation of the mesoscale ocean circulation response to the COAMPS® forcing in one-way and two-way interactive modes. COAMPS® also has been modified recently to predict electro-optical quantities of interest for directed-energy applications.

Results: In FY21, HPC resources were used to run COAMPS® simulations for a validation test report (VTR) to transition refraction index structure parameter calculations for COAMPS®. Two different refractive index structure parameters were tested and implemented: Wang et al. (2020) (W20) and Cherubuni and Businger (2012) (CB12). In Fig. 1, these two methods are compared against ship (FLIP) observations. HPC resources were also heavily leveraged in support of testing and evaluation for a number of other transitions to operations, including COAMPS® Forecast Sensitivity to Observation Impact (FSOI), new diagnostic fog output from the atmospheric model (COAMPS®), and an updated land surface model (LSM) from NOAHv3.2 to NOAHv3.6 in COAMPS® 2021. A number of research projects also resulted in publications in FY21, including observation impact data-assimilation experiments, high-resolution Arctic sea ice experiments that heavily depend upon accurate air-sea-ice coupling and the recently updated land surface model, an investigation of elevated Kelvin-Helmholtz billows on the atmospheric boundary layer, and a detailed performance evaluation on the prediction of cloud species and layers.

DoD Impact/Significance: COAMPS® continues to play a significant role in providing atmospheric forecasts in support of Navy missions involving the deployment of weapons systems, strike warfare, radar propagation, and search and rescue. Research and development performed at HPC DSRCs have led to significant improvements in the predictive skill of COAMPS® that will greatly benefit the operational performance of COAMPS®. The HPC DSRCs will be the primary computing resources in FY22 and beyond for the development of the fully coupled COAMPS® system including the emerging electromagnetic and electro-optical (EM/EO) and ensemble capabilities for COAMPS®.

[1] COAMPS® is a registered trademark of the Naval Research Laboratory.

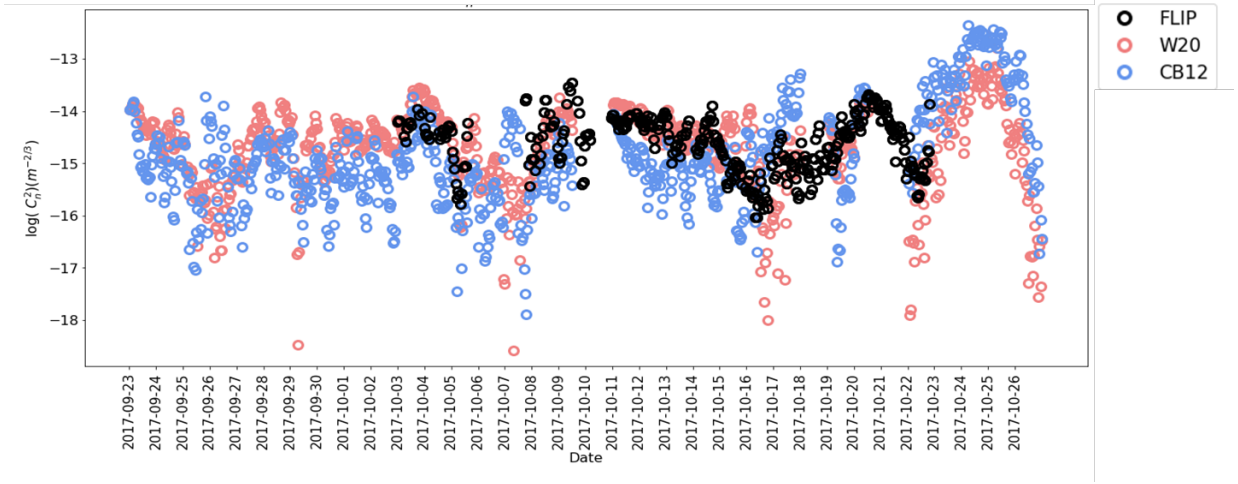

Figure 1. FLIP surface observations (black circles) and COAMPS® simulated 5 m log(cn^2) ($m^{-2/3}$) time series from the CB12 (blue) and W20 (red) methods.

Title: Eddy-Resolving Global/Basin-Scale Ocean Modeling
Author(s): E.J. Metzger and J.F. Shriver
Affiliation(s): Naval Research Laboratory, Stennis Space Center, MS
CTA: CWO

Computer Resources: HPE SGI 8600, Cray Shasta [NAVY, MS]; Cray XC40/50 [ERDC, MS]

Research Objectives: Modeling component of a coordinated 6.1–6.4 effort on the problem of eddy-resolving global and basin-scale ocean modeling and prediction. This includes increased understanding of ocean dynamics, model development, model validation, transitions to operations, naval applications, oceanic data assimilation, ocean predictability studies, observing system simulation studies, and nested models.

Methodology: The appropriate choice of vertical coordinate is a key factor in ocean model design. Traditional ocean models use a single coordinate type to represent the vertical, but no single approach is optimal for the global ocean. Isopycnal (density tracking) layers are best in the deep stratified ocean, Z-levels (constant depths) provide high vertical resolution in the mixed layer, and terrain-following levels are often the best choice in coastal regions. The HYbrid Coordinate Ocean Model (HYCOM) has a completely general vertical coordinate (isopycnal, terrain-following, and Z-level) via the layered continuity equation that allows for an accurate transition from the deep to shallow water. Two-way coupling to the Community Ice CodE (CICE) leads to a more realistic cryosphere in the polar latitudes.

Results: We have six refereed articles, three nonrefereed articles published, six invited talks in FY21.
South China Sea (SCS) Research: A 26-year global HYCOM reanalysis was used to explain the dynamics of the SCS Warm Current (Fig. 1). Yu et al. (2021) is the first paper to identify the area south of Taiwan Strait as the generation region as well as to provide statistics on the occurrence rate, duration, length, magnitude, and location of this current. Trott et al. (2021) also furthered the knowledge of the mesoscale eddy field in the northern SCS by using 26 years of altimeter data to obtain characteristics of both cyclonic and anti-cyclonic eddies.
North Atlantic Research: Nordic Sea simulations using both Navy Coastal Ocean Model (NCOM) and Modular Ocean Model version 6 (MOM6) have investigated fresh-water runoff from the melting Greenland ice sheet. The coastal fresh water alters the exchange across the continental shelf, modifying the current structure. Feature location and variability also were studied in this region as HPC resources were used to generate model output at different horizontal resolutions to facilitate the comparison between fronts as seen by different variables (sea surface height vs. sea surface temperature).
Winter Convection: The role of mesoscale eddies on the convective formation of water masses was studied using idealized eddy HYCOM 3D experiments to understand the response of eddy stratification to convective mixing. The mixed layer deepens disproportionally across the eddy with a deeper mixed layer in the eddy center.
Arctic Ocean: Seven observing system simulation experiments (OSSEs) were integrated to optimize sampling techniques and to determine the best data and way to use it in the Arctic Ocean. These showed the importance of different observation types and improved data assimilation in polar latitudes.

DoD Impact/Significance: Data-assimilative eddy-resolving models are important components of global ocean and sea ice prediction systems. Ocean forecasts are valuable for tactical planning, optimum-track ship routing, search-and-rescue operations, and the location of high-current shear zones. The sea ice environment has become increasingly important for strategic and economic reasons, given the diminishing trend in sea ice extent and thickness and the potential summertime opening of the Northwest Passage and Siberian sea routes. Fractures, leads, and polynya forecasts are also valuable to the naval submarine community.

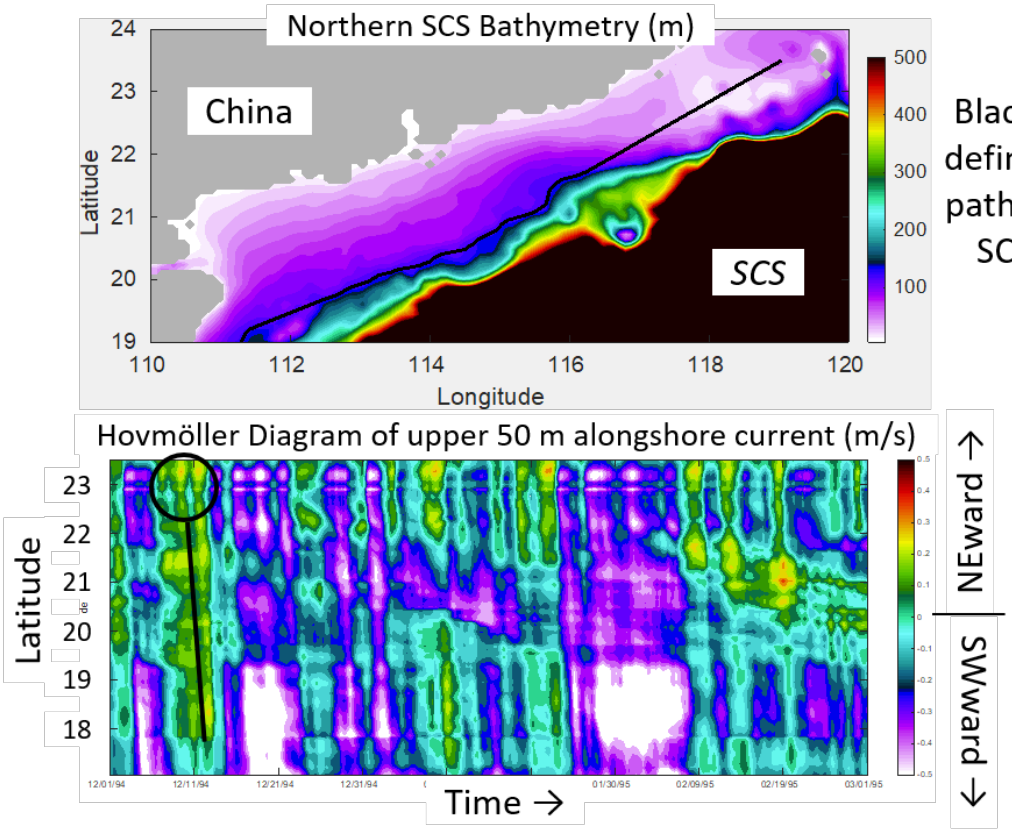

Figure 1. (top) Bathymetry (m) of the northern South China Sea. The black line defines the average path of the South China Sea Warm Current (SCSWC). (bottom) A Hovmöller diagram (time vs. latitude) of alongshore current (m/s) averaged over the top 50 m of the water column along the black line in the top panel. The green/yellow/red colors denote currents to the northeast that start south of the Taiwan Strait and propagate to the southwest. The SCSWC flows counter to the prevailing wintertime monsoon winds that generally blow toward the southwest in this region. The black circle and line denote the formation and propagation of the SCSWC.

Title: Coupled Ocean-Wave-Air-Ice Prediction System
Author(s): R. Allard,[1] T. Campbell,[1] E. Douglass,[1] D. Hebert,[1] T. Jensen,[1] A. Rydbeck,[1] T. Smith,[1] and M. Phelps[2]
Affiliations: [1]Naval Research Laboratory, Stennis Space Center, MS, [2]Peraton, Inc., Stennis Space Center, MS
CTA: CWO

Computer Resources: HPE SGI 8600, Cray Shasta [NAVY, MS]

Research Objectives: Perform research studies with the Coupled Ocean Atmosphere Prediction System (COAMPS®[1]), which consists of an atmosphere model, the Navy Coastal Ocean Model (NCOM), and the WAVEWATCHIII®[2](WW3) and SWAN wave models. Perform modeling studies with the Community Ice Code (CICE v6), which includes a landfast ice parameterization.

Methodology: For accurate simulation and prediction, we have used various configurations of NRL's state-of-the-art fully coupled COAMPS® with very high spatial and temporal resolution. For the Bay of Bengal (BoB) and simulation of cyclone Fani, the following model configuration was used: The atmospheric component has 60 vertical levels and 9 km resolution horizontally. The ocean model has a 0.5 m resolution in the upper 10 m, 45 sigma levels and up to 15 z-levels for a total of 60 levels in water deeper than 330 m, and includes eight semi-diurnal and diurnal tidal components. Horizontal resolution is 2 km. The numerical method for advection is a third-order upstream differencing scheme, a fourth-order pressure gradient, and Coriolis terms for increased accuracy. The turbulent closure scheme is the Kantha-Clayson 2.5 level scheme that includes Stokes drift from the wave model. For these configurations, we use SWAN, with 10 km spatial resolution, 34 frequency bands, and 48 directions. Coupling interval for data exchange between each of the two models is 6 min.

Results: Tropical cyclone Fani (Fig. 1) formed west of Sumatra on 25 April 2019 as a depression, moved north-northwestward, and intensified into a severe Category 4 storm before landfall in Odisha, India, on 3 May. The oceanic structure under Fani's track was captured by moorings, while the atmospheric and oceanic variability was studied using satellite observations and a coupled COAMPS® (Wijesekera et al., 2021a). The cold wake generated by Fani extended from 4°N to 21°N and persisted nearly two weeks, during which local atmospheric convection was suppressed above the wake. After the passage of Fani, the heat content in the upper 50 m increased steadily at a rate of ~200 W/m^2 for three weeks while the ocean surface was heating at a rate of 110–130 W/m^2. The heat budget indicates a large heat imbalance, pointing to the divergence of heat advection, and a lateral heat transport that can be as large as net surface heating. COAMPS® simulations support the view of mesoscale heat advection, and further illustrate that the East India Coastal Current transports warm, salty water from the eastern boundary of India to the northwest-central BoB through filaments/eddies, which, in turn, helps maintain a warm surface layer. We performed a series of regional CICE hindcast studies using a conjugate gradient technique to optimize the parameters for grounded ice keels in the Arctic. The simulations were performed for the period from October 1–July 1 for 2015/2016 and 2017/2018. Model solutions of landfast ice extent were compared against observed landfast ice to determine the optimized parameters.

DoD Impact/Significance: A coupled air-ocean-wave prediction system can have a pronounced effect on Navy forecasting by improving ASW performance, tropical cyclone prediction, search and rescue, and mission planning. The relocatable COAMPS-CICE system will provide high-resolution Arctic forecasting of ice thickness, ice drift, and concentration to support navigation. Inclusion of landfast ice in the Navy's global ice prediction systems will yield a more realistic representation of pan-Arctic sea ice.

[1] COAMPS® is a registered trademark of the Naval Research Laboratory.
[2]WAVEWATCH III® is a registered trademark of the National Oceanic and Atmospheric Administration.

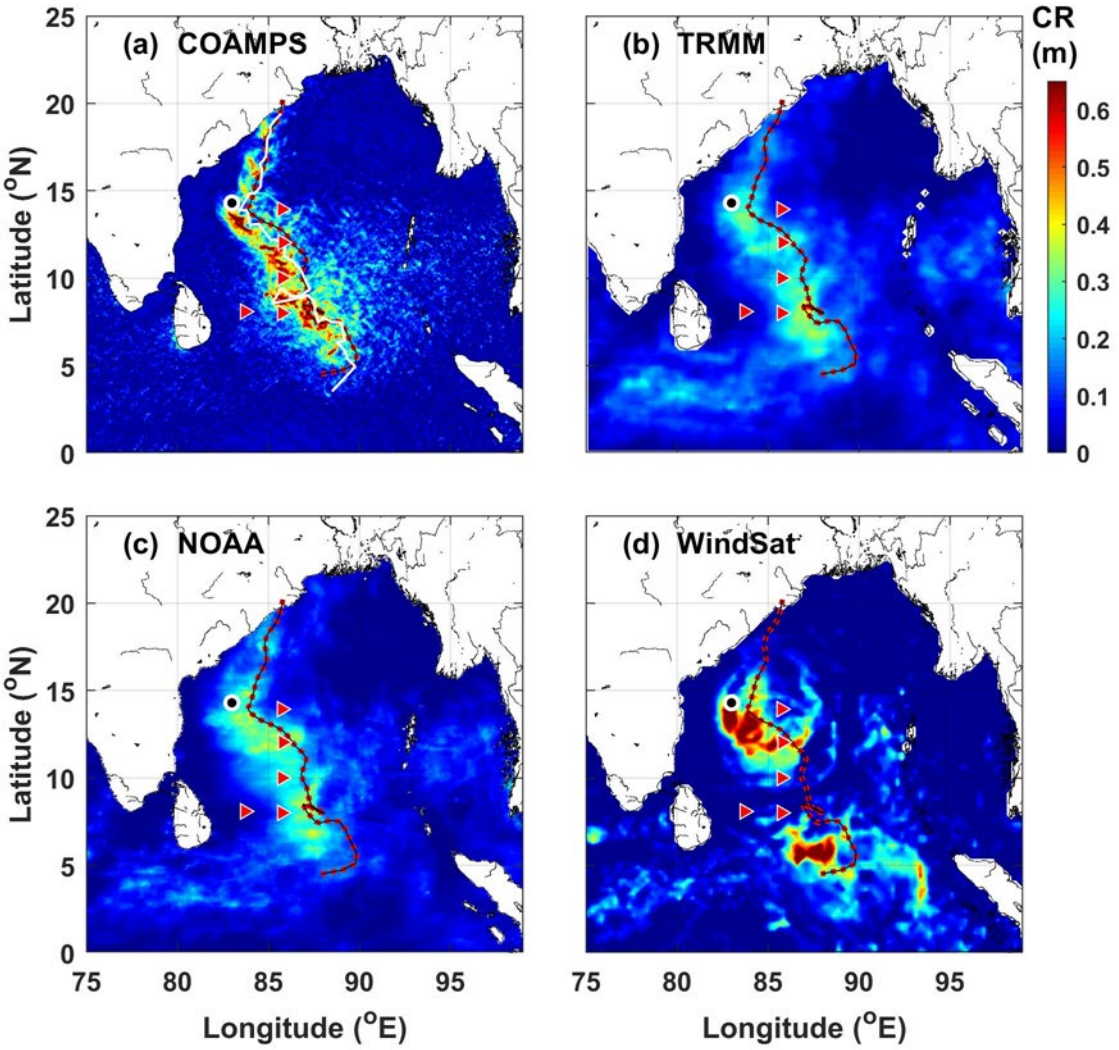

Figure 1. Cumulative Rainfall (CR) estimated between 27 April 2019 and 4 May 2019. (a) COAMPS®, (b) TRMM, (c) NOAA, and (d) WindSat. Note that each product has different spatial and temporal averages. The black line with red dots is the track of Fani, and the thin, white line in (a) is the COAMPS® track. The magenta triangles are the locations of NRL moorings. (From Wijesekera et al., 2021a)

Title: Multi-scale Characterization and Prediction of the Global Atmosphere from Ground to the Edge of Space using Next-Generation Navy Modeling Systems
Author(s): C.A. Barton,[1] S.D. Eckermann,[1] F. Sassi,[1] J.F. Kelly,[1] M.A. Herrera,[1] K.W. Hoppel,[1] D.D. Kuhl,[1] D.R. Allen,[1] J. Ma,[1] and J.L. Tate[2]
Affiliation(s): [1]Naval Research Laboratory, Washington, DC, [2]Computational Physics Inc., Springfield, VA
CTA: CWO

Computer Resources: HPE SGI 8600 [AFRL, OH], [NAVY, MS]; Cray XC40 [ARL, MD]; Cray XC40/50 [ERDC, MS]

Research Objectives: To develop and test new seamless atmospheric specification and prediction capabilities from 0 to 500 km altitude for future Navy Earth System Prediction Capability (ESPC) and Space Environment Prediction with High Resolution (SEPHIR) systems, linking prediction of the ocean, the atmosphere, and space over time scales from hours to decades.

Methodology: This project develops and tests key components of state-of-the-art systems required for improved modeling, prediction, and analysis of the extended operational environment for Navy applications, focusing on the atmosphere, the near space, and the geospace. Specific systems under development are: (a) a high-altitude version of the Navy Global Environmental Model (NAVGEM-HA), based on an upward extension of the Navy's operational global numerical weather prediction (NWP) system, (b) the next-generation Navy NWP model NEPTUNE (Navy Environmental Prediction system Utilizing a Nonhydrostatic Engine), (c) the Coupled Ocean-Atmosphere Mesoscale Prediction System (COAMPS®[1]), the Navy's operational regional NWP system, and (d) the SEPHIR ground-to-space prediction prototype.

Results: Major results directly facilitated by HPC resources during FY21 include: (a) successful testing of NAVGEM-HA code for transition to operations at Fleet Numerical Meteorology and Oceanography Center through the Navy ESPC program in FY22, (b) continued development of a new NEPTUNE modeling capability extending from the surface to 400 km altitude using advanced numerical algorithms that enable the nonhydrostatic dynamical core to operate at high altitudes (e.g., new turbulent mixing schemes, high-altitude physics parameterizations, and integrated empirical models for variable composition) (Fig. 1), (c) development and testing of a new high-altitude data-assimilation capability incorporating wind measurements of the mesosphere and the lower thermosphere from meteor radar and satellite observations into the NAVGEM-HA system (Fig. 2), (d) new long-term contiguous NAVGEM-HA meteorological analysis products with high vertical resolution extending into the mesosphere, (e) COAMPS® simulations coupled to new Fourier-ray and multilayer gravity wave models and an ionospheric model for end-to-end physics-based prediction of traveling ionospheric disturbances seeded by waves generated in the lower atmosphere, (f) development and application of a new in-line algorithm for determining gravity wave drag parameterization settings minimizing analysis increments in the coupled NAVGEM-HA data-assimilation/forecast system.

DoD Impact/Significance: This research addresses Navy requirements to develop and test new high-altitude atmospheric specification and prediction capabilities leading to a planned Navy ESPC by 2022. This project performs the R&D needed to install an accurate, high-altitude specification and forecast capability in next-generation Navy NWP systems, ultimately providing improved near-space specification and prediction capabilities to the warfighter over both tactical and strategic time frames. HPC resources for this project also provide critical support for the development of a new ground-to-thermosphere prediction capability fully coupled to ionospheric models and data assimilation to address key space-environment prediction goals of the Defense Advanced Research Projects Agency's Space Environment Exploitation (DARPA SEE) program.

[1] COAMPS® is a registered trademark of the Naval Research Laboratory.

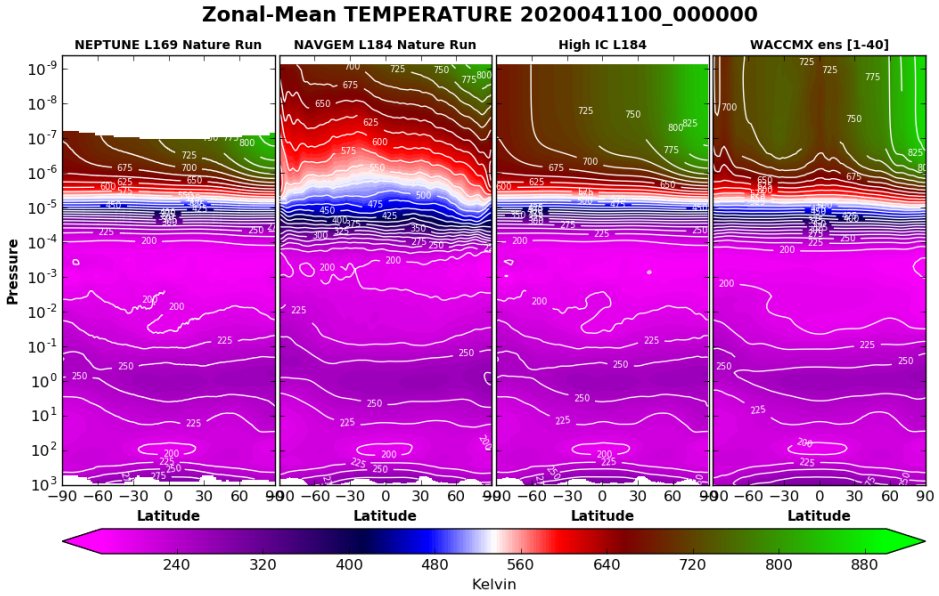

Figure 1. Pressure/latitude cross section of zonal-mean temperature from (left to right) the thermospheric version of NEPTUNE, the thermospheric extension of NAVGEM-HA, the "High ICs" initial condition blending NAVGEM-HA reanalysis with empirical models of the thermosphere, and WACCM-X.

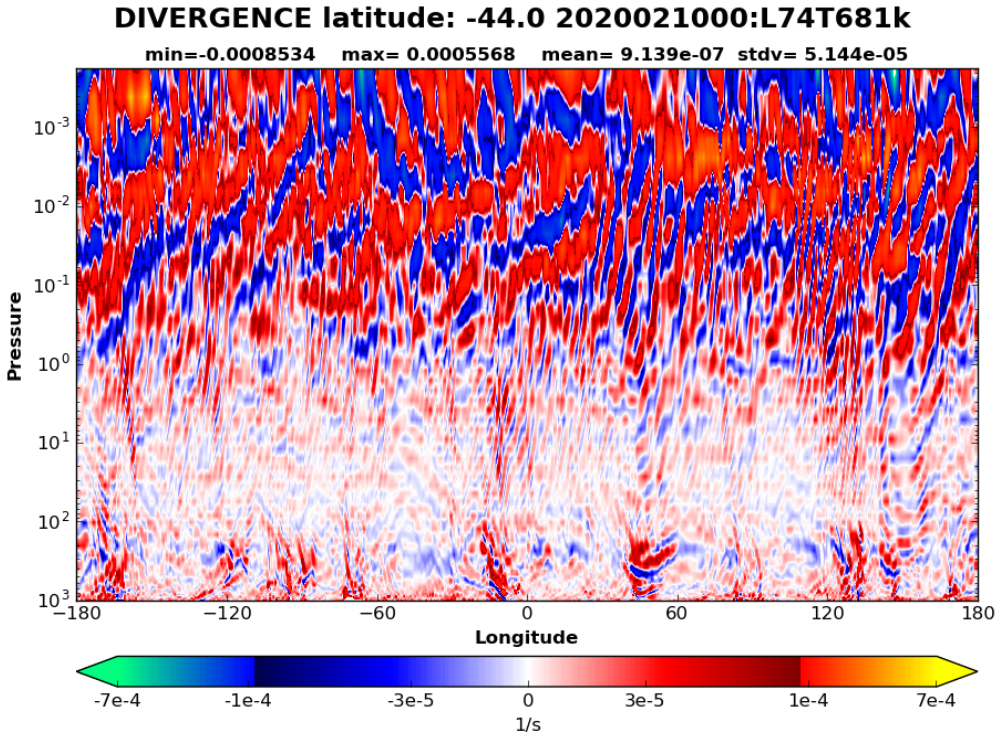

Figure 2. Pressure/longitude cross section of the horizontal wind divergence analyzed by NAVGEM-HA in a configuration with high horizontal resolution and including new meteor radar wind observations.

Title: Bio-Optical Modeling and Forecasting
Author(s): J.K. Jolliff, S. Ladner, T. Smith, and C. Wood
Affiliation(s): Naval Research Laboratory, Stennis Space Center, MS
CTA: CWO

Computer Resources: HPE SGI 8600 [NAVY, MS]

Research Objectives: The research objective for FY21 was to continue the development and implementation of operational data flow from satellite-estimated surface ocean optical properties into operational numerical ocean models in support of the 6.4 "Visible Band Satellite Data to Improve Ocean Model Radiative Transfer" (VISOR) program. Allocated HPC hours were devoted to this task, which includes evaluation and testing of the ocean model component within the Coupled Ocean-Atmosphere Mesoscale Prediction System (COAMPS®[1]).

Methodology: Numerical ocean models must have a designated numerical representation of the attenuation of solar shortwave radiation into the surface ocean. This attenuation calculation determines the potential ocean heating rate and thermal balance for each time step, and it broadly impacts thermal and density state variables. In the two-way coupled/ocean-atmosphere modeling system, the sensitivity of surface temperatures to this process also substantially impacts the simulated exchange of thermal energy between the respective planetary boundary layers. The default calculation for the present class of operational numerical ocean models is based upon a table of five optical (Jerlov) water types. This is the case for the Navy Coastal Ocean Model (NCOM), the ocean numerical model component within COAMPS®. Since these tabular attenuation functions do not recognize real-time optical data from the oceans, they are invariably in error. To remedy this error, we have initiated a program to obtain daily information about the optical state of the surface ocean from the operational constellation of ocean-viewing satellites and to ingest this information into the operational ocean models via the Navy Coupled Ocean Data Assimilation system (NCODA). Surface ocean optical data is a new data type for the NCODA system and requires its own quality control and analysis software architecture. The final analysis file then contains a complete spatial analysis field of surface ocean optical properties. In many cases, this may significantly impact thermal and other critical ocean and atmospheric variables as well as the simulated exchange of thermal energy. Thus, we also used HPC hours to investigate the coupled model behavior for instances in which the ocean is gaining substantial energy from solar shortwave (for example, boreal spring/summer in the northern Gulf of Mexico) as well as instances in which the ocean is subject to substantial heat loss (often during atmospheric cold fronts).

Results: Information from the Global Optical Processing System (GOPS) on surface ocean optics is fed directly into the NCODA optics branch to produce a continuous and updated estimate of solar shortwave attenuation. Under the conditions of low winds and high solar insolation, the differences in the improved model computations and the presently operational (default) are conspicuous. Final testing and evaluation of the VISOR end-to-end system was initiated in FY21, and transitions of the system subcomponents (NCODA + optics, and modified NCOM within COAMPS®) to operational centers is scheduled for FY22. The GOPS satellite data-processing software has been transitioned. An example of the validation results is shown in Fig. 1: in the default attenuation case (upper panel), there is too much penetration of solar shortwave below the density gradient due to freshwater runoff (halocline). This results in temperature inversions (warm water below colder water) that are not observed in this area.

DoD Impact/Significance: Improvement of operational ocean models when given realistic solar shortwave attenuation data has been demonstrated previously and moving this work to the operational level is of paramount importance. The flow of these data will improve model operations within the ocean and atmospheric domains.

[1] COAMPS® is a registered trademark of the Naval Research Laboratory.

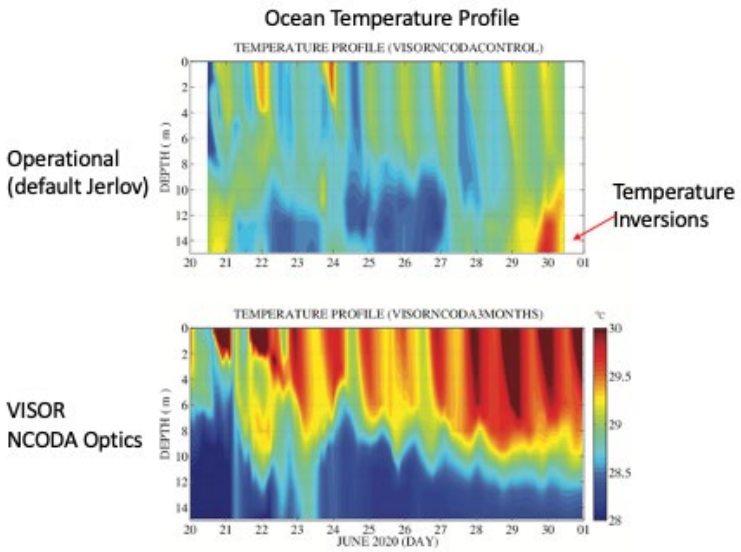

Figure 1. Results from the VISOR COAMPS® experiments in the Gulf of Mexico testbed domain. The upper panel is the default case that uses a table of attenuation values; the bottom panel is the improved model version that uses satellite data and results in an improved ocean temperature profile.

THIS PAGE INTENTIONALLY LEFT BLANK

SIP

Signal Image Processing

SIP covers the extraction of useful information from sensor outputs in real time. DoD applications include surveillance, reconnaissance, intelligence, communications, avionics, smart munitions, and electronic warfare. Sensor types include sonar, radar, visible and infrared images, and signal intelligence (SIGINT) and navigation assets. Typical signal-processing functions include detecting, tracking, classifying, and recognizing targets in the midst of noise and jamming. Image-processing functions include the generation of high-resolution, low-noise imagery, and the compression of imagery for communications and storage. The CTA emphasizes research, evaluation, and testing of the latest signal-processing concepts directed toward these embedded systems. Usually, such processors are aboard deployable military systems and hence require hefty packaging and minimum size, weight, and power. System affordability is expected to improve by an order of magnitude through the development of scalable codes running on flexible HPC systems. This will enable the traditional expensive military-unique “black boxes” required to implement high-speed signal/image processing to be replaced by COTS HPC-based equipment.

Title: Reducing the Burden of Massive Training Data for Deep Learning
Author(s): L.N. Smith
Affiliation(s): Naval Research Laboratory, Washington, DC
CTA: SIP

Computer Resources: Cray XC40/50 [ERDC, MS]

Research Objectives: The successes of deep learning in the past several years rely on three pillars: faster computer hardware, lots of labeled training data, and new algorithms. In this basic research project, we design, develop, and evaluate novel deep-learning algorithms for training deep neural networks that significantly reduce the training time and eliminate the current requirement for massive labeled training datasets in order to allow application of deep networks in situations where labeled data is scarce or expensive to label.

Methodology: Our methodology is primarily based on the following scientific process: Based on our understanding, we develop hypotheses, which often requires experimenting with many variations of neural networks and hyperparameters to determine which of those hypotheses are beneficial and when they are beneficial, and to develop a new understanding as to why they work. The majority of the work done was in the most popular deep-learning frameworks — TensorFlow, Torch, and PyTorch. Hence, it is valuable that the HPC staff installs and maintains these frameworks. Typically, our experiments build on previous work, so the first step is to download code from github.com, then to replicate previous results, and then to test our own hypotheses.

Results: In FY21, the majority of the work on this project attempted to combine our primary objective of reducing the amount of labeled data needed to train a neural network with other high-priority goals. In one effort, we demonstrated for the first time ever the potential for boosting one-shot, semi-supervised (BOSS) learning to attain test accuracies that are comparable to fully supervised learning. Our method combines novel methods such as class prototype refining and class balancing with the known method of self-training. In another effort, we used machine-learning techniques to speed up the computation of acoustic underseas factors needed by our fleet to understand their local environment (see Fig. 1). In addition, our software products are in the process of being transitioned to the fleet.

DoD Impact/Significance: It is widely accepted that large labeled datasets are an essential component of training deep neural networks, either directly for training or indirectly via transfer learning. To the best of our knowledge, we are the first to demonstrate performance comparable to fully supervised learning with semi-supervised learning with only one labeled sample per class. Eliminating the burden of labeling massive amounts of training data creates great potential for new neural network applications that attain high performance, which is especially important when labeling requires expertise.

Our work demonstrates that applying machine learning to acoustic problems is sound. We are now applying machine-learning methods to solve other challenges in the acoustics domain in order to enable substantially improved environmental and situational understanding by our fleet. In addition, the understanding gained by the experiments on the HPC GPU servers builds on all the previous understandings gained from previous experiments, and this understanding is crucial for our future progress in the field.

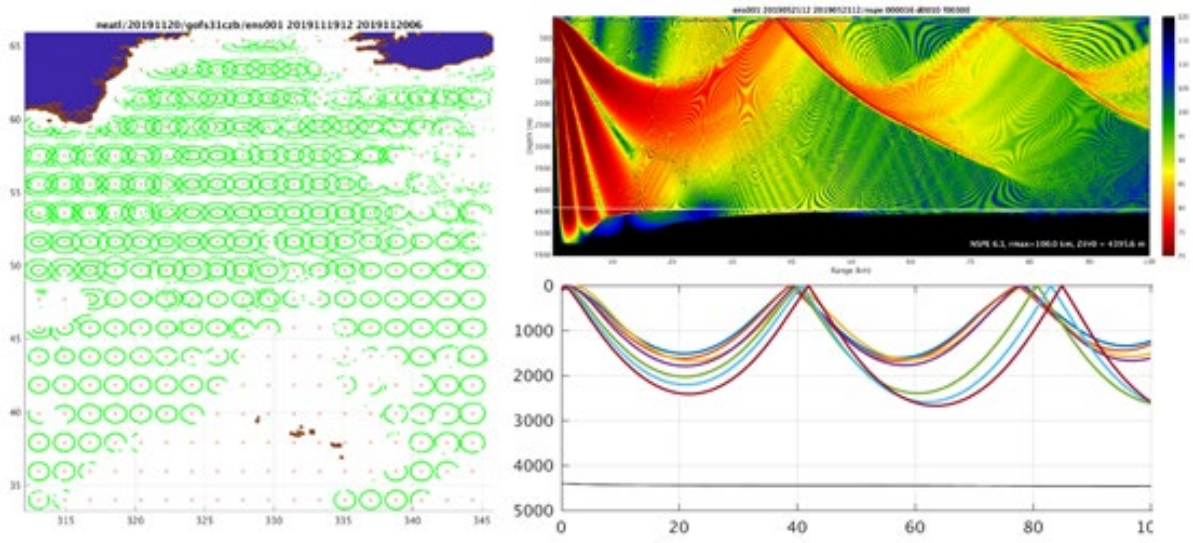

Figure 1. Diagrams of the acoustic performance that provides environmental intelligence desired by our fleet.

THIS PAGE INTENTIONALLY LEFT BLANK

SAS

Space and Astrophysical Science

Space and Astrophysical Sciences (SAS) research and development advance understanding, specification and prediction of the Earth's atmospheric and space domains to exploit the extended operational environment for military advantage and to minimize environmental impacts on military operations. The SAS Computational Technology Area (CTA) embodies the use of mathematics, computational science, and engineering in the analysis, design, identification, modeling, and simulation of the space and near-space environment, and of all objects therein, whether artificial or natural. The SAS CTA encompasses foundational discovery research to study the atmospheres of the Sun and the Earth, including solar activity and its effects on the Earth's atmosphere and ionosphere and near-Earth space, and the unique physics and properties of celestial sources. SAS employs an extensive array of physical and empirical models and analysis tools to integrate observations and theoretical understanding for ever-improving DoD enterprises within, and exploitation of, the extended operational environment. The CTA melds the strengths of a broad range of physical sciences — atomic and molecular physics, materials science, plasma physics, applied optics, radiation survivability, electronic warfare, directed-energy technology, astronautics and space propulsion, orbital mechanics, space situational awareness, and remote sensing – into a structure that helps the DoD multiply force combat effectiveness.

Title: Searches for Millisecond Pulsars and Pulsar Emission Modeling*
Author(s): P.S. Ray[1] and J. Deneva[2]
Affiliation(s): [1]Naval Research Laboratory, Washington, DC; [2]George Mason University, Fairfax, VA
CTA: SAS

Computer Resources: Cray XC40/50 [ERDC, MS]

Research Objectives: The first goal of this project is to search for millisecond pulsars in ground-based data from the Robert C. Byrd Green Bank Telescope (GBT) in West Virginia. These searches require high-performance computing resources because of the massive parameter spaces that must be searched. The second goal of the project is to model the X-ray emission of pulsars based on data from the NICER X-ray telescope, which is currently on the International Space Station.

Methodology: We use custom codes to search for pulsations in our radio data sets. These correct for frequency-dependent delays caused by interstellar dispersion and variable Doppler shifts caused by orbital acceleration in a binary system, then search over a broad range of candidate frequencies using very large Fourier transforms and harmonic summing. We split up the trials over a set of nodes on the cluster. We use another custom code to model pulsar emission. This is an iterative, computationally intensive process involving multithreaded calculations of the Bayesian likelihood of a number of model parameters.

Results: We used Onyx to fit several emission models to the NICER data of PSRs J0740+6620 and J1231-1411. Each model includes known pulsar parameters, like the rotation period and pulse shape, and unknown parameters, like the pulsar's mass and radius, and the locations and shapes of the hot spots on the pulsar's surface that produce the X-ray emissions. We also processed GBT data on 10-millisecond pulsars recently discovered in unidentified *Fermi* gamma-ray sources and were able to determine the orbital parameters of four of them so far. Ground-based radio observations of these pulsars are ongoing.

DoD Impact/Significance: This work is important because millisecond pulsars can be used as a basis of a GPS-independent navigation and timekeeping system for spacecraft, and these studies will assess the limiting accuracy of such systems. This supports the goals of the NRL Space Focus Area and addresses needs in the 2017 Naval Research and Development Framework and the DON 30 Year Research and Development Plans. This work will also maintain NRL leadership in this technical area and will provide expertise useful to USNO and other government partners.

*This work was supported by NASA and the Office of Naval Research.

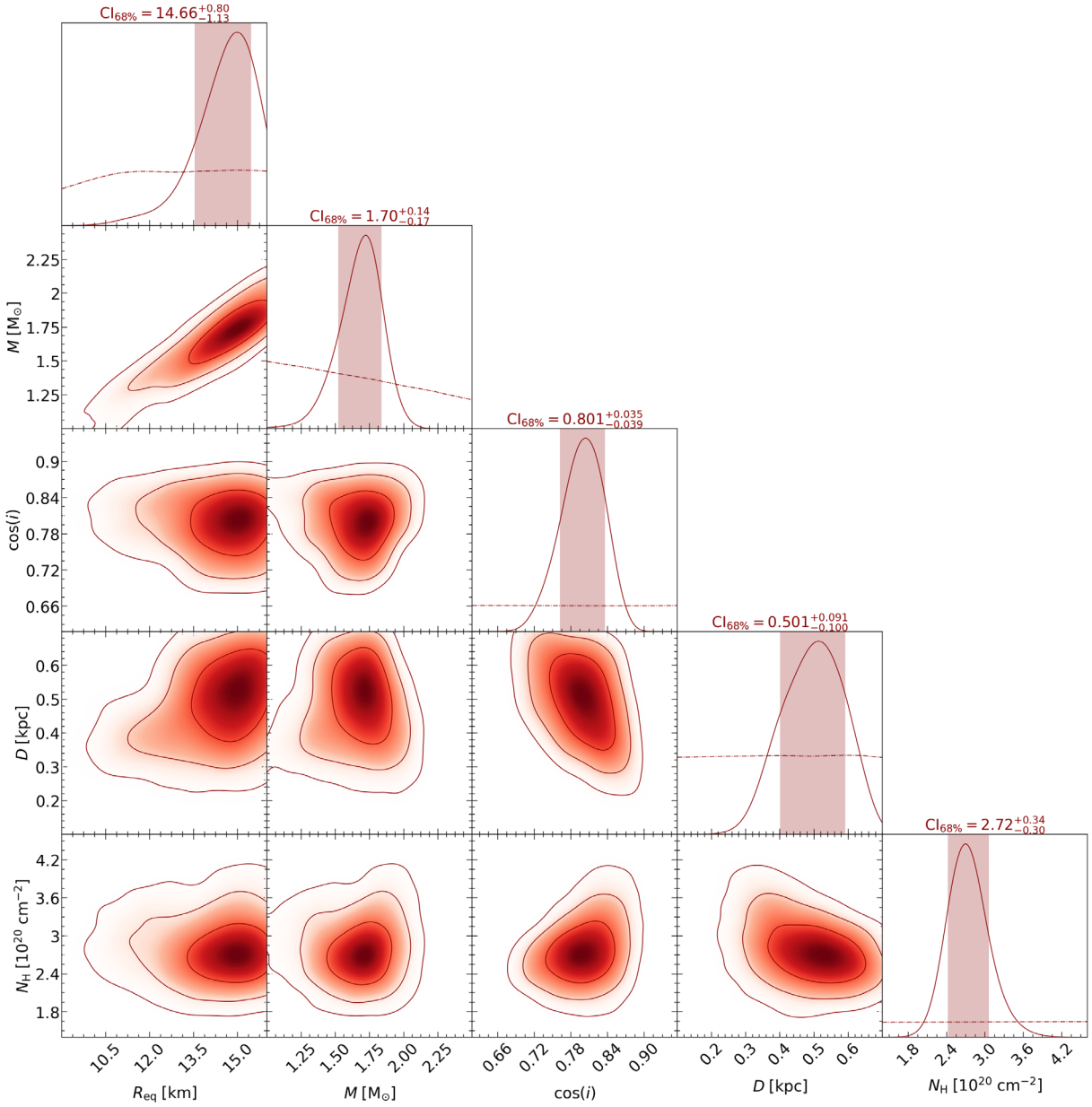

Figure 1. Results from one of our maximum-likelihood models of the X-ray emission of PSR J1231-1411based on NICER data. The emission was modeled as coming from two hot spots with independent shapes and locations on the pulsar's surface. The plot shows contours of the posterior distributions of the main parameters: radius, mass, inclination of the pulsar's orbit with respect to the line of sight to Earth, and distance to the pulsar. In the top panel in each column, dashed lines represent the prior for each parameter, a solid line shows the posterior distribution, and a shaded region represents the 68% posterior confidence interval.

Title: Modeling Propagation of Ionospheric Disturbances Initiated by Magnetospheric Substorms
Author(s): J. Haiducek and J. Helmboldt
Affiliation(s): Naval Research Laboratory, Washington, DC
CTA: SAS

Computer Resources: HPE SGI 8600 [AFRL, OH], [NAVY, MS]

Research Objectives: A traveling ionospheric disturbance (TID) consists of a wave-like density perturbation that moves through the ionosphere. Our primary objective is to improve understanding of TIDs, their spatial structures, and the physical processes that drive them. Our main focus will be on TIDs that are observed by the Very Large Array (VLA) Low-Band Ionosphere and Transient Experiment (VLITE), an observational capability developed jointly by the Naval Research Laboratory and the National Radio Astronomy Observatory. VLITE provides the capability to measure total electron content (TEC) in the ionosphere. Our computational efforts aim to model TIDs observed by VLITE in order to better understand how the area observed by VLITE interacts with the surrounding environment. A secondary objective is to better understand the production of TIDs by magnetospheric substorms, which are explosive releases of energy from the night-side magnetosphere. We aim to better understand these processes by using a combination of VLITE observations and numerical simulations.

Methodology: We are modeling TID propagation using the SAMI3 (SAMI is Another Model of the Ionosphere 3D) simulation code. SAMI3 is an MPI-parallel code that has a demonstrated ability to simulate TIDs from idealized initial conditions. In order to more realisticially simulate TID behavior with SAMI3, we are developing a parallel data-assimilation system called LightDA. LightDA uses an ensemble Kalman filter to assimilate TEC observations collected by GPS receivers and to update the SAMI3 simulation state. VLITE observations will be added to this system following initial tests with the GPS data. The system will be used to simulate TID events that are observed by VLITE, with a focus on TIDs that occur following magnetospheric substorms. By analyzing the output from the SAMI3 ensemble, we hope to gain insights into the physical processes governing the production and propagation of TIDs.

Results: We conducted basic functionality tests with LightDA on a variety of compilers and environments, including MacOS, Linux, and multiple versions of the Gnu and Intel compilers. It has been released as an open-source project under the MIT license. We conducted initial integration of LightDA components designed to read and write SAMI3 restart files and to read TEC observations. Scaling tests of the LightDA+SAMI3 combination on Mustang showed approximately linear speedup from 4 to 2,304 CPU processes, as shown in the upper left panel of Fig. 1.

DoD Impact/Significance: The density perturbations associated with TIDs can introduce errors in Global Navigation Satellite System (GNSS) positioning solutions, with particular impacts on applications requiring centimeter-level-or-better precision. TID activity also can impact radio communications. The assimilative modeling capabilities developed by this program will lead to predictive capabilities that can be used to provide advance notice of TID-related impacts on navigation and communications.

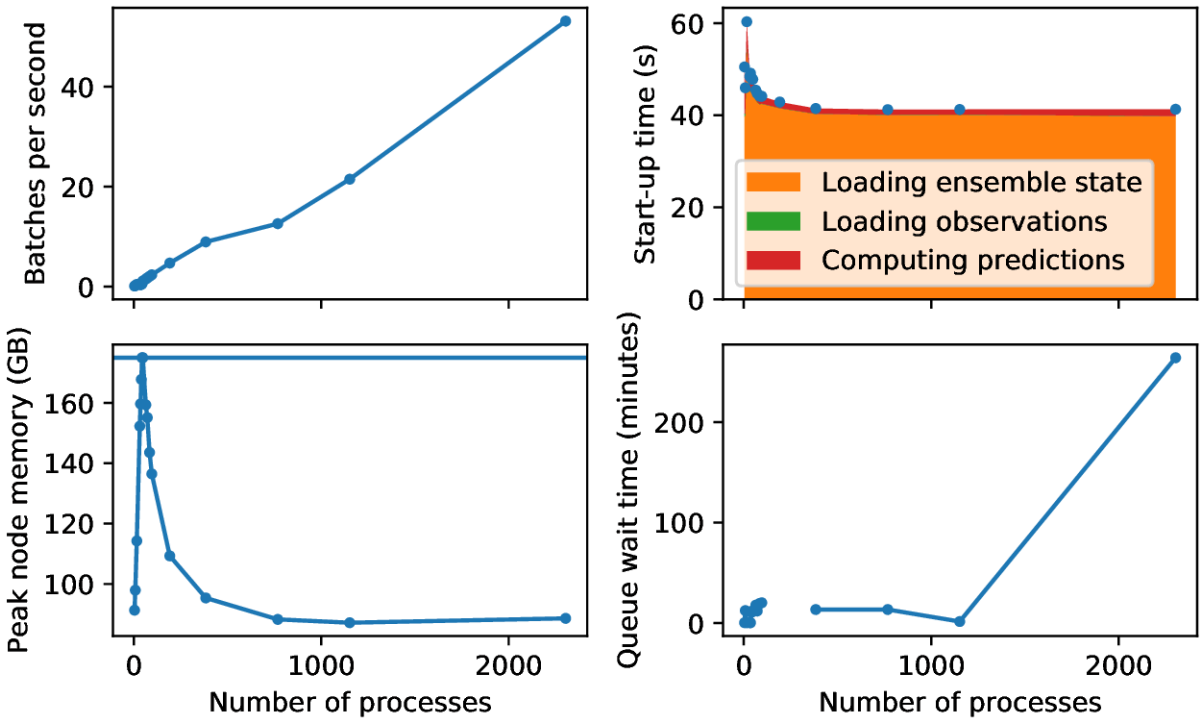

Figure 1. Scaling test results for 4 to 2,304 MPI processes. Upper left: batches (10,000 elements of the SAMI3 state array) assimilated per second. Upper right: Startup time in seconds. Lower left: Maximum per-node memory usage, with a horizontal line denoting the 175-GB-per-node memory limit. Lower right: Wait time in queue as a function of the number of processes.

Title: Dynamic Phenomena in the Solar Atmosphere
Author(s): K.J. Knizhnik
Affiliation(s): Naval Research Laboratory, Washington, DC
CTA: SAS

Computer Resources: SGI ICE X [ARL, MD]; Cray XC40/50 [ERDC, MS]

Research Objectives: The goal of this HPC program is to investigate the solar drivers of the space weather that disrupts DoD and civilian communications and navigation systems. The program is focused on understanding, and ultimately predicting, the initiation processes of the two key solar drivers: coronal mass ejections (CMEs) and solar flares. The fundamental questions that we are investigating are how the emergence of magnetic fields through the photosphere into the corona drives CMEs and flares, and how the reconnection that releases energy in these events occurs in both coronal and chromospheric conditions.

Methodology: Our work focuses on explorations of the emergence of magnetic fields from the convection zone into the solar corona, with the goal of determining how solar activity is generated. This year, we performed high-resolution 3D numerical simulations of the buoyant rise and emergence of twisted toroidal flux ropes through the convection zone and into the corona. We investigated how twist and rise speed affect the rise and emergence of toroidal magnetic flux ropes. In parallel, we focused on implementing and testing our new wave-characteristics-based boundary conditions, with the goal of driving the simulated coronal evolution with observed photospheric magnetic and velocity field information. In addition, we studied the reconnection of Y-type current sheets that form after solar flares. For these studies, we used our magnetohydrodynamics (MHD) code LAREXD for two- and three-dimensional simulations.

Results: We have worked this year to study the rise and emergence of twisted magnetic flux ropes. We showed that force balance on a twisted toroidal magnetic flux rope can be established by accounting for the magnetic tension, magnetic pressure and buoyant forces. We performed fully 3D simulations of rising magnetic flux ropes, which were initially placed in force balance and were given a small perturbation to make them buoyant. We performed a parameter study in which we varied the initial twist on these magnetic flux ropes to observe the effect this had on their rise and emergence. We found that more highly twisted flux ropes rose more quickly and emerged more coherently through the photosphere, whereas more weakly twisted flux ropes rose more slowly and emerged via a buoyancy instability. We then performed a parameter study in which we kept the initial twist constant but varied the initial perturbation in order to change the rise speed. We found that the initial perturbation did not play a large role in the rate of emergence of the flux rope through the photosphere, though did significantly influence the time it took for the magnetic flux rope to reach the photosphere. This effort addresses important aspects of how the convection zone affects the rise of magnetic fields, and reveals that the emergence rate of magnetic flux ropes is a key property that needs to be understood to accurately reproduce solar phenomena.

DoD Impact/Significance: These numerical simulations are providing new insight into how magnetic flux emerges at the solar photosphere, and how solar flares and coronal mass ejections are driven by this emergence. Furthering understanding of how solar activity is generated is a critical step toward building space weather prediction models and mitigating dangers of space weather.

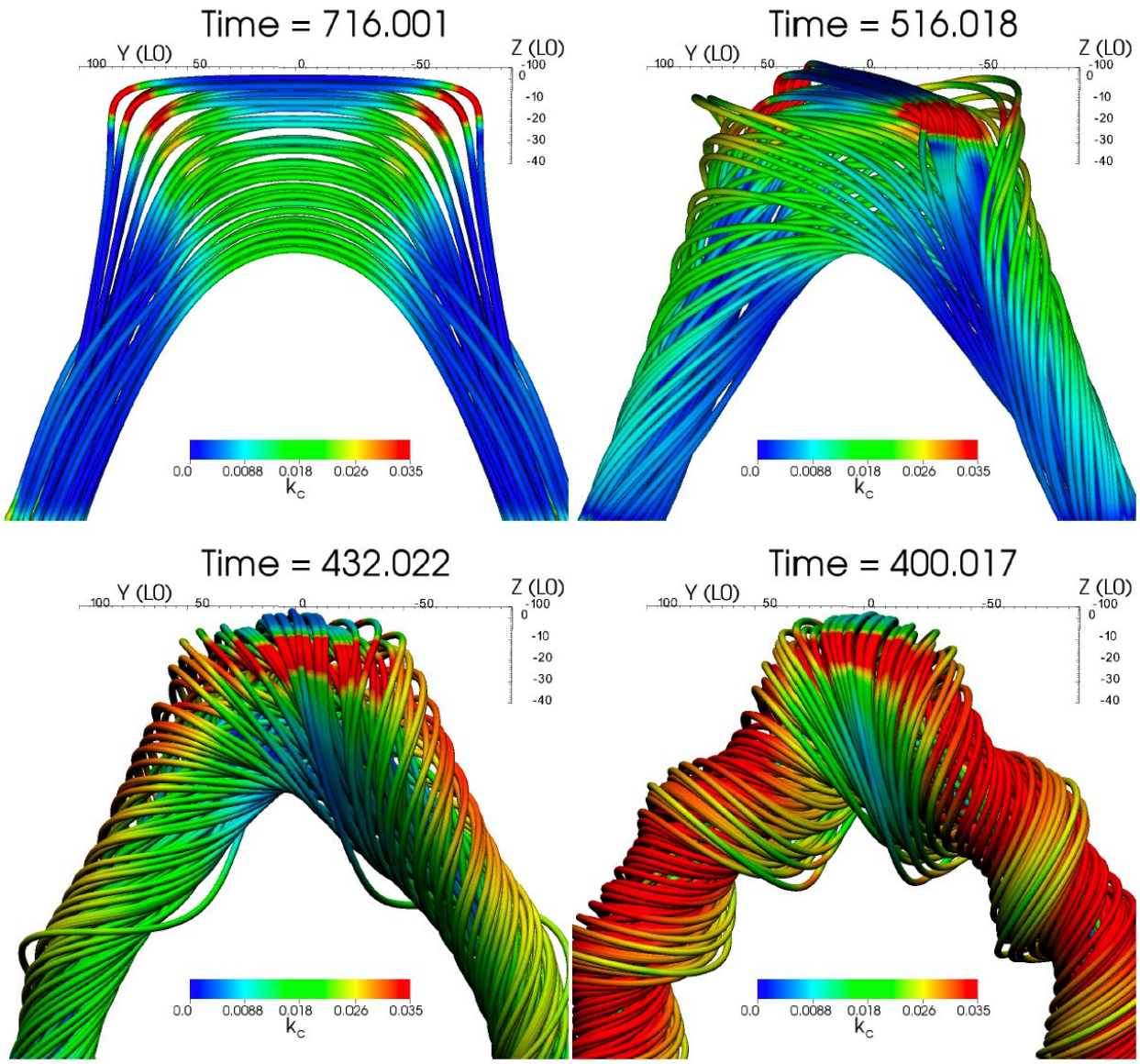

Figure 1. Field lines, colored by curvature magnitude, plotted just below the photosphere right before emergence for four magnetic flux ropes ranging from untwisted (top left) to highly twisted (bottom right).

Title: Global Kinetic Simulations of Space Plasma Waves and Turbulence
Author(s): A. Fletcher
Affiliation(s): Naval Research Laboratory, Washington, DC
CTA: SAS

Computer Resources: SGI ICE X [ARL, MD]

Research Objectives: The objectives of this project are 1) to support an NRL and DARPA sounding rocket experiment program, SMART (space measurement of a rocket-released turbulence, originally launching in fall 2021), by helping to choose mission parameters and understanding the data from the experiment, and 2) to develop the capability to simulate near-Earth space plasmas on both a global scale while including kinetic effects.

Methodology: We use a combination of four codes: 1) ALEGRA, a continuum dynamics code from Sandia National Laboratories, 2) VPIC, a particle-in-cell (PIC) code from Los Alamos National Laboratory, 3) an NRL-built direct-simulation Monte Carlo (DSMC) code, and 4) WICKED, a wave-in-cell (WIC) code developed at NRL. We will determine the density and optical/radar signature of the barium cloud, the amplitude and spectrum of the electrostatic and electromagnetic waves, and the rate of particle precipitation from the radiation belts. WIC, which could simulate the entire process, will need validation via comparable PIC runs. WIC will then be used to simulate as much of the cascade as possible within one simulation.

Results: We performed extensive simulations of shaped-charge detonation using ALEGRA hydrocode, both for predicting scientific results from SMART and to show compliance with NASA's safety guidelines. These simulations predicted yield of vapor, the initial distribution function, and the generation of debris. We showed that the production of barium beam will meet our science objectives. We repeated the calculation with symmetrized version of the entire payload to create a debris catalogue to do collision-avoidance analysis (debris depicted in Fig. 1). The simulations showed that the debris from SMART will not have the velocity to go orbital to threaten other space assets. Additionally, we built our first 3D electromagnetic simulation of the ring instability using the VPIC code. The full resolution version is being run right now. With additional diagnostics to examine energy conversion efficiency and the wave spectrum over time, this simulation confirms one of the key physical mechanisms underpinning the SMART experiment. We enhanced the DSMC code (and subsequent simulation results) with new collision cross sections for barium atoms. This cross-section data is not readily available for barium because it is an element that is rarely used or studied. With updated cross sections, the energy loss to the atmosphere is reduced, meaning more energy is available for plasma waves.

DoD Impact/Significance: The SMART experiment and associated simulations will study turbulence in the ionosphere coupling to waves in the magnetosphere. Given the DoD/Navy reliance on spaceborne assets, understanding the space environment is critical to assure uninterrupted C4ISR capability and to maintain information dominance.

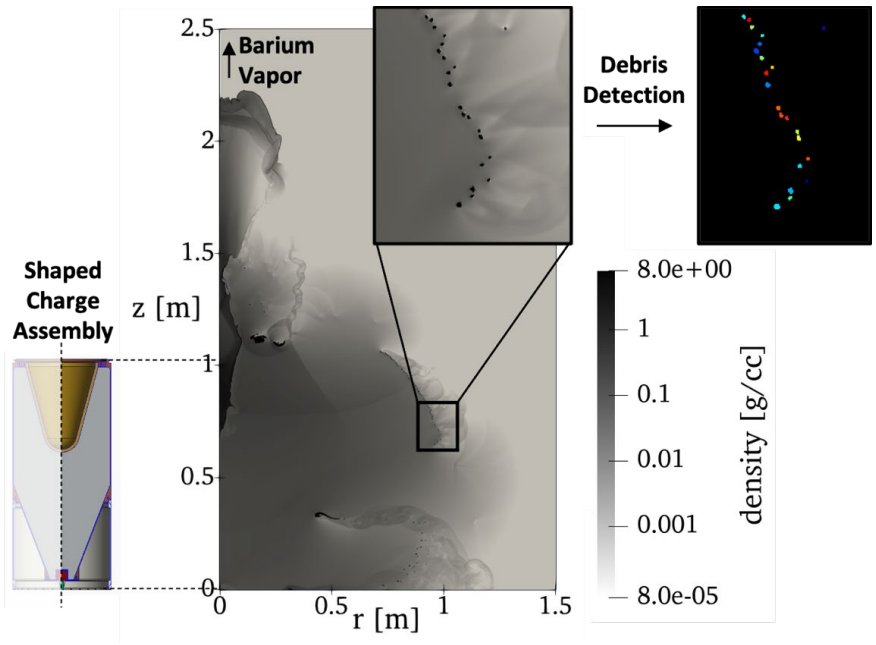

Figure 1. Simulation of neutral barium beam formation (in the positive z direction) and the debris generated by the device. Each piece of debris was detected by an algorithm (identified by unique colors above) to create Monte Carlo debris clouds. This debris is suborbital and quickly falls to Earth.

Title: Electromagnetic Pulses from Hypervelocity Impacts on Spacecraft
Author(s): A. Fletcher
Affiliation(s): Naval Research Laboratory, Washington, DC
CTA: SAS

Computer Resources: SGI ICE X [ARL, MD]

Research Objectives: The objective of this project is to use large-scale simulations to understand electromagnetic pulses (EMPs) and other electrical effects that are associated with hypervelocity impacts (HVIs) on spacecraft and to develop mitigation strategies.

Methodology: Hypervelocity impacts are simulated with two physical models: 1) a continuum-mechanics approach for the formation of the crater and plasma, and 2) a kinetic electromagnetic plasma approach for microscale physics and emission of radiation. ALEGRA, a hydrocode from Sandia National Laboratories, is used for the continuum-dynamics regime. VPIC, a particle-in-cell from Los Alamos National Laboratory, is used for the kinetic plasma regime. We run simulations to compare to both our theoretical predictions, in particular the generation of electromagnetic waves and interaction with the spacecraft potential, and to compare to experimental data from Van de Graaff experiments and NASA's Parker Solar Probe.

Results: There are three primary results this year. First, we compiled and incorporated a new particle-in-cell code that is faster and more robust called VPIC. We used VPIC to run the first 3D simulations of the plasma plume. We also incorporated neutral collisions into the PIC simulation in order to examine a critical assumption underlying the formation of an EMP from a hypervelocity impact. Second, we ran a series of simulations to quantify the change in momentum of the target and to characterize the pressure wave within the target from different impacts. We are using this information to procure sensors to measure these physical parameters. These sensors will be bench tested and then used in ground-based experiments. Third, we performed the first large-scale 3D magnetohydrodynamic (MHD) simulations of impact plasma plume, seen in Fig. 1. The 3D geometry is critical for the interaction of the plasma plume with the ambient environment due to the effects of the background magnetic field.

DoD Impact/Significance: Protection of critical DoD space assets from this threat is necessary to assure uninterrupted C4ISR capability, which is critical for operational success as envisioned in the Navy's S&T strategic plan for information dominance. Countermeasures against hypervelocity impacts of microprojectiles on DoD space assets depend on the knowledge of the electromagnetic power and the frequency spectrum of the impact-associated EMPs.

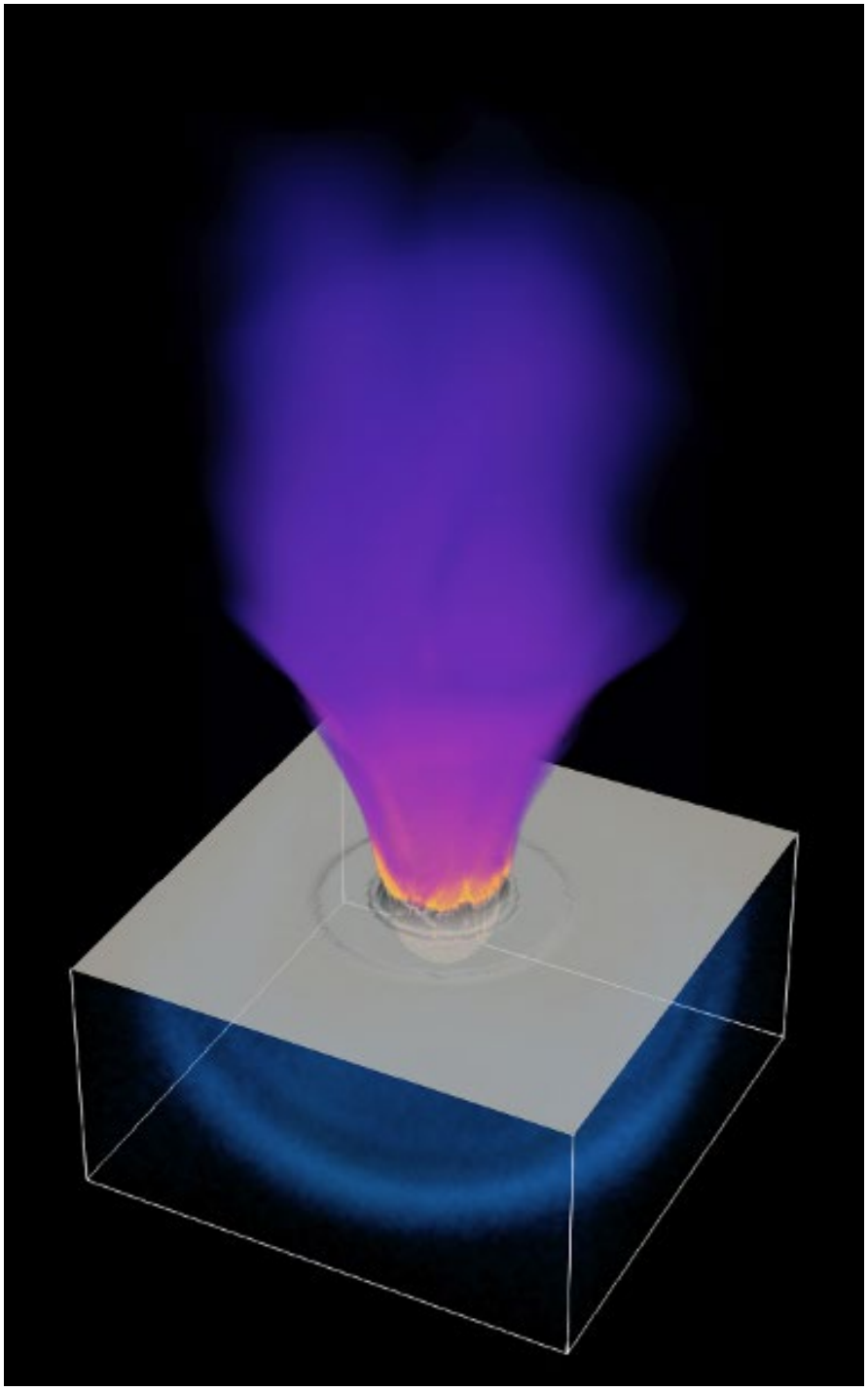

Figure 1. A hypervelocity impact on a spacecraft surface (72 km/s iron meteoroid on aluminum). The grey is the top of the surface; the formation of the crater can be seen. The blue hemispherical shock wave within the target is expanding away from the impact site. This pressure wave is what we intend to measure with acoustic sensors and accelerometers in order to diagnose the impact. The purple expanding out of the crater is the plasma generated by the impact. We ran subsequent simulations at the boundary of this plasma to examine kinetic instabilities that may form due to the extreme gradient there.

Title: Navy Ionosphere Model for Operations*
Author(s): S.E. McDonald,[1] C.A. Metzler,[1] F. Sassi,[1] J.L. Tate,[2] M.R. Burleigh,[1] D. Hodyss,[1] R.K. Schaefer,[3] G. Romeo,[3] R. Calfas[4]
Affiliation(s): [1]Naval Research Laboratory, Washington, DC, [2]Computational Physics, Inc., Springfield, VA, [3]The Johns Hopkins Applied Physics Laboratory, Laurel, MD, [4]The University of Texas at Austin Applied Research Laboratories, Austin, TX
CTA: SAS

Computer Resources: HPE SGI 8600 [NAVY, MS]; Cray XC40/50 [ERDC, MS]; Cray XC40 [ARL, MD]

Research Objectives: The objective of this effort is to develop a physics-based ionosphere model coupled to an ionospheric data-assimilation system that provides global and regional electron density specifications and short-term forecasts (0 to 24 hours). This capability forms the basis of a future Navy operational ionospheric forecasting system running at multiple resolutions and fully coupled to operational atmospheric forecast models. In FY21, the main objectives were to complete integration testing of the full system and to begin comprehensive validation of the model.

Methodology: The Next Gen Ionosphere Model for Operations (NIMO) is a physics-based model, SAMI3, and a 3DVAR ionospheric data-assimilation system (IDA4D) that can ingest a wide variety of ionospheric datasets. NIMO also includes couplers that use the Earth System Modeling Framework (ESMF) for interpolation the ionosphere and data-assimilation grids. IDA4D previously used an empirical ionosphere, the International Reference Ionosphere (IRI), as its background model. For NIMO, IRI has been replaced with SAMI3, which will enable improved specifications and short-term forecasts. The MPI-enabled Earth System Modeling Framework (ESMF) interpolation routines are used to interpolate between the unstructured IDA4D grid and the geomagnetic field-aligned SAMI3 grid. Cylc, a workflow tool, is used to manage the cycling of the system and the processing of late data, which occurs with a 15-minute cadence.

Results: In FY21, we began to transition NIMO to operations at Fleet Numerical Meteorology and Oceanography Center (FNMOC). As part of this effort, we have rigorously tested the full system to ensure the ionospheric datasets are properly ingested. NIMO is capable of ingesting a wide variety of ionospheric measurements that are linearly or nonlinearly related to electron density; these include line-of-sight measurements of total electron content (TEC) from ground-based Global Positioning System (GPS) receivers and space-based radio occultations from COSMIC-1 (and soon COSMIC-2), electron densities from ionosonde soundings and in situ satellite instruments, and ultraviolet (UV) radiances from space-based sensors. A monthlong run was successfully completed on the HPC systems using an archive of operational ionospheric datasets. Initial validation of this time period shows that the model is performing better than climatological models. Figure 1, for example, shows a comparison of a climatological run of SAMI3 (left column) to NIMO (right column). Total electron content (TEC) is shown for three consecutive days, 11–13 April 2020, at 18:00 UT. While the SAMI3 TEC shows very little variability over the three-day period, NIMO, with the ingestion of numerous datasets, shows considerable variation in TEC from day to day. In preparation for NIMO to ingest significantly more data in the near future, we continue to make improvements to the speed of the data-assimilation algorithms.

DoD Impact/Significance: The development of an operational ionospheric forecast model will aid in the numerical forecasting of high-frequency (HF) radio wave propagation through the Earth's atmosphere and ionosphere across the range of conditions relevant to DoD/Navy operations.

*This work is supported by the Office of Naval Research.

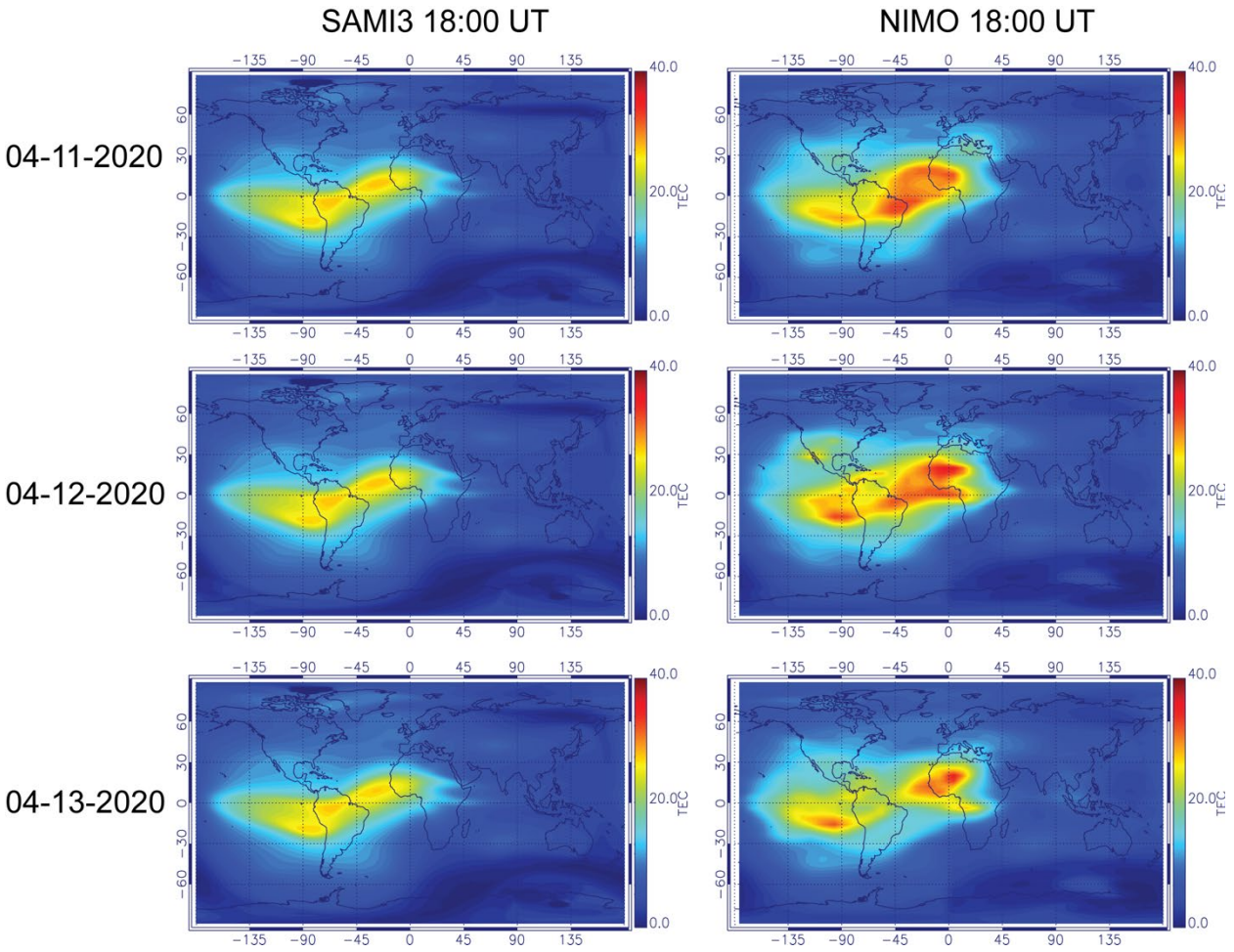

Figure 1. Global total electron content (TEC) shown at 18:00 UT on three consecutive days (11–13 April 2020). The left-hand column shows the SAMI3 simulation of TEC without data ingestion. The column on the right shows the NIMO analysis products in which GPS, COSMIC-2 radio occultations, and ionosonde measurments have been assimilated. The SAMI3 simulations use climatological thermospheric composition, temperature, and winds; therefore, this model cannot realistically capture the day-to-day variability. NIMO, on the other hand, is constrained by data and shows considerable variation in TEC during this three-day period.

Title: Thermosphere & Ionosphere Numerical Models and Ensemble Methods
Author(s): D.P. Drob and M. Jones
Affiliation(s): Naval Research Laboratory, Washington, DC
CTA: SAS

Computer Resources: HPE SGI 8600 [AFRL, OH]; Cray XC40/50 [ERDC, MS]; HPE SGI 8600, Cray Shasta [NAVY, MS]

Research Objectives: This effort seeks to specify the weather of Earth's thermosphere and ionosphere for high-frequency (HF) radio wave applications. Accurate and computationally efficient numerical models are needed to specify and forecast the density, ion-neutral composition, winds, and temperatures of the near-Earth space environment as perturbed from below by solar heating-driven tides and internal waves, as well as from above by ionizing extreme-ultraviolet solar radiation and fluctuations in the solar wind that interact with the Earth's magnetic field.

Methodology: For this effort, first-principles thermosphere and ionosphere numerical models are utilized together with ensemble data-assimilation methods to develop and test a first of its kind, global high-resolution (2.0 x 1.25 degree) medium-range (72-hour) ionosphere forecast model. SAMI4-EnKF (version 4.0, Ensemble Kalman Filter) is based on an updated version of the NRL SAMI model (Sami is Another Model of the Ionosphere). SAMI4-EnkF exists as an ensemble of members, each with slight random perturbation to uncertain system drivers and uncertain model parameters, and all run together in parallel. By tuning the ensemble mean and parameter variance to the past 24 hours of available ionosphere observations, a locally optimized set of model parameters, and initial conditions, the ensemble can be used to make unbiased ionosphere forecasts out to 72 hours, which also includes forecast uncertainty estimates.

Results: Numerous model parameter exploration and tuning experiments were performed this year, with particular emphasis on improving model physics, computational efficiency, resolution, and validation and verification of SAMI4-EnKF for transition to applied Navy and DoD applications. As a result of this year's efforts, SAMI4-EnKF now outperforms both existing research and operational physics-based and empirical models in terms of forecast skill, run time, and output resolution. Several studies were performed and documented to demonstrate and evaluated SAMI4-EnKF's capabilities for potential future transition into DoD space weather operations. For NRL basic research application, SAMI4-EnKF's improved computation efficiency enables high-resolution global ionosphere simulations for radio wave propagation calculations that previously have been unavailable. Long-range, high-frequency radio wave propagation depends on utilizing the ionosphere as a waveguide. The stability and smoothness of this waveguide impacts HF radio wave channel scattering and propagation path stability characteristics. SAMI4-EnKF was utilized to generate first-of-a-kind, high-cadence, time-resolved multiday, high-resolution, global specifications of important intermediate and small-scale ionosphere fluctuations and phenomena. Previously, this phenology could only be approximated with steady-state statistical random noise models. Two examples of this phenology resolved by SAMI4-EnKF for subsequent long-range HF radio wave propagation research calculations are shown in Figs. 1 and 2.

DoD Impact/Significance: The coupled physical-based thermosphere-ionosphere model validation studies performed here address the DoD/Navy long-term need for environmental prediction of space weather effects for tactical planning purposes, as well as the maximization of DoD HF and space systems performance though adaption to the variable environment (ref: SECNAVINST 2400.2A).

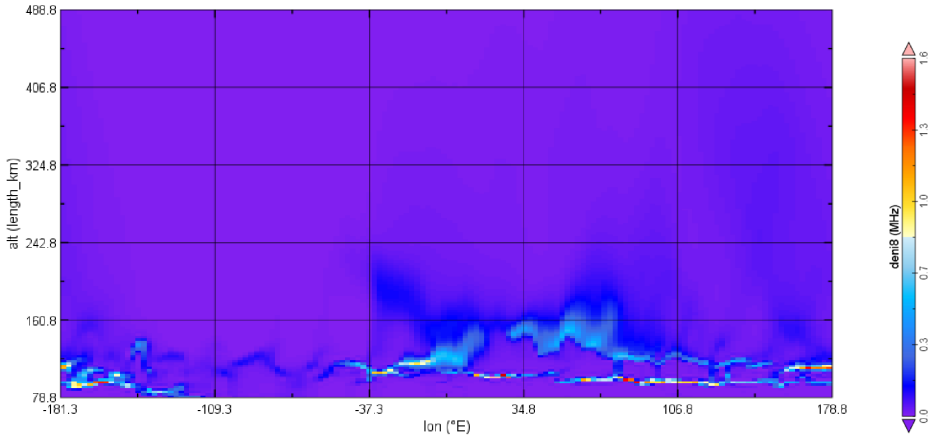

Figure 1. Longitudinal cross section at 20° N of long-lived [Mg^+] metallic ions continuously produced by micrometeorite ablation and entrained into dense, thin, slowly descending layers by vertically propagating, solar heating-driven tidal wind oscillations. These layers are often modulated and/or broken into smaller regional patches by vertically propagating mesoscale internal waves.

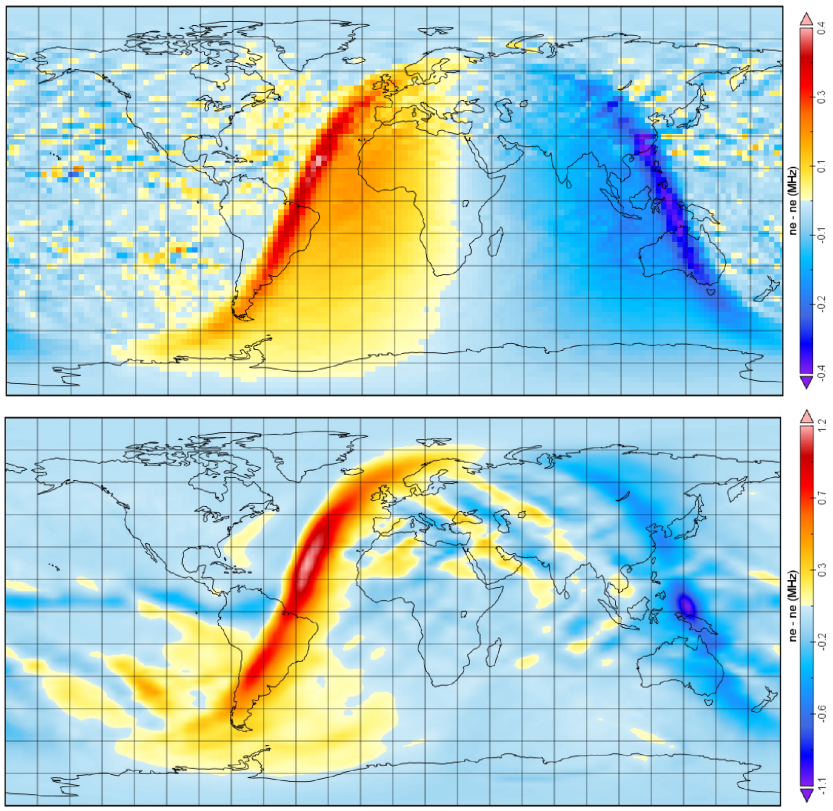

Figure 2. Difference images of electron density at two different altitudes (120 km and 250 km) above the Earth in units of plasma frequency (MHz) over 15 minutes from 09:00 to 9:15 UTC for December 9, 2021, from SAMI4 forecast model output at 2°×1.25° global resolution.

THIS PAGE INTENTIONALLY LEFT BLANK

Other

Work that is not easily categorized as one of the other computational technology areas.

Title: Simulation of High-Energy Radiation Environments
Author(s): J. Finke and W. Duvall
Affiliation(s): Naval Research Laboratory, Washington, DC
CTA: OTH

Computer Resources: Cray XC40/50 [ERDC, MS]

Research Objectives: (1) Apply three-dimensional (3D) Monte Carlo methods to simulate the transport of high-energy particles for use in space applications and for modeling detection systems, radiation environments, and the operational concepts relevant to the detection of special nuclear materials and other radiological/nuclear materials in maritime and urban scenarios of interest to DoD and other civilian agencies. (2) Create an improved model of the extragalactic background light (EBL) useful for the study of extragalactic sources by a number of instruments, including the Fermi Gamma-ray Telescope and the future Cherenkov Telescope Array.

Methodology: (1) We use three industry-standard ionizing radiation transport codes: two 3-D Monte Carlo packages, Geant4 (CERN) and MCNP (Los Alamos National Laboratory), and one discrete ordinates package, Denovo (Oak Ridge National Laboratory). We use an NRL-developed front-end package called SoftWare for Optimization of Radiation Detectors (SWORD) to quickly prototype geometries and radiation environments for running our simulations. (2) We use a model of the EBL created by Co-PI Finke and fit it with a Markov chain Monte Carlo (MCMC) to a wide variety of data from the literature to determine model parameters, and strongly constrain a number of quantities of astrophysical significance and of use to observations of extragalactic gamma-ray sources.

Results: (1) Several SWORD simulation runs contributed to an ongoing effort to validate the Nuclear Detection Figure of Merit (NDFOM) simulation environment. In this case, Monte Carlo results for specific detectors run on HPC resources were compared to the semi-analytical results from NDFOM. This work was done as part of the Data Mining Analysis and Modeling Cell (DMAMC), a program of DHS/CWMD. (2) Co-PI Finke's research has led to the measurement and constraints on a number of interesting quantities of astrophysical interest. This includes the mean metallicity and mass density evolution of the universe across cosmic time, and the cosmic star formation rate (SFR). The 68% constrain from the MCMC fit to luminosity density data is shown in Fig. 1 from an MCMC fit with our EBL model. The model provides a good fit to the data.

DoD Impact/Significance: (1) Our 3D Monte Carlo radiation modeling allows us to provide timely answers to the questions posed by DHS/CWMD, DTRA, NASA, DoD and other government sponsors about radiation environments and detectors. The science addressed by ionizing radiation simulations such as the studies described above is often impractical or not cost effective to study in any manner other than simulation. (2) The EBL absorbs gamma rays from extragalactic objects, and thus understanding the EBL is crucial to studying these types of high-energy sources. Understanding how high-energy particles are accelerated and producing ionizing radiation in these sources helps researchers understand the high-energy-radiation environment that can affect DoD space assets.

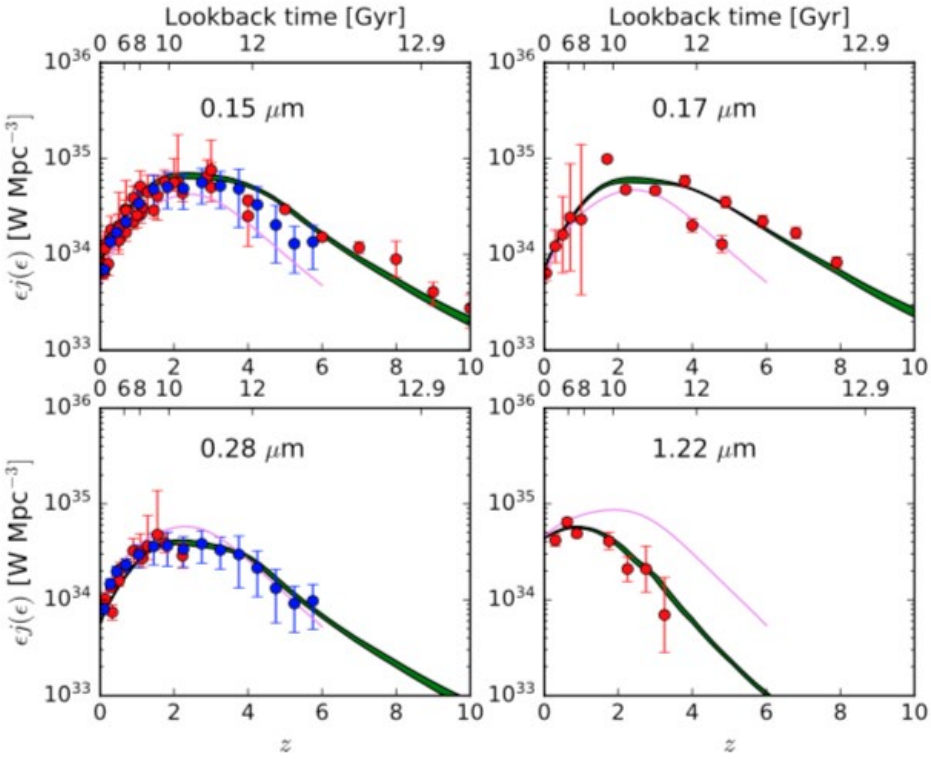

Figure 1. The luminosity as a function of redshift, or equivalently, lookback time, for several wavelengths. The green-shaded regions represent the 68% confidence intervals from MCMC fits to the gamma-ray and luminosity density data. The red and blue points represent measurements from galaxy sky surveys. The violet curves represent the model by Co-PI Finke published in 2010.

THIS PAGE INTENTIONALLY LEFT BLANK

Author Index

Author Index

Author Index

Division/Branch Index

Center for Biomolecular Science and Engineering (Code 6900)

Ocean and Atmospheric Science and Technology Directorate (Code 7000)

Acoustics Division (Code 7100)

Remote Sensing Division (Code 7200)

Ocean Sciences Division (Code 7300)

Marine Meteorology Division (Code 7500)

Space Science Division (Code 7600)

Naval Center for Space Technology (Code 8000)

Spacecraft Engineering Division (Code 8200)

Site Index

DSRCs